Entropy behavior for underresolved discontinuous Galerkin discretizations of the Navier-Stokes equations

by

Cory Frontin

B.S., University of Maryland (2014)

Submitted to the Department of Aeronautics and Astronautics
in partial fulfillment of the requirements for the degree of

Master of Science in Aeronautics and Astronautics

at the

MASSACHUSETTS INSTITUTE OF TECHNOLOGY

~~May 2018~~ [June 2018]

Signature redacted

Author .....
Department of Aeronautics and Astronautics
May 31, 2018

Signature redacted

Certified by .....
David L. Darmofal
Professor of Aeronautics and Astronautics
Thesis Supervisor

Signature redacted

Accepted by .....
Hamsa Balakrishnan
Associate Professor of Aeronautics and Astronautics
Chair, Graduate Program Committee

Entropy behavior for underresolved discontinuous Galerkin discretizations of the Navier-Stokes equations

by

Cory Frontin

Submitted to the Department of Aeronautics and Astronautics
on May 31, 2018, in partial fulfillment of the
requirements for the degree of
Master of Science in Aeronautics and Astronautics

Abstract

High-order methods are emerging as a crucial tool for aerodynamics. One application is for solving large eddy simulations (LES). The use of the discontinuous Galerkin (DG) discretization in particular has attractive properties for these simulations. The stabilization methods used for high-order DG for underresolved Navier Stokes perform some compensation for subgrid scale effects, like subgrid-scale modeling in explict LES. In this work, the mathematical formulation of the finite element method is used to create a new technique for quantifying the artificial generation of entropy due to stabilization in a common DG formulation, in order to clarify the necessity of explicit subgrid modeling and give insight into future modeling strategies for LES performed using high-order finite element methods.

Thesis Supervisor: David L. Darmofal
Title: Professor of Aeronautics and Astronautics

Dad: this thesis is the culmination so far of the engineering spirit you instilled in me. It is dedicated to you.

May you rest in peace.

Acknowledgments

Acknowledging everyone who deserves acknowledgement for this thesis is a herculean task. First and foremost, thanks to Prof. Dave Darmofal for supporting my research and giving the gifts of academic freedom and guidance in equal measure, allowing me to approach the problems in turbulent simulation here at MIT, and helping me to follow them even to the very end. Close behind, thanks to Dr. Steven Allmaras for constantly supporting my research as I quested into one of the many areas of his expertise. Thanks to them both for being examples for keeping my priorities straight, never placing work above those things vastly more important.

Thanks as well to Dr. Scott Murman of NASA Ames Research Center, as well as the entire `eddy` group working there for letting me crash for a summer, break their code, and eventually— at long last— use it productively.

Thanks to my parents, Curtis and Teri, and my sister Danielle for supporting me without fail, no matter what distance or workload might be separating us. Likewise to my fiancée, Judy, who liked me enough to follow me here and has loved me through the stress of a mutually graduate life. A lifetime of thanks to my extended family and to all of my teachers and mentors throughout the years.

Endless thanks to my friends from home (the triumvirate), DeMatha, University of Maryland, Habitat for Humanity of Metro Denver, the ACDL, AeroAstro, and the Muddy Charles in particular, and MIT in general. I am nothing without good friends. A huge thank you to the rest of the Darmofal research group. Thanks especially to the HyperCube and the HyperParallelopiped for the potent combination of both keeping me sane and also making me smarter.

Verso l'alto.

Contents

List of Figures

List of Tables

Chapter 1

Introduction

1.1 Fluid mechanics problems in aerospace engineering

When the Wright brothers first flew in late 1903, they took a leap above and beyond those would-be aviators who had come before them. They had little more than a high school education and a few years' experience in printing and bicycle shops, which starkly contrasts with today's aeronautical engineers. Nonetheless, they did share one advantage over their predecessors which is crucial even today: data. The Wright brothers innovated by building a wind tunnel and mastering its use, creating small experiments that were able to better inform them how to anticipate the way that their airplanes would fly.

Looking at the aerospace industry today, it is obvious that the same data-driven decision making process informs the modern designer. Despite over a hundred years of experience, aeronautical design is far from a closed problem. As an industry, we constantly seek new data and an improved ability to predict the characteristics of an aircraft or spacecraft's flight in the atmosphere. There are countless problems in aeronautics that are hard to solve, and, fittingly, aeronautics remains an active area of research interest. Some of the largest of these problems are in the domain of aerodynamics.

The applications of aerodynamics consists of two major areas, external flows, concerning the flow around an aircraft or spacecraft, and internal flows, which are inside of turboma-

chinery or other vehicle components. Regardless of which application area one considers, the primary goal of the aerodynamicist is to provide accurate and reliable predictions of the aerodynamic loading on vehicles or their components, as well as predicting the coupled thermodynamics that are involved in the case of high-speed and reacting flows. These predictions are complicated by the nonlinear and time-dependent nature of real fluid mechanical flows.

1.2 Time-dependent phenomena in fluid mechanics

Considering the high-resolution simulation of fluid flows, we must take care to capture the variations of the flow in time and space. Chaotic behavior can arise from the huge number of interactions involved in a real fluid flow, and this, in turn, can lead to an unpredictable state of the flow. In other words, the snapshot of a real fluid flowfield at any given time can be strongly dependent on the infinite sequence of previous snapshots of the flowfield. This leads to unpredictable states, and as the flow's complexity grows we are quickly unable to simply and accurately describe the flow state by using simplifying variables or assumptions. These effects make predicting or simulating fluid flows extremely challenging. Some of the most important predictions that aerodynamicists need to make are directly complicated by the challenges of the fundamental unsteadiness of many relevant fluid flows.

One such example is known as laminar-turbulent transition. When a viscous flow in a free stream encounters a flat plate or airfoil, the flow will, at first, remain laminar. Viscosity has the effect of slowing the flow that is nearest the boundary, but nonlinear interactions between scales are both small and stable in the laminar case. This leaves a region in which the only significant effect of friction is decelerating the flow near the wall; the region where the flow is slowed down is called a laminar boundary layer. After traveling some distance along the surface, the boundary begins to exhibit some additional nonlinear effects. As these nonlinear effects appear, the transition region begins. In the transition region, initially small interactions between the viscous and inertial effects in the flow grow in an unstable fashion. Eventually, these interactions introduced by the boundary excite vortical flow features. As transition progresses to fully-developed turbulence, these interactions progress to a state of

chaotic, three-dimensional vortices. These are often referred to as "eddies", and the region of the boundary layer in which they occur is the turbulent boundary layer. This process, referred to as "laminar-turbulent transition", is a key point of study for aircraft design today. With some effort, this transition point can be experimentally observed, and predicting where it will be on a new airfoil or aerodynamic surface is quite hard. This fact has large consequences on aircraft design, for instance, because the stresses imparted by the fluid on the aerodynamic surface are different for laminar and turbulent boundary layers, and, thus, predicting the laminar-turbulent transition is crucial to making accurate estimates of drag.

Another example can be found in separation. When flow past an aerodynamic body experiences a strong adverse pressure gradient (e.g. in the case of an airfoil at high angle of attack), flow can separate from the body, leaving a strongly vortical wake region characterized by reversal of flow downstream of the separation point. In the design field, this is an important phenomena to predict. Flow separation often results in a sudden and substantial increase in drag and decrease in lift. For aircraft in particular, the realization of this phenomenon is known as "stall"; in fact, the unsteady flow reversal at stall onset is known to aviators as "stall buffeting". Stall, like transition, is hard to predict, and for this reason it is usually roughly estimated using theorerical insights and only later more accurately found using wind tunnel and flight testing.

These examples, though just a subset of the applications that exist, make it clear that prediction of time-dependent flows is a problem of crucial importance in the development of the next generation of aeronautical design tools.

1.3 Compressible Navier-Stokes equations

Many fluid flows are well modeled by the Navier-Stokes equations. Developed by Claude-Louis Navier and George Gabriel Stokes, these equations consider the conservation of mass, momentum, and energy of a fluid flow. The derivation of these equations can be found in the literature [1].

The resulting governing equations are as follows. The continuity equation, given by:

$$\frac{\partial \rho}{\partial t} + \frac{\partial}{\partial x_j}(\rho u_j) = 0 \tag{1.1}$$

where ρ is the density, and u_j is the velocity in the x_j direction. The momentum equations:

$$\frac{\partial}{\partial t}(\rho u_i) + \frac{\partial}{\partial x_j}(\rho u_i u_j) + \frac{\partial p}{\partial x_i} = \frac{\partial \tau_{ij}}{\partial x_j} \tag{1.2}$$

for $i \in \{1, 2, 3\}$, where p is the pressure and the stress tensor $\underline{\underline{\tau}}$ is given by:

$$\tau_{ij} = \mu\left(\frac{\partial u_i}{\partial x_j} + \frac{\partial u_j}{\partial x_i}\right) + \lambda \frac{\partial u_k}{\partial x_k}\delta_{ij} \tag{1.3}$$

where μ is the dynamic viscosity and λ is the bulk viscosity, which by the Stokes hypothesis is $\lambda = -\frac{2}{3}\mu$. Finally, the energy equation is given by:

$$\frac{\partial}{\partial t}(\rho E) + \frac{\partial}{\partial x_j}\left(\rho u_j\left(E + \frac{p}{\rho}\right)\right) = \frac{\partial}{\partial x_j}\left(u_i \tau_{ij} + \kappa_T \frac{\partial T}{\partial x_j}\right) \tag{1.4}$$

where E is the total energy of the system, T is the temperature, and κ_T is the thermal conductivity of the system. The temperature, pressure, and density are related by the ideal gas law:

$$p = \rho R T \tag{1.5}$$

An equivalent and useful form relates the pressure to the total energy and the velocities by:

$$p = (\gamma - 1)\left(\rho E - \frac{1}{2}\rho u_i u_i\right) \tag{1.6}$$

where, here, $\gamma \equiv c_p / c_V$ is the specific heat ratio.

1.4 Numerical solutions of the Navier-Stokes equations

With the Navier-Stokes equations defined, we now have a set of partial differential equations that will describe fluid flow. However, solving these equations is not a trivial endeavor. The Navier-Stokes equations are nonlinear, and they are known to have strong interactions between all scales of the flow; even the smallest scales will have a substantial effect on the largest scales (and vice-versa). For this reason, computational fluid dynamics remains an active research area, with active research in both solving the equations as-derived and using different modeling strategies.

1.4.1 Direct Numerical Simulation

The solution of the Navier-Stokes equations such that the entire range of both spatial and temporal scales is accurately represented is known as Direct Numerical Simulation (DNS). The smallest scales that must be resolved can be estimated by the Kolmogorov scales. The Kolmogorov length scale, η, refers to the length scale at which friction effects are dominated by molecular diffusion and the Kolmogorov time scale, τ_η, refers to the corresponding time scale. They are given by:

$$\eta = \left(\frac{\nu^3}{\varepsilon}\right)^{1/4} \tag{1.7}$$

and

$$\tau_\eta = \left(\frac{\nu}{\varepsilon}\right)^{\frac{1}{2}} \tag{1.8}$$

where $\nu = \mu/\rho$ is the kinematic viscosity and ε is the rate of dissipation of energy in the fluid.

At the same time, DNS must also capture the scale, L, of the largest eddies that will be present in the flow. Rogallo and Moin [24] show that in order to resolve the Kolmogorov scales spatially, the number of gridpoints would scale with Reynolds number by about $N^3 \sim Re^{9/4}$, and considering temporal requirements, the number of degrees of freedom would scale with Re^3, where Reynolds number is defined by $Re = \frac{\rho_0 V_0 L}{\mu}$, with ρ_0 and V_0, the reference density and reference velocity for the problem. This scaling proves far too costly to be practical for

high Reynolds number flows.

1.4.2 Reynolds Averaged Navier-Stokes

Since the time dependence and complex relationships between the small, unsteady scales and the larger scales create a substantial burden for the simulation of real viscous flows, fluid dynamicists have sought ways to reduce the resolution requirements for Navier-Stokes simulations. One such option is to use the RANS equations. RANS simulations use the Reynolds decomposition [21] to separate a flow into a time-averaged and fluctuating part.

We describe the Reynolds decomposition for an arbitrary choice of variable X:

$$X = \bar{X} + \tilde{X} \tag{1.9}$$

where $\bar{X}$ and $\tilde{X}$ represent the Reynolds-averaged part and fluctuating parts of X, respectively. For compressible flows, the concept of Favre averaging [8] is necessary to find the compressible RANS equations. The Favre average is given by:

$$\tilde{X} = \frac{\overline{\rho X}}{\bar{\rho}} \tag{1.10}$$

where ρ gives the density of a flow, $\tilde{X}$ represents the Favre average of a general quantity X, and $\overline{()}$ represents the Reynolds average of a quantity, as above.

Using these techniques, the compressible RANS equations can be found, which are solved to find the Reynolds-averaged state [29]. The most crucial implications of these simplifications are two. First, the time dependence of the averaged quantity goes effectively to zero. In other words, the turbulent fluctuations are completely unresolved. This, in turn, leads to the second implication, which is that the effects of turbulence need to be modeled to close the equations. These models include, prominently, the Spalart-Allmaras model [25], the k-ε model [16], and the k-ω model [29].

These choices have two results of immediate importance to the CFD engineer. They collapse the resolution requirement of RANS relative to DNS, to the point that simulations

using RANS are not only tractible but even industrially practical. On the other hand, even in the limit of infinite resolution, solutions to the RANS equations do not approach DNS solutions. In CFD parlance, they are not "scale-resolving". While they are a decent model for some engineering problems involving turbulent flows, there remains a necessity for modeling techniques that capture time-dependent flows in a scale-resolving way.

1.4.3 Large Eddy Simulation

With a perfectly resolved solution to the Navier-Stokes equations out of reach for high Reynolds number flows, we must find a way to generate approximations to a time-resolved Navier-Stokes system. Where the RANS method uses an a priori global averaging operation in time to reduce the computational cost necesary for a solution, Large Eddy Simulation (LES) uses a filtering operation in space and/or time to reduce cost. From a physical perspective, LES tries to capture the large eddies, which carry the majority of the energy of the flow, while modeling the smaller eddies [17]. This notion is underpinned by the idea that the small eddies of the flow are much more likely to be described by universal behavior which can be accurately captured by a model. The historical development of LES is described well in the literature [18, 20].

The formal description of LES is to take a variable of interest $f(\underline{x})$ and define its "large-scale" component $\overline{f}(\underline{x})$:

$$\overline{f}(\underline{x}) = \int_{\Omega} f(\underline{x}')G(\underline{x}, \underline{x}'; \overline{\Delta})\ \mathrm{d}\underline{x}' \tag{1.11}$$

In this section, we use the overline $\overline{()}$ to represent the large-scale component, and G is the filter kernel, which in the literature varies from Gaussian functions to top hat functions and others [20]. Using this transformation, the LES equations can be found, which introduce a small number of terms to capture the effect of the unresolved parts of the flow, which need to be modeled. Now, we use the same concept of Favre averaging, except applied to the filter. For an arbitrary choice of variable X, the so-called Favre-filtered [8] version is given

by:

$$\widetilde{X} = \frac{\overline{\rho X}}{\overline{\rho}} \tag{1.12}$$

This can be used to write a statement of the compressible LES equations [19]:

$$\frac{\partial \overline{\rho}}{\partial t} + \frac{\partial}{\partial x_j}\left(\overline{\rho}\tilde{u}_j\right) = 0 \tag{1.13}$$

$$\frac{\partial}{\partial t}\left(\overline{\rho}\tilde{u}_i\right) + \frac{\partial}{\partial x_j}\left(\overline{\rho}\tilde{u}_i\tilde{u}_j\right) + \frac{\partial \overline{p}}{\partial x_i} = -\frac{\partial \tilde{\tau}_{ij}}{\partial x_j} = -\frac{\partial \sigma_{ij}}{\partial x_j} \tag{1.14}$$

$$\begin{aligned}\frac{\partial}{\partial t}\left(\overline{\rho}\widetilde{E}\right) + \frac{\partial}{\partial x_j}\left(\overline{\rho}\tilde{u}_j\left(\tilde{E} + \frac{\overline{p}}{\overline{\rho}}\right)\right) - \frac{\partial}{\partial x_j}\left(\tilde{u}_j\tilde{\tau}_{ij} + \tilde{\kappa}_T\frac{\partial \tilde{T}}{\partial x_j}\right) \\ = -\frac{\partial}{\partial x_j}\left(\gamma c_V Q_j\right) - \frac{\partial}{\partial x_j}\left(\frac{1}{2}\mathcal{J}_j\right) + \frac{\partial \mathcal{D}_j}{\partial x_j}\end{aligned} \tag{1.15}$$

In these equations, it should be noted that $\tilde{\mu}$ and $\tilde{\kappa_T}$ are the viscosity and thermal conductivity associated to the filtered temperature $\tilde{T}$. It has been assumed in this formulation that:

$$\overline{\mu(T)\left(\frac{\partial u_i}{\partial x_j} + \frac{\partial u_j}{\partial x_i}\right)} \approx \mu(\tilde{T})\left(\frac{\partial \tilde{u}_i}{\partial x_j} + \frac{\partial \tilde{u}_j}{\partial x_i}\right)$$

We now see that the terms on the right hand side of (1.14) and (1.15), have to do with the effect of the subgrid scales. The terms on the left hand side all have counterparts in (1.2) and (1.4). The resolved scale terms can be well described by the filtered state variables, density $\bar{\rho}$, momentum $\bar{\rho}\tilde{u}_i$, and energy $\bar{\rho}\tilde{E}$. The subgrid terms have to be modeled. These terms represent, in turn, the subgrid scale stresses:

$$\sigma_{ij} = \bar{\rho}\left(\widetilde{u_i u_j} - \tilde{u}_i\tilde{u}_j\right) \tag{1.16}$$

the subgrid scale heat flux:

$$Q_j = \bar{\rho}\left(\widetilde{u_j T} - \tilde{u}_j\tilde{T}\right) \tag{1.17}$$

the subgrid scale turbulent diffusion, given by $\partial \mathcal{J}_j / \partial x_j$, where:

$$\mathcal{J}_j = \bar{\rho}\left(\widetilde{u_j u_k u_k} - \tilde{u}_j\widetilde{u_k u_k}\right) \tag{1.18}$$

and the subgrid scale viscous dissipation, given by $\partial \mathcal{D}_j / \partial x_j$, where:

$$\mathcal{D}_j = \overline{u_i \sigma_{ij}} - \tilde{u}_i \tilde{\tau}_{ij} \tag{1.19}$$

Various techniques for modeling the subgrid scales can be found in the literature [19, 10, 20].

1.5 Implicit and explicit LES methods

The issue of modeling subgrid scales is of significant interest to researchers. Some authors, however, claim that subgrid scale modeling is not necessary for optimal LES. This claim is based on the fact that for a discrete simulation of a Navier-Stokes flow, there will be "numerical dissipation", an artificial error induced by the finite numerical representation. In a simplified mathematical form, we seek to solve a conservation law for Navier-Stokes given by:

$$\frac{\partial \mathbf{u}}{\partial t} + \nabla \cdot \mathcal{F}_{\text{NS}} = 0 \tag{1.20}$$

We can not, however, solve this perfectly using numerics, and we effectively solve a discrete version:

$$\frac{\partial \mathbf{u}_h}{\partial t} + \nabla \cdot \mathcal{F}_{\text{NS}} + \nabla \cdot \mathcal{F}_{\text{discrete}} = 0 \tag{1.21}$$

When we solve DNS, we must solve (1.21) such that the effect of the discretization, $\mathcal{F}_{\text{discrete}}$, is very small relative to that of the physical flux, $\mathcal{F}_{\text{NS}}$.

When we run a large eddy simulation, we design $\mathcal{F}_{\text{SGS}}^{\text{model}}$ such that we solve, as nearly as possible:

$$\frac{\partial \widetilde{\mathbf{u}}}{\partial t} + \nabla \cdot \mathcal{F}_{\text{NS}} + \nabla \cdot \mathcal{F}_{\text{SGS}}^{\text{model}} = 0 \tag{1.22}$$

where $\widetilde{\mathbf{u}}$ is the approximation of the filtered state. However, some authors claim that using a stable scheme and neglecting the modeling term could result in an adequate model of real flow [2, 7, 22]. This technique of relying on the numerical dissipation inherent in the discretization is known as implicit LES (ILES). In these cases, (1.21) is solved, but, this time, the effect of the discretization, $\mathcal{F}_{\text{discrete}}$, will no longer be negligible compared to the

effect of the physical flux, $\mathcal{F}_{\text{NS}}$. On the other hand, we can refer to the classical approach as explicit LES, in which the subgrid scale effects are modeled through the inclusion of a subgrid scale model as in (1.22). For high-order discontinuous Galerkin discretizations in particular, it has been demonstrated that implicit methods might outperform explicit LES at predicting flow features of interest [9, 11], especially when comparing implicit and explicit LES methods at equal cost [26].

We can now tie these notions together. Comparing (1.22) with (1.21), we can see that, when $\mathcal{F}_{\text{discrete}}$ functionally replaces $\mathcal{F}_{\text{SGS}}^{\text{model}}$, the discretization can be interpreted as a model in ILES. Looking back to (1.13), (1.14), and (1.15), it can be seen that the subgrid scale terms in the LES governing equations will be the ones that are effectively modeled by the discrete stabilization of a scheme. A key insight for the future of modeling efforts for LES is to understand what physics are induced by the stabilization process of discretization. With this insight, we can delineate the cases for which explicit modeling is and is not necessary, and we can design models that are complementary to the stabilization induced by the discretization process.

1.6 Contributions

In this thesis, we attempt to investigate the subgrid scale modeling effect induced by one particular choice of discretization method, the discontinuous Galerking spacetime finite element method.

We begin by introducing the analytic entropy behavior of a Navier-Stokes flow. From here, we outline the method we will be using to solve the Navier-Stokes equations using the spacetime entropy variable formulation for DG, which represents one particular state-of-the-art high-order solver. We also select numerical flux functions that are commonly used in the literature, as a representative example. Next, we derive a method to compute exactly the entropy evolution equation for this DG scheme, including entropy contributions by the discretization choices. This method allows for quantifying exactly how each of the stabilization terms inherent to our discretization contribute to the entropy evolution for the

discretized system.

Finally, we perform a series of numerical experiments that leverage this method in order to show how entropy is generated at various levels of underresolution of the scheme. This study will provide some insight into what the physical effects of the DG discretization will be—- in the form of entropy production—- and how they vary with the order of polynomials as well as the number of elements used to represent the solution.

Chapter 2

Entropy behavior of the compressible Navier-Stokes equations

In this chapter, the thermodynamic entropy of a compressible flow is defined, and equations governing its behavior in analytical solutions to flow problems are derived for useful forms of the governing equations.

2.1 Thermodynamic entropy

Entropy is a measure of the disorder of a physical system. For fluid flows, the thermodynamic entropy is a measure of the irreversible processes that occur in the flow, either due to heating in the system or due to the viscous dissipation of momentum into heat. The nondimensional thermodynamic entropy per unit mass is given by s. The generation of entropy is governed by the Gibbs relation, which is given by:

$$\mathrm{d}h = c_V T \, \mathrm{d}s + \frac{1}{\rho} \, \mathrm{d}p \tag{2.1}$$

where the enthalpy h is defined by:

$$h = U + \frac{p}{\rho} \tag{2.2}$$

The internal energy and enthalpy are related to the temperature by

$$\begin{aligned} U &= c_V T \\ h &= c_p T \end{aligned} \tag{2.3}$$

with the specific heat at constant volume given by c_V and the specific heat at constant pressure given by c_p. For these relations, and throughout this work, we assume a calorically perfect gas. For an ideal gas, the specific heats are related by: $R = c_p - c_V$. The internal energy is also related to the total energy by:

$$\rho E = \rho U + \frac{1}{2}\rho u_i u_i \tag{2.4}$$

Using (2.1), (2.2), and (2.3), we can relate the entropy s to the state of the system by:

$$s = \ln\left(\frac{p}{\rho^\gamma}\right) \tag{2.5}$$

for a calorically perfect gas.

2.2 Second law of thermodynamics for Navier-Stokes flows

The process by which entropy is generated in and transported by a flow can be seen by multiplying (1.2) by u_i then subtracting it from (1.4) and substituting (2.4). This gives:

$$\rho\frac{\mathrm{D}U}{\mathrm{D}t} = \rho\frac{\partial U}{\partial t} + \rho u_j \frac{\partial}{\partial x_j}(U) = -p\frac{\partial u_j}{\partial x_j} + \frac{\partial}{\partial x_j}\left(\kappa_T \frac{\partial T}{\partial x_j}\right) + \tau_{ij}\frac{\partial u_i}{\partial x_j} \tag{2.6}$$

The Gibbs relation, (2.1), can be generalized to the substantial derivative:

$$\frac{\mathrm{D}h}{\mathrm{D}t} = c_V T\frac{\mathrm{D}s}{\mathrm{D}t} + \frac{1}{\rho}\frac{\mathrm{D}p}{\mathrm{D}t} \tag{2.7}$$

Now, (2.2), (2.6), and (2.7) are combined to find:

$$\frac{\mathrm{D}s}{\mathrm{D}t} = \rho\frac{\partial s}{\partial t} + \rho u_j \frac{\partial s}{\partial x_j} = \frac{1}{c_V T}\frac{\partial}{\partial x_j}\left(\kappa_T \frac{\partial T}{\partial x_j}\right) + \frac{1}{c_V T}\tau_{ij}\frac{\partial u_i}{\partial x_j} \tag{2.8}$$

Some rearrangement leaves:

$$\frac{\partial}{\partial t}(\rho s) + \frac{\partial}{\partial x_j}(\rho u_j s) - \frac{\partial}{\partial x_j}\left(\frac{\kappa_T}{c_V T}\frac{\partial T}{\partial x_j}\right) = \frac{\kappa_T}{c_V T^2}\left(\frac{\partial T}{\partial x_j}\right)^2 + \frac{1}{c_V T}\tau_{ij}\frac{\partial u_i}{\partial x_j} \tag{2.9}$$

This result allows us to describe the production and transport of entropy by a fluid flow. The first term, $\partial(\rho s)/\partial t$ gives the change in entropy per unit volume in time. The second term, $\partial(\rho u_j s)/\partial x_j$, gives change in entropy due to convection out of a control volume. The third term $\partial((\kappa_T\, \partial T/\partial x_j)/T)/\partial x_j$ describes the flux of entropy out of the control volume due to the reversible heat processes. On the right hand side, the first term, $\kappa_T(\partial T/\partial x_j)^2/T^2$ gives the production of entropy due to irreversible heating processes, and it is evidently nonnegative. Similarly the second term on the right-hand side, $\tau_{ij}(\partial u_i/\partial x_j)/T$, can be shown to be nonnegative. This term represents the production of entropy by the viscous dissipation of kinetic energy into heat.

In order to show that $\tau_{ij}(\partial u_i/\partial x_j)/T$ is positive, we expand it using the definition of τ_{ij} in (1.3) and setting λ according to Stokes theorem:

$$\begin{aligned}\frac{1}{c_V T}\tau_{ij}\frac{\partial u_i}{\partial x_j} &= \frac{1}{c_V T}\left(\mu\left(\frac{\partial u_i}{\partial x_j} + \frac{\partial u_j}{\partial x_i}\right) - \frac{2}{3}\mu\frac{\partial u_k}{\partial x_k}\delta_{ij}\right)\frac{\partial u_i}{\partial x_j} \\ &= \frac{\mu}{c_V T}\left(\frac{\partial u_i}{\partial x_j}\frac{\partial u_i}{\partial x_j} + \frac{\partial u_i}{\partial x_j}\frac{\partial u_j}{\partial x_i} - \frac{2}{3}\left(\frac{\partial u_k}{\partial x_k}\right)^2\right)\end{aligned} \tag{2.10}$$

Unwrapping this statment for $\{i,j\} \in \{1,2,3\}$ gives:

$$\begin{aligned}\frac{1}{T}\tau_{ij}\frac{\partial u_i}{\partial x_j} = \frac{\mu}{T}\Bigg(&\left(\frac{\partial u}{\partial x}\right)^2 + \left(\frac{\partial v}{\partial x}\right)^2 + \left(\frac{\partial w}{\partial x}\right)^2 + \left(\frac{\partial u}{\partial y}\right)^2 + \left(\frac{\partial v}{\partial y}\right)^2 + \left(\frac{\partial w}{\partial y}\right)^2 \\ &+ \left(\frac{\partial u}{\partial z}\right)^2 + \left(\frac{\partial v}{\partial z}\right)^2 + \left(\frac{\partial w}{\partial z}\right)^2 + \left(\frac{\partial u}{\partial x}\right)^2 + \left(\frac{\partial v}{\partial y}\right)^2 + \left(\frac{\partial w}{\partial z}\right)^2 \\ &+ 2\frac{\partial u}{\partial y}\frac{\partial v}{\partial x} + 2\frac{\partial u}{\partial z}\frac{\partial w}{\partial x} + 2\frac{\partial v}{\partial z}\frac{\partial w}{\partial y} - \frac{2}{3}\left(\frac{\partial u_k}{\partial x_k}\right)^2\Bigg) \\ = \frac{\mu}{T}\Bigg(&2\left(\left(\frac{\partial u}{\partial x}\right)^2 + \left(\frac{\partial v}{\partial y}\right)^2 + \left(\frac{\partial w}{\partial z}\right)^2\right) - \frac{2}{3}\left(\frac{\partial u_k}{\partial x_k}\right)^2 \\ &+ \left(\frac{\partial u}{\partial y} + \frac{\partial v}{\partial x}\right)^2 + \left(\frac{\partial u}{\partial z} + \frac{\partial w}{\partial x}\right)^2 + \left(\frac{\partial v}{\partial z} + \frac{\partial w}{\partial y}\right)^2\Bigg) \geq 0\end{aligned} \tag{2.11}$$

Next, it is integrated over some control volume $\mathbb{V}$:

$$\begin{aligned}\frac{\partial}{\partial t}\int_{\mathbb{V}} \rho s \ \mathrm{d}\mathbb{V} + \int_{\mathbb{V}} \frac{\partial}{\partial x_j}\left(\rho u_j s\right) \ \mathrm{d}\mathbb{V} - \int_{\mathbb{V}} \frac{\partial}{\partial x_j}\left(\frac{\kappa_T}{T}\frac{\partial T}{\partial x_j}\right) \ \mathrm{d}\mathbb{V} = \\ \int_{\mathbb{V}} \frac{\kappa_T}{T^2}\left(\frac{\partial T}{\partial x_j}\right)^2 \ \mathrm{d}\mathbb{V} + \int_{\mathbb{V}} \frac{\tau_{ij}}{T}\frac{\partial u_i}{\partial x_j} \ \mathrm{d}\mathbb{V} \geq 0\end{aligned} \tag{2.12}$$

By applying the divergence theorem, we find:

$$\begin{aligned}\frac{\partial}{\partial t}\int_{\mathbb{V}} \rho s \ \mathrm{d}\mathbb{V} + \int_{\mathbb{V}} \frac{\partial}{\partial x_j}\left(\rho u_j s\right) \ \mathrm{d}\mathbb{V} - \int_{\mathbb{V}} \frac{\partial}{\partial x_j}\left(\frac{\kappa_T}{T}\frac{\partial T}{\partial x_j}\right) \ \mathrm{d}\mathbb{V} = \\ \frac{\partial}{\partial t}\int_{\mathbb{V}} \rho s \ \mathrm{d}\mathbb{V} + \oint_{\partial\mathbb{V}} \rho u_j s n_j \ \mathrm{dS} - \oint_{\partial\mathbb{V}} \frac{\kappa_T}{T}\frac{\partial T}{\partial x_j} n_j \ \mathrm{dS}\end{aligned} \tag{2.13}$$

Assuming that there is no normal flow through or heat flux across $\partial\mathbb{V}$ results in:

$$\frac{\partial}{\partial t}\int_{\mathbb{V}} \rho s \ \mathrm{d}\mathbb{V} \geq 0 \tag{2.14}$$

At last, it can be seen that the total specific entropy for a Navier-Stokes system on a control volume with no flow or heat flux across its boundary will only increase.

This is the statement of the Clausius-Duhem inequality or the second law of thermodynamics for a viscous flow.

2.3 Entropy properties of the weighted residual forms of the Navier-Stokes equations

The Clausius-Duhem entropy inequality can be derived in an alternative approach by utilizing a weak form of the compressible Navier-Stokes equations. This approach also has a direct connection to the weak form used in finite element methods. In this section, we discuss this weak form derivation, so that we can apply it to the discontinuous Galerkin finite element method that we will use in our numerical simulations.

2.3.1 Conservative form

The Navier-Stokes equations can be written in a conservative form:

$$\frac{\partial \mathbf{u}}{\partial t} + \nabla \cdot \left(\underline{\mathbf{F}}^I - \underline{\mathbf{F}}^V \right) = 0 \tag{2.15}$$

where the state vector is given by:

$$\mathbf{u} = \begin{pmatrix} \rho \\ \rho \underline{V} \\ \rho E \end{pmatrix} = \begin{pmatrix} \rho \\ \rho u \\ \rho v \\ \rho w \\ \rho E \end{pmatrix} \tag{2.16}$$

with:

$$\underline{V} = \begin{pmatrix} u & v & w \end{pmatrix}^T \tag{2.17}$$

and the fluxes are defined:

$$\underline{\mathbf{F}}^I = \begin{bmatrix} \rho \underline{V}^T \\ \rho \underline{V}\underline{V}^T + p\underline{\underline{I}} \\ \rho \underline{V}^T (E + \frac{p}{\rho}) \end{bmatrix} = \begin{bmatrix} \rho u & \rho v & \rho w \\ \rho uu + p & \rho uv & \rho uw \\ \rho uv & \rho vv + p & \rho vw \\ \rho uw & \rho vw & \rho ww + p \\ \rho u \left(E + \frac{p}{\rho}\right) & \rho v \left(E + \frac{p}{\rho}\right) & \rho w \left(E + \frac{p}{\rho}\right) \end{bmatrix} \tag{2.18}$$

and

$$\underline{\mathbf{F}}^V = \begin{bmatrix} \underline{0}^T \\ \underline{\underline{\tau}} \\ \underline{V}^T \underline{\underline{\tau}} + \kappa_T \nabla T \end{bmatrix} = \begin{bmatrix} 0 & 0 & 0 \\ \tau_{11} & \tau_{12} & \tau_{13} \\ \tau_{21} & \tau_{22} & \tau_{23} \\ \tau_{31} & \tau_{32} & \tau_{33} \\ \underline{V} \cdot \underline{\tau}_1 + \kappa_T \frac{\partial T}{\partial x} & \underline{V} \cdot \underline{\tau}_2 + \kappa_T \frac{\partial T}{\partial y} & \underline{V} \cdot \underline{\tau}_3 + \kappa_T \frac{\partial T}{\partial z} \end{bmatrix} \tag{2.19}$$

It will be useful later to write the viscous flux as a function of the gradient of the state:

$$\underline{\mathbf{F}}^V = \overline{\underline{\mathbf{K}}} \, \nabla \mathbf{u} \tag{2.20}$$

where the diffusion tensor $\overline{\underline{\mathbf{K}}}$ is given by:

$$\left[\overline{\underline{\mathbf{K}}}_j\right]_{lm} = \begin{bmatrix} 0 \\ \mu(\delta_{1l}\delta_{jm} + \delta_{jl}\delta_{1m}) - \frac{2}{3}\mu(\delta_{kl}\delta_{km})\delta_{1j} \\ \mu(\delta_{2l}\delta_{jm} + \delta_{jl}\delta_{2m}) - \frac{2}{3}\mu(\delta_{kl}\delta_{km})\delta_{2j} \\ \mu(\delta_{3l}\delta_{jm} + \delta_{jl}\delta_{3m}) - \frac{2}{3}\mu(\delta_{kl}\delta_{km})\delta_{3j} \\ \mu v_i(\delta_{jl}\delta_{im} + \delta_{il}\delta_{jm}) - \frac{2}{3}\mu v_j(\delta_{kl}\delta_{km}) + \frac{\kappa_T}{R}\frac{p}{\rho^2}\delta_{jm}\delta_{l0} - \frac{\kappa_T}{R}\frac{1}{\rho}\delta_{jm}\delta_{l4} \end{bmatrix} \tag{2.21}$$

such that $\mathbf{F}_j^V = \overline{\underline{\mathbf{K}}}_j \, \nabla \mathbf{u}$.

2.3.2 Entropy variable formulation

In this section, an entropy variable form of the Navier-Stokes equations is discussed that closely follows previous work [14, 3]. Additional information about the entropy variable formulation can be found in Appendix B.

A set of symmetrizing entropy variables can be written,

$$\mathbf{v} = \begin{bmatrix} -\frac{s}{\gamma-1} + \frac{\gamma+1}{\gamma-1} - \frac{\rho E}{p} \\ \frac{\rho u}{p} \\ \frac{\rho v}{p} \\ \frac{\rho w}{p} \\ -\frac{\rho}{p} \end{bmatrix} \tag{2.22}$$

A nonlinear transformation exists from these entropy variables to the conservative variables: $\mathbf{u} = \mathbf{u}(\mathbf{v})$. Further details on this transformation can be found in Appendix B. Using the transformation a version of the conservative Navier-Stokes equations can be written as:

$$\overline{\mathbf{A}}_0 \frac{\partial \mathbf{v}}{\partial t} + \overline{\underline{\mathbf{A}}} \nabla \mathbf{v} - \nabla \cdot \left(\overline{\underline{\mathbf{K}}} \nabla \mathbf{v} \right) = 0 \tag{2.23}$$

where $\overline{\mathbf{A}}_0 = \frac{\partial \mathbf{u}}{\partial \mathbf{v}}$ is a symmetric positive definite system, $\overline{\underline{\mathbf{A}}} = \frac{\partial \underline{\mathbf{F}}^I}{\partial \mathbf{u}} \overline{\mathbf{A}}_0 = \frac{\partial \underline{\mathbf{F}}^I}{\partial \mathbf{v}}$ is symmetric, and $\overline{\underline{\mathbf{K}}} = \frac{\partial \underline{\mathbf{F}}^V}{\partial (\nabla \mathbf{u})} \overline{\mathbf{A}}_0 = \frac{\partial \underline{\mathbf{F}}^V}{\partial (\nabla \mathbf{v})}$ is a symmetric positive semi-definite system [3, 3, 14].

2.3.3 Weighted residual form

The weighted residual form can be found by specifying a domain of interest, Ω. Because we desire to use a spacetime formulation as well, we must also specify a time domain I, on which a solution is sought:

$$I \in [t_0, t] \tag{2.24}$$

The conservation equations are weighted with a function $\mathbf{w}$ from some appropriately smooth space $\mathcal{V} : \Omega \times I \rightarrow \mathcal{R}^m$ and the result is integrated to give the weighted residual

form:

$$\int_I \int_\Omega \mathbf{w}^T \frac{\partial \mathbf{u}}{\partial t} \; \mathrm{d}\mathbb{V} \; \mathrm{d}t + \int_I \int_\Omega \mathbf{w}^T \left(\nabla \cdot \left(\underline{\mathbf{F}}^I - \underline{\mathbf{F}}^V \right) \right) \; \mathrm{d}\mathbb{V} \; \mathrm{d}t = 0 \tag{2.25}$$

Now, testing using the entropy variables as has been done in the literature [3, 14], such that $\mathbf{w} = \mathbf{v}$, gives:

$$\int_I \int_\Omega \mathbf{v}^T \frac{\partial \mathbf{u}}{\partial t} \; \mathrm{d}\mathbb{V} \; \mathrm{d}t + \int_I \int_\Omega \mathbf{v}^T \left(\nabla \cdot \underline{\mathbf{F}}^I \right) \; \mathrm{d}\mathbb{V} \; \mathrm{d}t - \int_I \int_\Omega \mathbf{v}^T \left(\nabla \cdot \underline{\mathbf{F}}^V \right) \; \mathrm{d}\mathbb{V} \; \mathrm{d}t = 0 \tag{2.26}$$

The terms in (2.26) can be translated into the Clausius-Duhem inequality. The derivation of these relations can be found in Appendix B. First, the temporal term of Clausius-Duhem inequality, the variation of entropy:

$$\mathbf{v}^T \frac{\partial \mathbf{u}}{\partial t} = -\frac{1}{\gamma - 1} \frac{\partial}{\partial t} \left[\rho s \right] \tag{2.27}$$

Next, the inviscid entropy flux term can be found:

$$\mathbf{v}^T (\nabla \cdot \underline{\mathbf{F}}^I) = -\frac{1}{\gamma - 1} \left(\nabla \cdot (\rho s \underline{V}) \right) \tag{2.28}$$

The viscous interior flux term is divided into into a viscous shearing contribution and a heating contribution, respectively:

$$\mathbf{v}^T (\nabla \cdot \underline{\mathbf{F}}^V) = \mathbf{v}^T (\nabla \cdot \underline{\mathbf{F}}^{V^*}) - \mathbf{v}^T (\nabla \cdot \underline{\mathbf{F}}^{H^*}) \tag{2.29}$$

The heat flux component of the viscous term is given by:

$$\mathbf{v}^T (\nabla \cdot \underline{\mathbf{F}}^{H^*}) = \frac{1}{R} \nabla \cdot \left(\frac{\kappa_T \nabla T}{T} \right) + \frac{1}{R} \kappa_T \left(\frac{\nabla T \cdot \nabla T}{T^2} \right) \tag{2.30}$$

The viscous shearing contribution can be written:

$$\mathbf{v}^T(\nabla \cdot \underline{\mathbf{F}}^{V^*}) = -\frac{\rho}{p}\left[2\mu\left(\left(\frac{\partial u}{\partial x}\right)^2 + \left(\frac{\partial v}{\partial w}\right)^2 + \left(\frac{\partial w}{\partial z}\right)^2\right) - \frac{2}{3}\mu\left(\frac{\partial u_k}{\partial x_k}\right)^2 + \mu\left(\frac{\partial u}{\partial y} + \frac{\partial v}{\partial x}\right)^2 + \mu\left(\frac{\partial u}{\partial z} + \frac{\partial w}{\partial x}\right)^2 + \mu\left(\frac{\partial u}{\partial z} + \frac{\partial w}{\partial x}\right)^2\right] \tag{2.31}$$

This gives, finally,

$$\mathbf{v}^T(\nabla \cdot \underline{\mathbf{F}}^{V}) = -\frac{1}{R}\nabla \cdot \left(\frac{\kappa_T \nabla T}{T}\right) - \frac{1}{R}\kappa_T\left(\frac{\nabla T \cdot \nabla T}{T^2}\right) - \frac{\rho}{p}\left[2\mu\left(\left(\frac{\partial u}{\partial x}\right)^2 + \left(\frac{\partial v}{\partial w}\right)^2 + \left(\frac{\partial w}{\partial z}\right)^2\right) - \frac{2}{3}\mu\left(\frac{\partial u_k}{\partial x_k}\right)^2 + \mu\left(\frac{\partial u}{\partial y} + \frac{\partial v}{\partial x}\right)^2 + \mu\left(\frac{\partial u}{\partial z} + \frac{\partial w}{\partial x}\right)^2 + \mu\left(\frac{\partial u}{\partial z} + \frac{\partial w}{\partial x}\right)^2\right] \tag{2.32}$$

It is easy to see that $\frac{1}{R}\kappa_T\left(\frac{\nabla T \cdot \nabla T}{T^2}\right)$ is always nonnegative, and that $\mathbf{v}^T(\nabla \cdot \underline{\mathbf{F}}^{V^*})$ is always negative or zero. Plugging these into (2.26), results in a statement of the Clausius-Duhem inequality for the analytical weak form:

$$\int_I \int_\Omega \frac{\partial}{\partial t}(\rho s)\ \ \mathrm{d}\mathbb{V}\ \mathrm{d}t + \int_I \int_\Omega (\nabla \cdot (\rho s \underline{V}))\ \ \mathrm{d}\mathbb{V}\ \mathrm{d}t - \int_I \int_\Omega \frac{(\gamma-1)}{R}\nabla \cdot \left(\frac{\kappa_T \nabla T}{T}\right)\ \ \mathrm{d}\mathbb{V}\ \mathrm{d}t = -(\gamma-1)\int_I \int_\Omega \mathbf{v}^T(\nabla \cdot \underline{\mathbf{F}}^{V*}) + \int_I \int_\Omega \frac{(\gamma-1)}{R}\kappa_T\left(\frac{\nabla T \cdot \nabla T}{T^2}\right)\ \ \mathrm{d}\mathbb{V}\ \mathrm{d}t \geq 0 \tag{2.33}$$

By rearranging and applying the divergence theorem, it can be stated equivalently:

$$\frac{\mathrm{d}}{\mathrm{d}t}\int_I \int_\Omega \rho s\ \ \mathrm{d}\mathbb{V}\ \mathrm{d}t + \int_I \int_{\partial\Omega} (\rho s \underline{V}) \cdot \underline{n}\ \ \mathrm{dS}\ \mathrm{d}t - \int_I \int_{\partial\Omega} \frac{(\gamma-1)}{R}\frac{\kappa_T \nabla T \cdot \underline{n}}{T}\ \ \mathrm{dS}\ \mathrm{d}t = -(\gamma-1)\int_I \int_\Omega \mathbf{v}^T(\nabla \cdot \underline{\mathbf{F}}^{V*}) + \int_I \int_\Omega \frac{(\gamma-1)}{R}\kappa_T\left(\frac{\nabla T \cdot \nabla T}{T^2}\right)\ \ \mathrm{d}\mathbb{V}\ \mathrm{d}t \geq 0 \tag{2.34}$$

Again, for problems where there is no normal velocity through and no heat flux across the boundary $\partial\Omega$, we can see the same result is generated here, that total specific entropy is only produced on the domain:

$$\frac{\mathrm{d}}{\mathrm{d}t}\int_I\int_\Omega \rho s \;\; \mathrm{d}\mathbb{V}\,\mathrm{d}t \geq 0 \tag{2.35}$$

or equivalently:

$$\int_\Omega \rho(t)s(t) \;\; \mathrm{d}\mathbb{V} - \int_\Omega \rho(t_0)s(t_0) \;\; \mathrm{d}\mathbb{V} \geq 0 \tag{2.36}$$

This result, (2.33) in particular, gives us a useful statement of the Clausius-Duhem statment for the forthcoming discretization. While promising, it still does not provide insight into the effect of discretization on the entropy budget. The next chapter will dive into uncovering this effect.

Chapter 3

Entropy behavior of the discontinuous Galerkin discretization of the compressible Navier-Stokes equations

For the discontinuous Galerkin discretization it should be possible to make a similar statement about the entropy satisfaction of the DG solution. This new statement will account for the entropy production induced by the stabilization inherent to the scheme as well as the resolved physical entropy behaviors.

3.1 Discontinuous Galerkin discretization of the Navier-Stokes equations

In order to approximate the solution to a Navier-Stokes problem numerically, we discretize the domain as a set of non-overlapping elements:

$$\Omega = \{\kappa_i\} \quad \forall i \tag{3.1}$$

$$\kappa_i \cap \kappa_j = \varnothing \quad i \neq j$$

The space $\mathcal{V}$ is then approximated by the space of polynomials of order d_x in space and d_t in time:

$$\mathcal{V}_h = \left\{ \mathbf{w} \,\middle|\, \mathbf{w} \in \left[\mathcal{P}^{(d_x,d_t)}(\kappa \times I) \right]^m, \ \forall \kappa \in \Omega \right\} \tag{3.2}$$

where $\mathcal{P}^{(d_x,d_t)}(\kappa \times I)$ is the space of polynomials that span the element κ in space with order d_x and the timeslab I in time with order d_t. This space is selected such that the approximate solution is a function of the entropy variables: $\mathbf{u}_h = \mathbf{u}(\mathbf{v}_h)$, with $\mathbf{v}_h \in \mathcal{V}_h$. The definition of the timeslab I is modified to be a finite subdivision of the temporal domain:

$$I \in \left[t^n, t^{n+1} \right] \tag{3.3}$$

For this work, the partitioning of the domain will be structured in both space and time, such that any temporal spacetime element faces have normal vectors that coincide always to the time direction, and generally spacetime element faces should have normal vectors to either time or one of the spatial coordinate directions.

When solved numerically, the weighted residual form of the equations are not satisfied exactly. In fact, (2.25) is effectively solved on each element κ, and the flux contributions for the element boundaries $\partial\kappa$ come from integrating by parts this weighted residual form. On each boundary face, however, description of the fluxes is ambiguous. This results from the fact that the elements are not required to be continuous and the values of the fluxes can therefore differ on either side of a face f. This necessitates a numerical flux function on element boundaries in both space and time. For this case, the second method of Bassi and Rebay (BR2) [4] is used to compute the viscous numerical flux functions, and the Roe flux formulation of Ismail [15, 23] is used for the inviscid fluxes, and full upwinding is used in time.

These choices result in the following DG weak form:

$$
\begin{aligned}
&-\sum_{\kappa}\int_{I}\int_{\kappa}\frac{\partial \mathbf{w}}{\partial t}^{T}\mathbf{u}_h \;\mathrm{d}\mathbb{V}\,\mathrm{d}t+\sum_{\kappa}\int_{\kappa}\left(\mathbf{w}(t_{-}^{n+1})^{T}\mathbf{u}_h(t_{-}^{n+1})-\mathbf{w}(t_{+}^{n})^{T}\mathbf{u}_h(t_{-}^{n})\right)\;\mathrm{d}\mathbb{V}\\
&\quad-\sum_{\kappa}\int_{I}\int_{\kappa}\nabla\mathbf{w}^{T}\cdot\underline{\mathbf{F}}^{I}\;\mathrm{d}\mathbb{V}\,\mathrm{d}t+\sum_{\kappa}\int_{I}\int_{\kappa}\nabla\mathbf{w}^{T}\cdot\underline{\mathbf{F}}^{V}\;\mathrm{d}\mathbb{V}\,\mathrm{d}t\\
&\quad+\sum_{f\in\Gamma_i}\int_{I}\int_{f}\left(\left(\mathbf{w}^{T}\widehat{\underline{\mathbf{F}}^{I}\cdot\underline{n}}\right)^{+}+\left(\mathbf{w}^{T}\widehat{\underline{\mathbf{F}}^{I}\cdot\underline{n}}\right)^{-}\right)\;\mathrm{dS}\,\mathrm{d}t\\
&\quad-\sum_{f\in\Gamma_i}\int_{I}\int_{f}\left\{\left(\underline{\underline{\mathbf{K}}}(\mathbf{u}_h)\right)^{T}(\nabla\mathbf{w})\right\}\cdot[[\mathbf{u}_h]]\;\mathrm{dS}\,\mathrm{d}t\\
&\quad-\sum_{f\in\Gamma_i}\int_{I}\int_{f}[[\mathbf{w}]]\cdot\left\{\underline{\underline{\mathbf{K}}}(\mathbf{u}_h)\left(\nabla\mathbf{u}_h+\eta_f\underline{r}_f([[\mathbf{u}_h]])\right)\right\}\;\mathrm{dS}\,\mathrm{d}t=0
\end{aligned}
\tag{3.4}
$$

for all $\mathbf{w}\in\mathcal{V}_h$. Here, the lifting operator $\underline{r}_f:[\mathcal{V}_h(f)]^d\mapsto[\mathcal{V}_h]^d$ associated with a face f is given by:

$$
\sum_{\kappa\in\kappa_f}\int_{\kappa}\nabla\boldsymbol{\phi}\cdot^{T}\underline{r}_f(\boldsymbol{\psi})\;\;\mathrm{d}\mathbb{V}=-\int_{f}\{\boldsymbol{\phi}\cdot\underline{n}\}^{T}\boldsymbol{\psi}\;\;\mathrm{dS}\;\;\forall\,\boldsymbol{\phi}\in[\mathcal{V}_h]^d \tag{3.5}
$$

and κ_f is defined as the set of all elements sharing a face f. A jump operator is also introduced here. On a face f, the jump operator applied to an arbitrary quantity X is given by:

$$
[[X]]=(X)^{+}\underline{n}^{+}+(X)^{-}\underline{n}^{-} \tag{3.6}
$$

Here, the value of X^{+} is the value of X as defined on one side of the face, and X^{-} is the value of X as defined on the opposite side of the face, and $\underline{n}^{\pm}$ are the corresponding normal vectors pointing out of the element from which comes the definition of $X^{\pm}$.

Lastly, an averaging operator is introduced for brevity. The averaging operator of an arbitrary quantity X across a face f is given by:

$$
\{X\}=\frac{1}{2}\left((X)^{+}+(X)^{-}\right) \tag{3.7}
$$

This is the form of the equations that are solved natively in the **eddy** solver developed by the NASA Advanced Supercomputing division [5], which is used to perform the simulations

mentioned in this thesis. Further details of the temporal, inviscid, and viscous numerical flux functions can be found in Appendix A.

3.2 Manipulation of the weak form solution

In order to investigate the entropy behavior of the DG discretization, terms analogous to (2.33) are necessary. In order to get them, we can leverage the divergence theorem applied to the temporal fluxes:

$$\int_I \int_\kappa \frac{\partial \mathbf{w}}{\partial t}^T \mathbf{u}_h \ \mathrm{d}\mathbb{V}\ \mathrm{d}t = -\int_I \int_\kappa \mathbf{w}^T \frac{\partial \mathbf{u}_h}{\partial t} \ \mathrm{d}\mathbb{V}\ \mathrm{d}t + \int_\kappa \left(\mathbf{w}^T \mathbf{u}_h\right)\Big|_{t_+^n}^{t_-^{n+1}} \ \mathrm{d}\mathbb{V} \tag{3.8}$$

and to the inviscid fluxes:

$$\int_I \int_\kappa \nabla \mathbf{w}^T \cdot \underline{\mathbf{F}}^I \ \mathrm{d}\mathbb{V}\ \mathrm{d}t = \int_I \oint_{\partial\kappa} \mathbf{w}^T \left(\underline{\mathbf{F}}^I \cdot \underline{n}\right) \ \mathrm{dS}\ \mathrm{d}t - \int_I \int_\kappa \mathbf{w}^T \left(\nabla \cdot \underline{\mathbf{F}}^I\right) \ \mathrm{d}\mathbb{V}\ \mathrm{d}t \tag{3.9}$$

and finally to the viscous fluxes:

$$\int_I \int_\kappa \nabla \mathbf{w}^T \cdot \underline{\mathbf{F}}^V \ \mathrm{d}\mathbb{V}\ \mathrm{d}t = \int_I \oint_{\partial\kappa} \mathbf{w}^T \left(\underline{\mathbf{F}}^V \cdot \underline{n}\right) \ \mathrm{dS}\ \mathrm{d}t - \int_I \int_\kappa \mathbf{w}^T \left(\nabla \cdot \underline{\mathbf{F}}^V\right) \ \mathrm{d}\mathbb{V}\ \mathrm{d}t \tag{3.10}$$

Practically speaking, this equation will be solved numerically, so there will exist a residual due to quadrature error. A residual statement can be written for the temporal quadrature errors:

$$E_\kappa^{t,\mathrm{quad}} = -\int_I \int_\kappa \frac{\partial \mathbf{w}}{\partial t}^T \mathbf{u}_h \ \mathrm{d}\mathbb{V}\ \mathrm{d}t - \int_I \int_\kappa \mathbf{w}^T \frac{\partial \mathbf{u}_h}{\partial t} \ \mathrm{d}\mathbb{V}\ \mathrm{d}t + \int_\kappa \left(\mathbf{w}^T \mathbf{u}_h\right)\Big|_{t_+^n}^{t_-^{n+1}} \ \mathrm{d}\mathbb{V} \tag{3.8a}$$

for the inviscid quadrature errors:

$$\begin{aligned} E_\kappa^{I,\mathrm{quad}} = &-\int_I \int_\kappa \nabla \mathbf{w}^T \cdot \underline{\mathbf{F}}^I \ \mathrm{d}\mathbb{V}\ \mathrm{d}t + \int_I \oint_{\partial\kappa} \mathbf{w}^T \left(\underline{\mathbf{F}}^I \cdot \underline{n}\right) \ \mathrm{dS}\ \mathrm{d}t \\ &- \int_I \int_\kappa \mathbf{w}^T \left(\nabla \cdot \underline{\mathbf{F}}^I\right) \ \mathrm{d}\mathbb{V}\ \mathrm{d}t \end{aligned} \tag{3.9a}$$

and for the viscous quadrature errors:

$$E_\kappa^{V,\text{quad}} = -\int_I \int_\kappa \nabla \mathbf{w}^T \cdot \underline{\mathbf{F}}^V \ \mathrm{d}\mathbb{V}\ \mathrm{d}t + \int_I \oint_{\partial\kappa} \mathbf{w}^T \left(\underline{\mathbf{F}}^V \cdot \underline{n}\right) \ \mathrm{dS}\ \mathrm{d}t - \int_I \int_\kappa \mathbf{w}^T \left(\nabla \cdot \underline{\mathbf{F}}^V\right) \ \mathrm{d}\mathbb{V}\ \mathrm{d}t \tag{3.10a}$$

Summing these over the entire domain, we now write:

$$E^{t,\text{quad}} = -\sum_\kappa \int_I \int_\kappa \frac{\partial \mathbf{w}^T}{\partial t} \mathbf{u}_h \ \mathrm{d}\mathbb{V}\ \mathrm{d}t - \sum_\kappa \int_I \int_\kappa \mathbf{w}^T \frac{\partial \mathbf{u}_h}{\partial t} \ \mathrm{d}\mathbb{V}\ \mathrm{d}t + \sum_\kappa \int_\kappa \left(\mathbf{w}(t_-^{n+1})^T \mathbf{u}_h(t_-^{n+1}) - \mathbf{w}(t_+^n)^T \mathbf{u}_h(t_+^n)\right) \ \mathrm{d}\mathbb{V} \tag{3.11}$$

$$E^{I,\text{quad}} = -\sum_\kappa \int_I \int_\kappa \nabla \mathbf{w}^T \cdot \underline{\mathbf{F}}^I \ \mathrm{d}\mathbb{V}\ \mathrm{d}t - \sum_\kappa \int_I \int_\kappa \mathbf{w}^T \left(\nabla \cdot \underline{\mathbf{F}}^I\right) \ \mathrm{d}\mathbb{V}\ \mathrm{d}t + \sum_{f \in \Gamma_i} \int_I \int_f \left(\left(\mathbf{w}^T \left(\underline{\mathbf{F}}^I \cdot \underline{n}\right)\right)^+ + \left(\mathbf{w}^T \left(\underline{\mathbf{F}}^I \cdot \underline{n}\right)\right)^-\right) \ \mathrm{dS}\ \mathrm{d}t \tag{3.12}$$

and

$$E^{V,\text{quad}} = -\sum_\kappa \int_I \int_\kappa \nabla \mathbf{w}^T \cdot \underline{\mathbf{F}}^V \ \mathrm{d}\mathbb{V}\ \mathrm{d}t - \sum_\kappa \int_I \int_\kappa \mathbf{w}^T \left(\nabla \cdot \underline{\mathbf{F}}^V\right) \ \mathrm{d}\mathbb{V}\ \mathrm{d}t + \sum_{f \in \Gamma_i} \int_I \int_f \left(\left(\mathbf{w}^T \left(\underline{\mathbf{F}}^V \cdot \underline{n}\right)\right)^+ + \left(\mathbf{w}^T \left(\underline{\mathbf{F}}^V \cdot \underline{n}\right)\right)^-\right) \ \mathrm{dS}\ \mathrm{d}t \tag{3.13}$$

Combining (3.11), (3.12), and (3.13) with (3.4) gives:

$$\begin{aligned}
&\sum_{\kappa}\int_I\int_\kappa \mathbf{w}^T\frac{\partial \mathbf{u}_h}{\partial t}\ \mathrm{d}\mathbb{V}\ \mathrm{d}t - \sum_{\kappa}\int_\kappa \mathbf{w}(t_+^n)^T\left(\mathbf{u}_h(t_-^n)-\mathbf{u}_h(t_+^n)\right)\ \mathrm{d}\mathbb{V}\\
&\quad+\sum_{\kappa}\int_I\int_\kappa \mathbf{w}^T\left(\nabla\cdot\underline{\mathbf{F}}^I\right)\ \mathrm{d}\mathbb{V}\ \mathrm{d}t - \sum_{\kappa}\int_I\int_\kappa \mathbf{w}^T\left(\nabla\cdot\underline{\mathbf{F}}^V\right)\ \mathrm{d}\mathbb{V}\ \mathrm{d}t\\
&+\sum_{f\in\Gamma_i}\int_I\int_f\left(\left(\mathbf{w}^T\left(\widehat{\underline{\mathbf{F}}^I\cdot\underline{n}}-\underline{\mathbf{F}}^I\cdot\underline{n}\right)\right)^+ + \left(\mathbf{w}^T\left(\widehat{\underline{\mathbf{F}}^I\cdot\underline{n}}-\underline{\mathbf{F}}^I\cdot\underline{n}\right)\right)^-\right)\ \mathrm{dS}\ \mathrm{d}t\\
&\quad-\sum_{f\in\Gamma_i}\int_I\int_f\left\{\overline{\underline{\mathbf{K}}}\left((\mathbf{u}_h)\right)^T(\nabla\mathbf{w})\right\}\cdot[[\mathbf{u}_h]]\ \mathrm{dS}\ \mathrm{d}t\\
&\quad-\sum_{f\in\Gamma_i}\int_I\int_f[[\mathbf{w}]]\cdot\left\{\overline{\underline{\mathbf{K}}}(\mathbf{u}_h)\left(\nabla\mathbf{u}_h+\eta_f\underline{r}_f([[\mathbf{u}_h]])\right)\right\}\ \mathrm{dS}\ \mathrm{d}t\\
&\quad+\sum_{f\in\Gamma_i}\int_I\int_f\left[\left(\mathbf{w}^T\left(\underline{\mathbf{F}}^V\cdot\underline{n}\right)\right)^+ + \left(\mathbf{w}^T\left(\underline{\mathbf{F}}^V\cdot\underline{n}\right)\right)^-\right]\ \mathrm{dS}\ \mathrm{d}t + E^{\mathrm{quad}} = 0
\end{aligned} \tag{3.14}$$

We note that the quadrature errors, $E^{t,\mathrm{quad}}$, $E^{I,\mathrm{quad}}$, and $E^{V,\mathrm{quad}}$ are zero when integrating exactly, and we define their sum $E^{\mathrm{quad}} = E^{t,\mathrm{quad}} + E^{I,\mathrm{quad}} - E^{V,\mathrm{quad}}$ for brevity. This error is not a residual error term in the solution of the equations themselves, rather, they are an error introduced in transforming the data into a more useful form using the divergence theorem under quadrature. A small E^{quad}, then, indicates that this analysis is not tainted by quadrature errors.

Now we can see that this form of the governing equation gives us a new outlook on the entropy behavior of the system. There will be a contribution in both space and time from the "jump terms" which exist because of discontinuities at the spacetime element boundaries. These contributions can be interpreted as the implicit subgrid scale model induced by this DG discretization.

3.3 Entropy conservation and the second law of thermodynamics

As seen in Section 2.3.3, testing using the entropy variables, such that $\mathbf{w} = \mathbf{v}$, results in a statement that gives the Clausius-Duhem inequality or the second law of theromodynamics. We can use our expanded form in (3.14) to investigate the artificial generation of entropy due to the underresolution of the scheme:

$$\begin{aligned}
&\sum_{\kappa}\int_I\int_\kappa \mathbf{v}_h^T\frac{\partial \mathbf{u}_h}{\partial t}\ \mathrm{d}\mathbb{V}\ \mathrm{d}t - \sum_{\kappa}\int_\kappa \mathbf{v}_h(t_+^n)^T\left(\mathbf{u}_h(t_-^n)-\mathbf{u}_h(t_+^n)\right)\ \mathrm{d}\mathbb{V}\\
&\qquad+\sum_{\kappa}\int_I\int_\kappa \mathbf{v}_h^T\left(\nabla\cdot\underline{\mathbf{F}}^I\right)\ \mathrm{d}\mathbb{V}\ \mathrm{d}t - \sum_{\kappa}\int_I\int_\kappa \mathbf{v}_h^T\left(\nabla\cdot\underline{\mathbf{F}}^V\right)\ \mathrm{d}\mathbb{V}\ \mathrm{d}t\\
&\quad+\sum_{f\in\Gamma_i}\int_I\int_f\left(\left(\mathbf{v}_h^T\left(\widehat{\underline{\mathbf{F}}^I\cdot\underline{n}}-\underline{\mathbf{F}}^I\cdot\underline{n}\right)\right)^+ + \left(\mathbf{v}_h^T\left(\widehat{\underline{\mathbf{F}}^I\cdot\underline{n}}-\underline{\mathbf{F}}^I\cdot\underline{n}\right)\right)^-\right)\ \mathrm{dS}\ \mathrm{d}t\\
&-\sum_{f\in\Gamma_i}\int_I\int_f\frac{1}{2}\left(\left(\overline{\underline{\underline{\mathbf{K}}}}(\mathbf{u}_h^+)\right)^T(\nabla\mathbf{v}_h)^+ + \left(\overline{\underline{\underline{\mathbf{K}}}}(\mathbf{u}_h^-)\right)^T(\nabla\mathbf{v}_h)^-\right)\cdot\left(\mathbf{u}_h^+\underline{n}^+ + \mathbf{u}_h^-\underline{n}^-\right)\ \mathrm{dS}\ \mathrm{d}t \qquad (3.15)\\
&\qquad-\sum_{f\in\Gamma_i}\int_I\int_f\left\{\overline{\underline{\underline{\mathbf{K}}}}\left((\mathbf{u}_h)\right)^T(\nabla\mathbf{v}_h)\right\}\cdot[[\mathbf{u}_h]]\ \mathrm{dS}\ \mathrm{d}t\\
&\quad-\sum_{f\in\Gamma_i}\int_I\int_f[[\mathbf{v}_h]]\cdot\left\{\overline{\underline{\underline{\mathbf{K}}}}(\mathbf{u}_h)\left(\nabla\mathbf{u}_h+\eta_f\underline{r}_f([[\mathbf{u}_h]])\right)\right\}\ \mathrm{dS}\ \mathrm{d}t\\
&\quad+\sum_{f\in\Gamma_i}\int_I\int_f\left[\left(\mathbf{v}_h^T\left(\underline{\mathbf{F}}^V\cdot\underline{n}\right)\right)^+ + \left(\mathbf{v}_h^T\left(\underline{\mathbf{F}}^V\cdot\underline{n}\right)\right)^-\right]\ \mathrm{dS}\ \mathrm{d}t + E^{\text{quad}} = 0
\end{aligned}$$

A number of the terms in (B.11) can be translated into simple expressions of the entropy transport terms in the Clausius-Duhem inequality, as we have seen already in Equations (2.27), (2.28), and (2.32). Taking these relations and substituting them into (B.11) gives a new statement of the Clausius-Duhem inequality that includes the terms from the

discretization. These terms constitute artificial sources of entropy production or destruction:

$$
\begin{aligned}
&\sum_{\kappa}\int_I\int_\kappa \frac{\partial}{\partial t}\left[\rho s\right]\ \mathrm{d}\mathbb{V}\ \mathrm{d}t + \sum_{\kappa}\int_I\int_\kappa \nabla\cdot\left[\rho s\underline{V}\right]\ \mathrm{d}\mathbb{V}\ \mathrm{d}t \\
&\qquad - \sum_{\kappa}\int_I\int_\kappa \frac{(\gamma-1)}{R}\nabla\cdot\left(\frac{\kappa_T\nabla T}{T}\right)\ \mathrm{d}\mathbb{V}\ \mathrm{d}t \\
&\qquad + (\gamma-1)\sum_{\kappa}\int_\kappa \mathbf{v}_h(t_+^n)^T\left(\mathbf{u}_h(t_-^n)-\mathbf{u}_h(t_+^n)\right)\ \mathrm{d}\mathbb{V} \\
&-(\gamma-1)\sum_{f\in\Gamma_i}\int_I\int_f\left(\left(\mathbf{v}_h^T\left(\widehat{\underline{\mathbf{F}}^I\cdot\underline{n}}-\underline{\mathbf{F}}^I\cdot\underline{n}\right)\right)^+ + \left(\mathbf{v}_h^T\left(\widehat{\underline{\mathbf{F}}^I\cdot\underline{n}}-\underline{\mathbf{F}}^I\cdot\underline{n}\right)\right)^-\right)\ \mathrm{d}\mathrm{S}\ \mathrm{d}t \\
&\qquad + (\gamma-1)\sum_{f\in\Gamma_i}\int_I\int_f\left\{\left(\underline{\underline{\mathbf{K}}}(\mathbf{u}_h)\right)^T\left(\nabla\mathbf{v}_h\right)\right\}\cdot\left[\left[\mathbf{u}_h\right]\right]\ \mathrm{d}\mathrm{S}\ \mathrm{d}t \\
&\qquad -(\gamma-1)\sum_{f\in\Gamma_i}\int_I\int_f\left[\left[\mathbf{v}_h\right]\right]\cdot\left\{\underline{\underline{\mathbf{K}}}(\mathbf{u}_h)\left(\nabla\mathbf{u}_h+\eta_f\underline{r}_f\left(\left[\left[\mathbf{u}_h\right]\right]\right)\right)\right\}\ \mathrm{d}\mathrm{S}\ \mathrm{d}t \\
&\qquad -(\gamma-1)\sum_{f\in\Gamma_i}\int_I\int_f\left(\mathbf{v}_h^T\left(\underline{\mathbf{F}}^V\cdot\underline{n}\right)\right)^+ + \left(\mathbf{v}_h^T\left(\underline{\mathbf{F}}^V\cdot\underline{n}\right)\right)^-\ \mathrm{d}\mathrm{S}\ \mathrm{d}t = \\
&-(\gamma-1)\sum_{\kappa}\int_I\int_\kappa \mathbf{v}_h^T(\nabla\cdot\underline{\mathbf{F}}^{V^*})\ \mathrm{d}\mathbb{V}\ \mathrm{d}t + \sum_{\kappa}\int_I\int_\kappa \frac{\gamma-1}{R}\kappa_T\left(\frac{\nabla T\cdot\nabla T}{T^2}\right)\ \mathrm{d}\mathbb{V}\ \mathrm{d}t
\end{aligned}
\tag{3.16}
$$

Now it can be seen that in (3.16), as opposed to (2.33), there are a set of terms that are free to produce or destroy entropy on a timeslab. One way to think about these terms could be as the entropy effects created by the implicit model for the unresolved subgrid scales, similar to what has been suggested in the literature [6].

With the form given in (3.16), all of the terms are readily computable from the state, except for the reversible heat entropy term that includes a second derivative of T. We can

apply the divergence theorem to write:

$$\begin{aligned}\sum_{\kappa}\int_I\int_\kappa \frac{1}{R}\kappa_T\nabla\cdot\left(\frac{\nabla T}{T}\right)\ \mathrm{d}\mathbb{V}\ \mathrm{d}t = \\ \sum_{\kappa}\int_I\oint_{\partial\kappa}\frac{\kappa_T}{R}\left(\frac{\nabla T\cdot\underline{n}}{T}\right)\ \mathrm{dS}\ \mathrm{d}t = \\ \sum_{f\in\Gamma_i}\int_I\int_f\left[\left(\frac{\kappa_T}{R}\left(\frac{\nabla T\cdot\underline{n}}{T}\right)\right)^+ + \left(\frac{\kappa_T}{R}\left(\frac{\nabla T\cdot\underline{n}}{T}\right)\right)^-\right]\ \mathrm{dS}\ \mathrm{d}t\end{aligned} \tag{3.17}$$

This allows the calculation of $\sum_\kappa\int_I\int_\kappa\frac{1}{R}\kappa_T\nabla\cdot\left(\frac{\nabla T}{T}\right)\ \mathrm{d}\mathbb{V}\ \mathrm{d}t$ without explicit calculation of any second derivative terms. As a downside, it contributes additional quadrature error when we calculate $E^{V,\text{quad}}$ in (3.13).

At this point, we introduce a shorthand for each of the terms in (3.16). The first set of terms concern the resolved entropy transport. The total entropy is defined by:

$$S(t)\equiv\int_\kappa \rho s\ \ \mathrm{d}\mathbb{V} \tag{3.18}$$

and its variation on a timeslab I defined on $t\in[t^n,t^{n+1}]$ is denoted by $(\Delta S)^t_{\text{total}}=S(t_-^{n+1})-S(t_-^n)$. The resolved component of this entropy change is given by:

$$(\Delta S)^t_{\text{flux}}=\sum_\kappa\int_I\int_\kappa\frac{\partial}{\partial t}(\rho s)\ \ \mathrm{d}\mathbb{V}\ \mathrm{d}t=-(\gamma-1)\sum_\kappa\int_I\int_\kappa\mathbf{v}^T\frac{\partial\mathbf{u}_h}{\partial t}\ \ \mathrm{d}\mathbb{V}\ \mathrm{d}t \tag{3.19}$$

The total flux of entropy across the spatial boundaries of a DG discretization is given by:

$$(\Delta S)^I_{\text{flux}}=\sum_\kappa\int_I\int_\kappa\nabla\cdot\left[\rho s\underline{V}\right]\ \ \mathrm{d}\mathbb{V}\ \mathrm{d}t=-(\gamma-1)\sum_\kappa\int_I\int_\kappa\mathbf{v}^T\left(\nabla\cdot\underline{\mathbf{F}}^I\right)\ \ \mathrm{d}\mathbb{V}\ \mathrm{d}t \tag{3.20}$$

Rounding out the resolved entropy transport is a term that captures the diffusion of entropy:

$$(\Delta S)^{\text{heat}}_{\text{diff}}=-(\gamma-1)\sum_{f\in\Gamma_i}\int_I\int_f\left[\left(\frac{\kappa_T}{R}\frac{(\nabla T\cdot\underline{n})}{T}\right)^+ + \left(\frac{\kappa_T}{R}\frac{(\nabla T\cdot\underline{n})}{T}\right)^-\right]\ \mathrm{dS}\ \mathrm{d}t \tag{3.21}$$

Once the resolved transport of entropy is accounted for, the resolved production of entropy must be considered. Entropy is produced on the domain by two sources. The first is production by the action of viscous shearing in the resolved scales:

$$\begin{aligned}(\Delta S)_{\text{prod}}^{\text{shear}} &= -(\gamma-1)\int_I\int_\kappa \mathbf{v}^T(\nabla\cdot\underline{\mathbf{F}}^{V^*})\ \mathrm{d}\mathbb{V}\ \mathrm{d}t \\ &= (\gamma-1)\int_I\int_\kappa \frac{\rho}{p}\left[\frac{4}{3}\mu\left(\left(\frac{\partial u}{\partial x}\right)^2+\left(\frac{\partial v}{\partial w}\right)^2+\left(\frac{\partial w}{\partial z}\right)^2\right)\right. \\ &\quad \left.+\mu\left(\frac{\partial u}{\partial y}+\frac{\partial v}{\partial x}\right)^2+\mu\left(\frac{\partial u}{\partial z}+\frac{\partial w}{\partial x}\right)^2+\mu\left(\frac{\partial u}{\partial z}+\frac{\partial w}{\partial x}\right)^2\right]\ \mathrm{d}\mathbb{V}\ \mathrm{d}t \geq 0\end{aligned} \tag{3.22}$$

Entropy is also produced by the irreversible effects of heating on the domain:

$$(\Delta S)_{\text{prod}}^{\text{heat}} = \sum_\kappa \int_I\int_\kappa \frac{\gamma-1}{R}\kappa_T\left(\frac{\nabla T\cdot\nabla T}{T^2}\right)\ \mathrm{d}\mathbb{V}\ \mathrm{d}t \geq 0 \tag{3.23}$$

With these terms, all of the resolved scales are accounted for. However, when the flow is underresolved, there is some production or destruction of entropy due to the stabilization scheme. There are three entropy terms from the stabilization, due to the temporal upwinding:

$$(\Delta S)_{\text{disc}}^{t} = (\gamma-1)\sum_\kappa \int_\kappa \mathbf{v}(t_+^n)^T\left(\mathbf{u}_h(t_-^n)-\mathbf{u}_h(t_+^n)\right)\ \mathrm{d}\mathbb{V} \tag{3.24}$$

due to the inviscid numerical flux:

$$\begin{aligned}(\Delta S)_{\text{disc}}^{I} = (\gamma-1)\sum_{f\in\Gamma_i}\int_I\int_f \Bigg(&\left(\mathbf{v}^T\left(\widehat{\underline{\mathbf{F}}^I\cdot\underline{n}}-\underline{\mathbf{F}}^I\cdot\underline{n}\right)\right)^+ \\ &+\left(\mathbf{v}^T\left(\widehat{\underline{\mathbf{F}}^I\cdot\underline{n}}-\underline{\mathbf{F}}^I\cdot\underline{n}\right)\right)^-\Bigg)\ \mathrm{dS}\ \mathrm{d}t\end{aligned} \tag{3.25}$$

and due to the viscous numerical flux:

$$
\begin{aligned}
(\Delta S)^V_{\text{disc}} = &-(\gamma-1)\sum_{f\in\Gamma_i}\int_I\int_f \left\{\left(\overline{\underline{\mathbf{K}}}(\mathbf{u}_h)\right)^T(\nabla\mathbf{v}_h)\right\}\cdot[[\mathbf{u}_h]] \;\; \mathrm{dS}\;\mathrm{d}t \\
&+(\gamma-1)\sum_{f\in\Gamma_i}\int_I\int_f [[\mathbf{v}_h]]\cdot\left\{\overline{\underline{\mathbf{K}}}(\mathbf{u}_h)\left(\nabla\mathbf{u}_h+\eta_f\underline{r}_f\left([[\mathbf{u}_h]]\right)\right)\right\} \;\; \mathrm{dS}\;\mathrm{d}t \\
&+(\gamma-1)\sum_{f\in\Gamma_i}\int_I\int_f \left(\mathbf{v}_h^T\left(\underline{\mathbf{F}}^V\cdot\underline{n}\right)\right)^+ + \left(\mathbf{v}_h^T\left(\underline{\mathbf{F}}^V\cdot\underline{n}\right)\right)^- \;\; \mathrm{dS}\;\mathrm{d}t
\end{aligned}
\tag{3.26}
$$

We can now restate (3.16) using this shorthand:

$$
\begin{aligned}
&\underbrace{(\Delta S)^t_{\text{flux}}+(\Delta S)^I_{\text{flux}}+(\Delta S)^{\text{heat}}_{\text{diff}}}_{\text{resolved transport terms}} \\
&\qquad+\underbrace{(\Delta S)^t_{\text{disc}}+(\Delta S)^I_{\text{disc}}+(\Delta S)^V_{\text{disc}}}_{\text{numerical stabilization terms}}= \\
&\qquad\qquad\underbrace{(\Delta S)^{\text{shear}}_{\text{prod}}+(\Delta S)^{\text{heat}}_{\text{prod}}}_{\text{resolved production terms}}\geq 0
\end{aligned}
\tag{3.27}
$$

Here, of course, we have assumed that the quadrature error is negligible with respect to the dominant terms in (3.16) and (3.27). With this form written out, we can see that the stabilization terms have the effect of artificially producing (or destroying) entropy.

Chapter 4

Numerical experiments

In this chapter, we perform some numerical experiments to use this new technique to characterize the entropy behavior of the DG scheme. These experiments have the twofold goals of evaluating the merits of the ILES concept and help elucidate strategies for new explicit subgrid physical models designed for high-order discretizations.

4.1 Problem setup

4.1.1 Taylor-Green vortex problem

The Taylor-Green vortex problem is a classic canonical problem in turbulent flow. The Taylor-Green vortex system was first developed and analyzed by Taylor and Green in the late 1930s [12]. The behavior of the Taylor-Green vortex problem has been well studied and its behavior is well known. The flow exists in a cube which is periodic in three directions,

with each of x, y, and z spanning $[0, 2\pi L]$. The initial conditions are given by:

$$\begin{aligned} u &= V_0 \sin\left(\frac{x}{L}\right) \cos\left(\frac{y}{L}\right) \cos\left(\frac{z}{L}\right) \\ v &= -V_0 \cos\left(\frac{x}{L}\right) \sin\left(\frac{y}{L}\right) \cos\left(\frac{z}{L}\right) \\ w &= 0 \\ p &= \rho_0 V_0^2 \left[\frac{1}{\gamma M_0^2} + \frac{1}{16}\left(\cos\left(\frac{2x}{L}\right) + \cos\left(\frac{2y}{L}\right)\right)\left(\cos\left(\frac{2z}{L}\right) + 2\right)\right] \end{aligned} \tag{4.1}$$

with density ρ, velocity components in x, y, and z, respectively, u, v, and w, and pressure p. The Mach number is given by:

$$M_0 = \frac{V_0}{a_0} \tag{4.2}$$

The flow is initialized to be isothermal, such that:

$$\frac{p}{\rho} = \frac{p_0}{\rho_0} = RT_0 \tag{4.3}$$

and the cases are run at a variety of specified Reynolds numbers, which are defined by:

$$Re = \frac{\rho_0 V_0 L}{\mu} \tag{4.4}$$

Finally, the nondimensional time scale is given by:

$$t_0 = \frac{L}{V_0} = \frac{L}{M_0 a_0} \tag{4.5}$$

The Taylor-Green vortex problem is characterized by the convection of the initial conditions, which relatively quickly leads to the stretching of the initial vortices. Eventually, the flow undergoes a transition to turbulence at a critical point. From here, the turbulence continues through a range of scales until all of the kinetic energy is dissipated to heat.

4.1.2 Discretization

We will discretize the system using a uniform spacetime mesh of $N \times N \times N$ hexahedral elements in space, with timeslabs of uniform timestep Δt. We set the timestep using a constant CFL number according to the resolved scales. We can approximate the resolved scales with a length scale δx and timsecale δt, for polynomial representations of order p_x and p_t in space and time respectively, given by:

$$\delta x = \frac{\Delta x}{p_x} = \frac{L}{p_x N} \tag{4.6}$$

and

$$\delta t = \frac{\Delta t}{p_t} \tag{4.7}$$

We use the CFL number, C_{CFL}, as a parameter to specify a resolved time scale:

$$\delta t = C_{\text{CFL}} \frac{\delta x}{c} \tag{4.8}$$

where c a physical wavespeed we want to resolve. Using this and the specified polynomial order in time, p_t, we can set Δt:

$$\Delta t = \frac{C_{\text{CFL}}}{c} \frac{L}{N} \frac{p_t}{p_x} \tag{4.9}$$

The values that specify the discretization that we use for the majority of this work can be found in Table 4.1. These discretization choices will be used for all simulations in this work unless otherwise noted.

Specifications	
Re	1600
c	1.0
a_0	1.0
ρ_0	1.0
M_0	0.1
L	1.0
C_{CFL}	16

Table 4.1: Specifications of discretization choices for the Taylor-Green vortex problem.

4.2 Results

4.2.1 Case selection

For this work, we consider discretizations that are in the range typical for LES. To do this, we consider the Kolmogorov length scale and time scale for the problem. We recall that these are given by, respectively:

$$\eta = \left(\frac{\nu^3}{\varepsilon}\right)^{1/4} \tag{1.7, reprise}$$

and

$$\tau_\eta = \left(\frac{\nu}{\varepsilon}\right)^{\frac{1}{2}} \tag{1.8, reprise}$$

We use specification constants as shown in Table 4.1. Via scaling analysis, we can estimate ε:

$$\varepsilon \sim \frac{V_0^3}{L} \tag{4.10}$$

A slightly better approximation is to estimate the rate of dissipation of TKE per unit mass by:

$$\varepsilon \approx \frac{1}{\rho_0 L^3}\left(\frac{\partial E_k}{\partial t}\right)_{\max} \tag{4.11}$$

Pulling from later results, we use $(\frac{\partial E_k}{\partial t})_{\max} \approx 0.012$. Table 4.2 gives the approximate Kolmogorov scales given by these estimates, and shows them to be in decent agreement.

	approximation order	
	0th	1st
η	0.00395	0.00212
τ_η	0.25	0.0722

Table 4.2: Estimates of Kolmogorov scales.

In Table 4.3, we show a series of discretizations that we will use in this text and compare their resolved length scales to the zeroth-order and first-order approximations of the Kolmogorov length scale.

We can see in Table 4.3 that the most resolved cases ($p_x = 8$, $N = 64$) are in the range of a DNS simulation. The less-resolved cases ($N = 32$) tend to be between about two and

N	p_x	p_t	C_{CFL}	δx	Δt	δt	$(\delta x/\eta)_{\text{0th}}$	$(\delta t/\tau_\eta)_{\text{0th}}$	$(\delta x/\eta)_{\text{1st}}$	$(\delta t/\tau_\eta)_{\text{1st}}$
32	2	2	16	0.0156	0.5	0.25	3.95	1	7.36	3.46
32	4	2	16	0.00781	0.25	0.125	1.98	0.5	3.68	1.73
32	8	2	16	0.00391	0.125	0.0625	0.988	0.25	1.84	0.866
32	2	4	16	0.0156	1	0.25	3.95	1	7.36	3.46
32	4	4	16	0.00781	0.5	0.125	1.98	0.5	3.68	1.73
32	8	4	16	0.00391	0.25	0.0625	0.988	0.25	1.84	0.866
48	2	2	16	0.0104	0.333	0.167	2.64	0.667	4.90	2.31
48	4	2	16	0.00521	0.167	0.0833	1.32	0.333	2.45	1.15
48	8	2	16	0.00260	0.0833	0.0417	0.659	0.167	1.23	0.577
48	2	4	16	0.0104	0.667	0.167	2.64	0.667	4.90	2.31
48	4	4	16	0.00521	0.333	0.0833	1.32	0.333	2.45	1.15
48	8	4	16	0.00260	0.167	0.0417	0.659	0.167	1.23	0.577
64	2	2	16	0.00781	0.25	0.125	1.98	0.5	3.68	1.73
64	4	2	16	0.00391	0.125	0.0625	0.988	0.25	1.84	0.866
64	8	2	16	0.00195	0.0625	0.0313	0.494	0.125	0.920	0.433
64	2	4	16	0.00781	0.5	0.125	1.98	0.5	3.68	1.73
64	4	4	16	0.00391	0.25	0.0625	0.988	0.25	1.84	0.866
64	8	4	16	0.00195	0.125	0.0313	0.494	0.125	0.920	0.433

Table 4.3: Resolved scales for various discretization choices.

eight times less resolved than is necessary for a direct numerical simulation. These represent a range of tractible resolutions for performing LES simulations of the Taylor-Green vortex problem.

4.2.2 Controlling quadrature errors

In the discrete setting, we use numerical quadrature to perform integrations. Gaussian quadrature approximates the integral of some function f as:

$$\int_a^b f(x)\,\mathrm{d}x \approx \sum_{i=1}^{N^{\text{quad}}} w_i f(x_i) \tag{4.12}$$

where the paired set of nodes and weights, x_i and w_i, are well known Gauss nodes and weights. Gaussian quadrature is exact for polynomials of order $p \leq 2N^{\text{quad}} - 1$, and as N^{quad} is increased, the error between the exact integral and the approximation will converge to

zero.

Before we can proceed, we must ensure that the errors induced by using numerical quadrature to evaluate the integrals are not large with respect to the actual quantities of interest. Thus we must evaluate $E^{t,\text{quad}}$, $E^{I,\text{quad}}$, and $E^{V,\text{quad}}$.

We can evaluate trivially $E^{t,\text{quad}}$, $E^{I,\text{quad}}$, and $E^{V,\text{quad}}$ easily using (3.11), (3.12) and (3.13), from data easily accessible in the simulation. In Figure 4-1, we show that $E^{t,\text{quad}}$ normalized by $|(\Delta S)^t_{\text{flux}}|$ is small, and, in Figure 4-2, we show that $E^{I,\text{quad}}$ normalized by $|(\Delta S)^I_{\text{flux}}|$ is small.

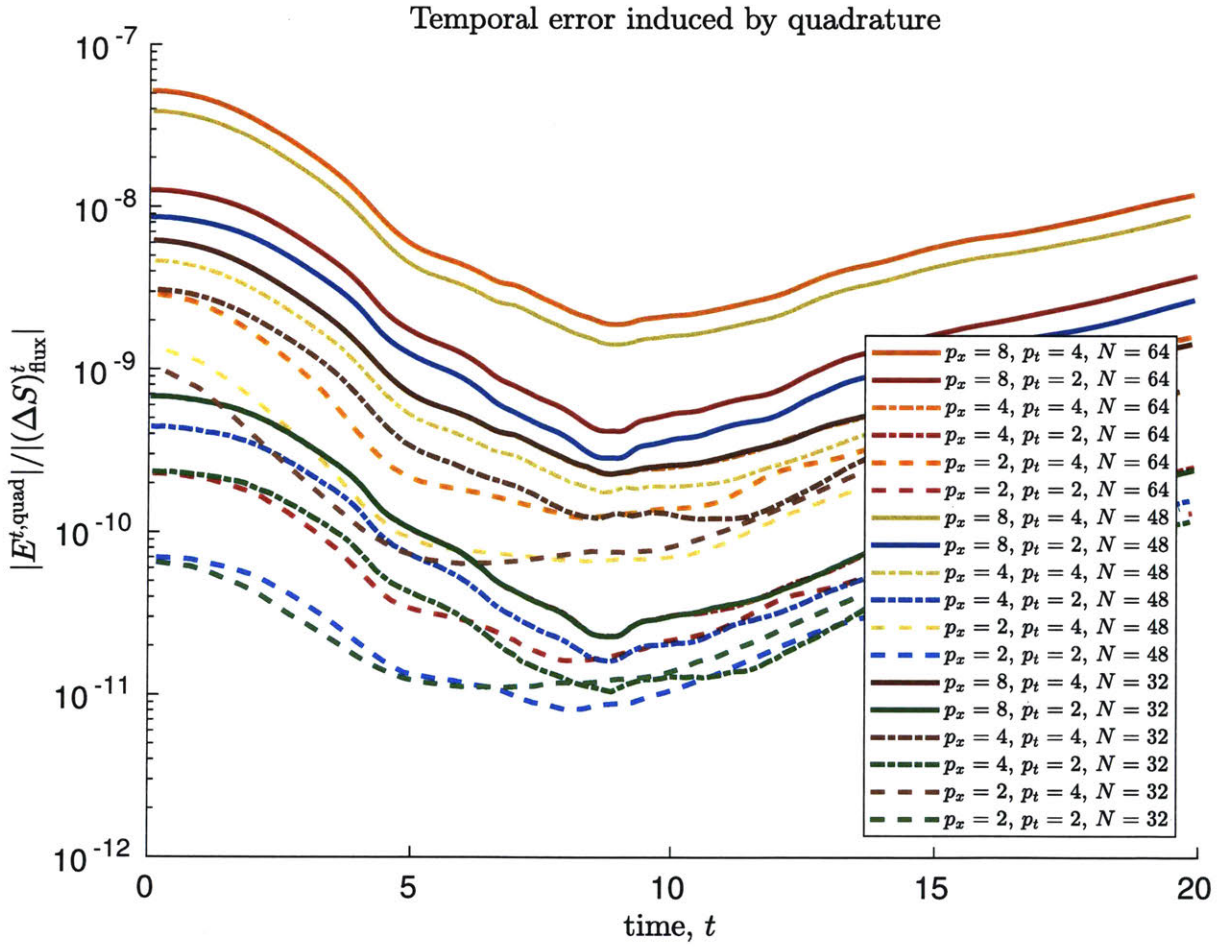

Figure 4-1: Quadrature error due to temporal flux transformation.

Finally, in Figure 4-3, we show that $E_{V,\text{quad}}$ normalized by $(\Delta S)^{\text{shear}}_{\text{prod}} + (\Delta S)^{\text{heat}}_{\text{prod}}$ is small, such that the quadrature error does not dominate the values of interest. The quadrature

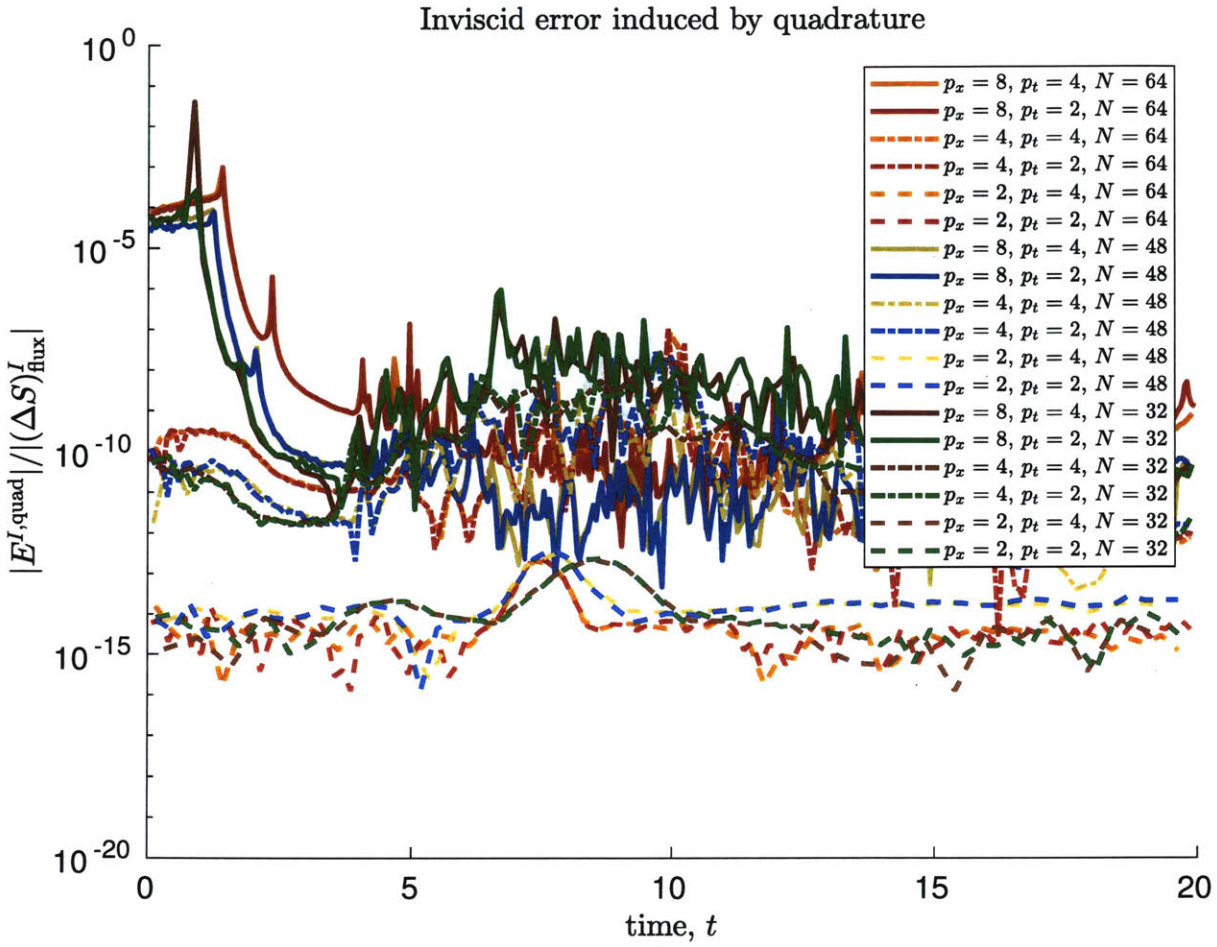

Figure 4-2: Quadrature error due to inviscid flux transformation.

error for these terms is not as small as for the inviscid and temporal terms. Nonetheless, the quadrature error will be less than 1% of the magnitude of the production terms, which is reasonably small to distinguish the effects we are interested in.

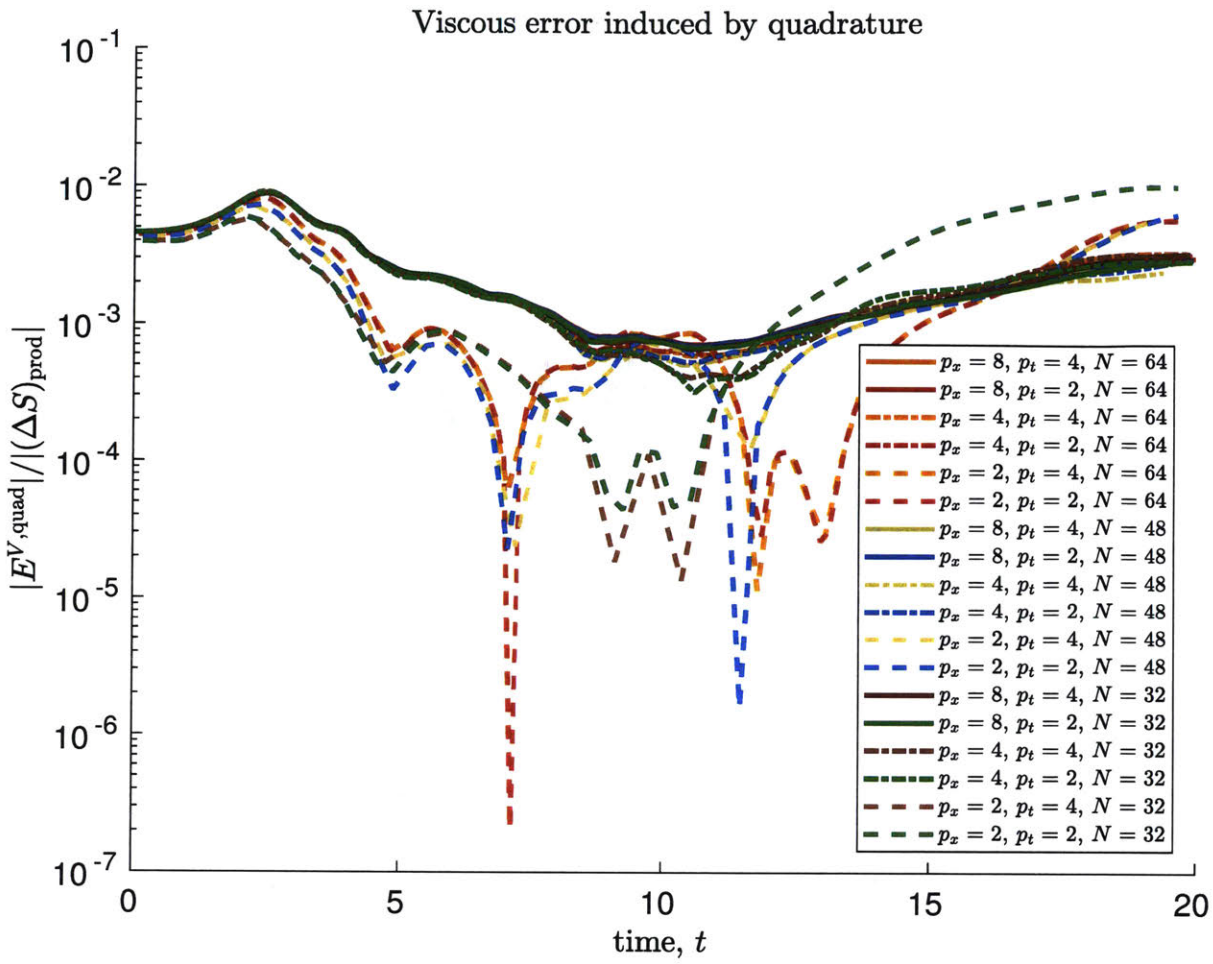

Figure 4-3: Quadrature error due to viscous flux transformation.

4.2.3 Kinetic energy evolution of the Taylor-Green vortex problem

It is a standard practice in the literature to study the kinetic energy evolution of a Taylor-Green vortex problem. The kinetic energy is defined as:

$$E_k(t) = \sum_{\kappa} \int_{\kappa} \frac{1}{2} \rho \, \underline{V} \cdot \underline{V} \; \mathrm{d}\mathbb{V} \tag{4.13}$$

Figure 4-4 shows the kinetic energy evolution for various discretization choices with $p_t = 2$. In this plot, we can see that the kinetic energy evolution converges as both the polynomial order of approximation and the number of elements are increased. The kinetic energy is decreasing, which is an expected behavior for a low Mach number flow. It seems that

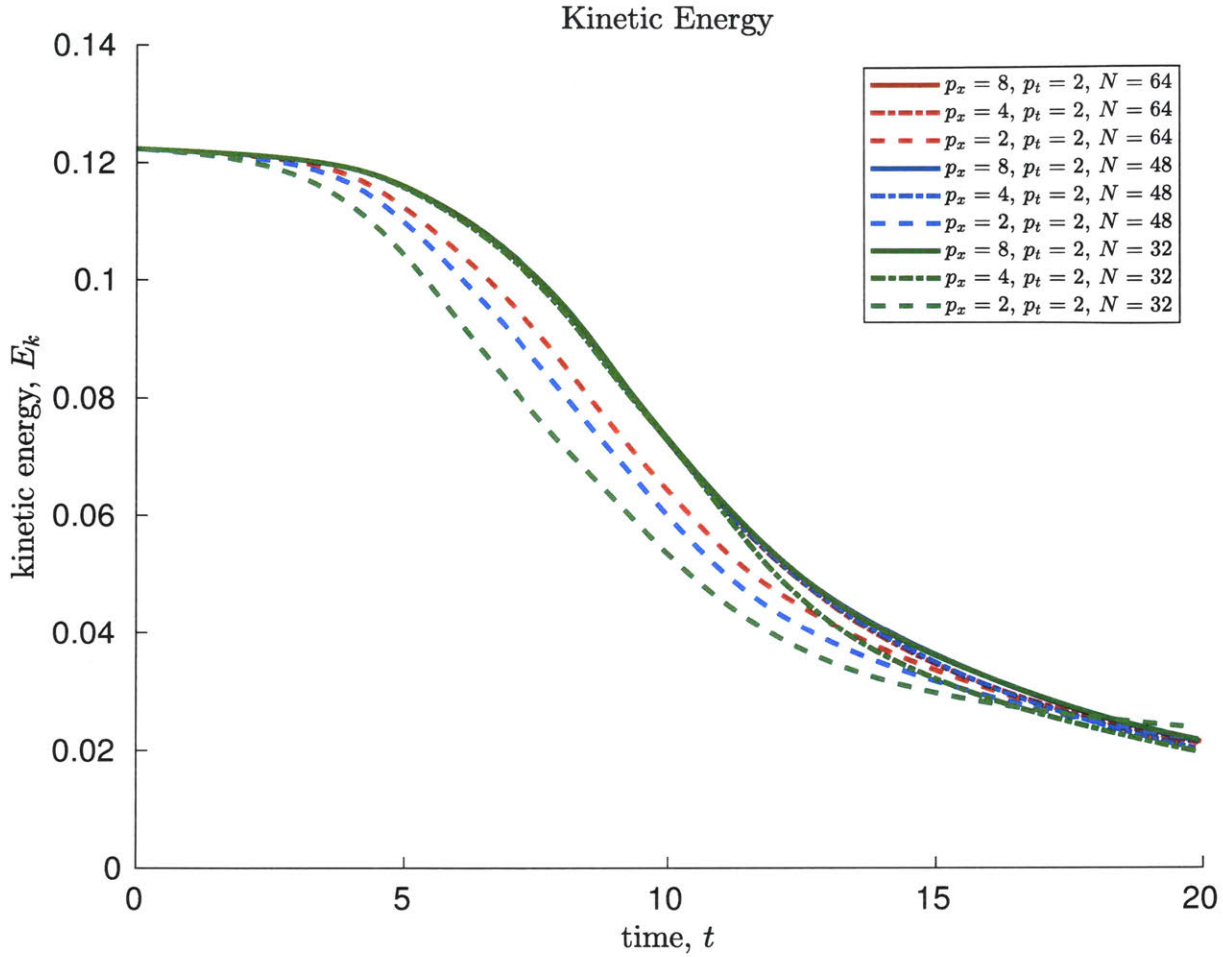

Figure 4-4: Evolution of kinetic energy for Taylor-Green vortex problem under varied discretizations with $p_t = 2$.

the lowest order terms, with $p_x = 2$ and regardless of the number of elements, tend to be prematurely dissipative. As N is decreased, the onset of dissipation is increasingly premature. In these cases, it seems the stabilization of the DG scheme is adding excessive dissipation early in the process of transition to turbulence.

Moving to the $p_x = 4$ simulations, we can see a different behavior. Early in the evolution, before $t \approx 4$, the kinetic energy curves are in very good agreement for all $p_x = 4$ or greater simulations, for all N tested. After $t \approx 4$, the $p_x = 4$, $N = 32$ simulation begins to diverge from the more highly resolved simulations, now dissipating more kinetic energy than the others. It continues this behavior until the end of the simulated window, ultimately

resulting in a solution with significant underprediction of the kinetic energy. Again, the other $p_x = 4$ simulations exhibit a similar behavior, albeit one that is more closely aligned with the highest resolution simulations.

In particular, the behavior of the $p_x = 2$, $N = 64$ simulation can be compared to the behavior of the $p_x = 4$, $N = 32$ simulation, as they both have 128^3 spatial degrees of freedom for the simulation. It can be seen that, at a fixed count of degrees of freedom, the low order solution dissipates the kinetic energy more rapidly. Increasing the order of a solution seems to more closely approximate the most resolved solutions than increasing the number of elements.

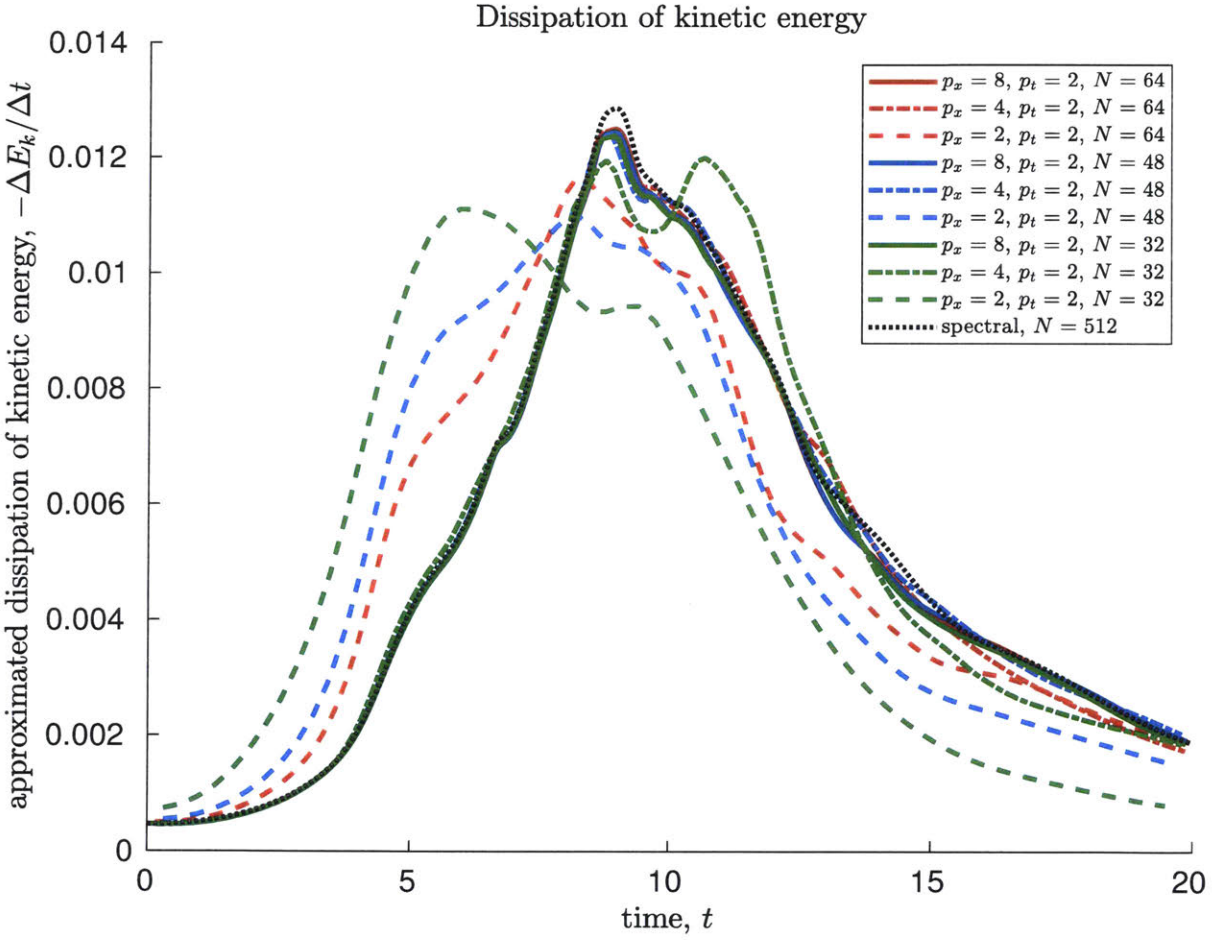

Figure 4-5: Evolution of kinetic energy dissipation for Taylor-Green vortex problem under varied discretizations with $p_t = 2$.

In Figure 4-5, we consider the dissipation of kinetic energy for the same cases. We now

introduce an $N = 512$ spectral incompressible solution from the literature [28] for comparison with our results. This confirms and informs what we witness in Figure 4-4. We can see that the solutions converge on a peak dissipation at $t \approx 9$. The $p_x = 8$ solutions have good agreement, while on the other hand, the $p_x = 2$ solutions all demonstrate early dissipation. Additionally, we can see that the $p_x = 4$ solutions exhibit good resolution of the dissipation on the whole, with, however, some interesting secondary peaks in dissipation after the peak dissipation that are not seen in the highest-order solutions.

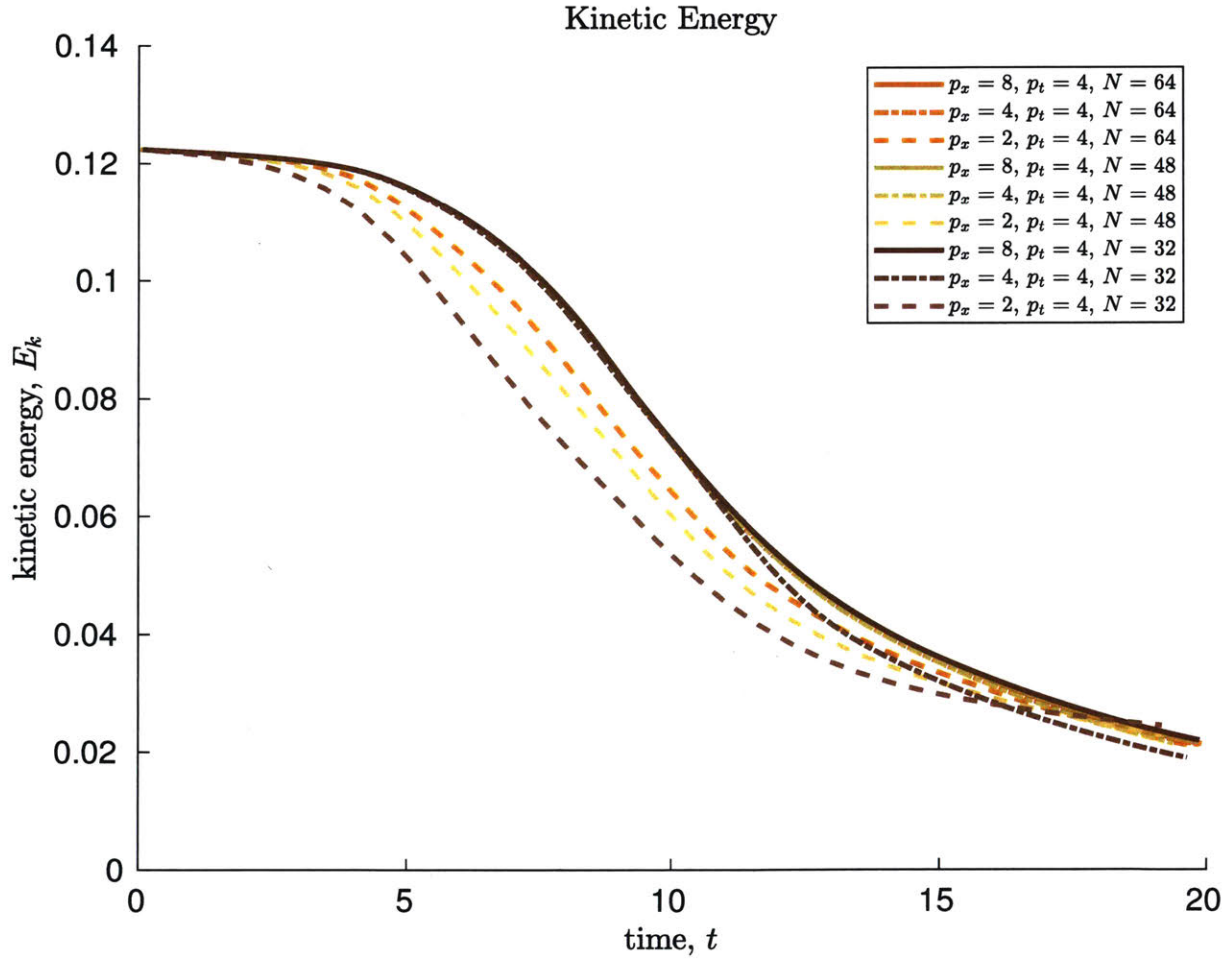

Figure 4-6: Evolution of kinetic energy for Taylor-Green vortex problem under varied discretizations with $p_t = 4$.

In Figures 4-6 and 4-7, we look at the same analysis for simulations with $p_t = 4$. It can seen that the change in temporal order of approximation does very little to change the

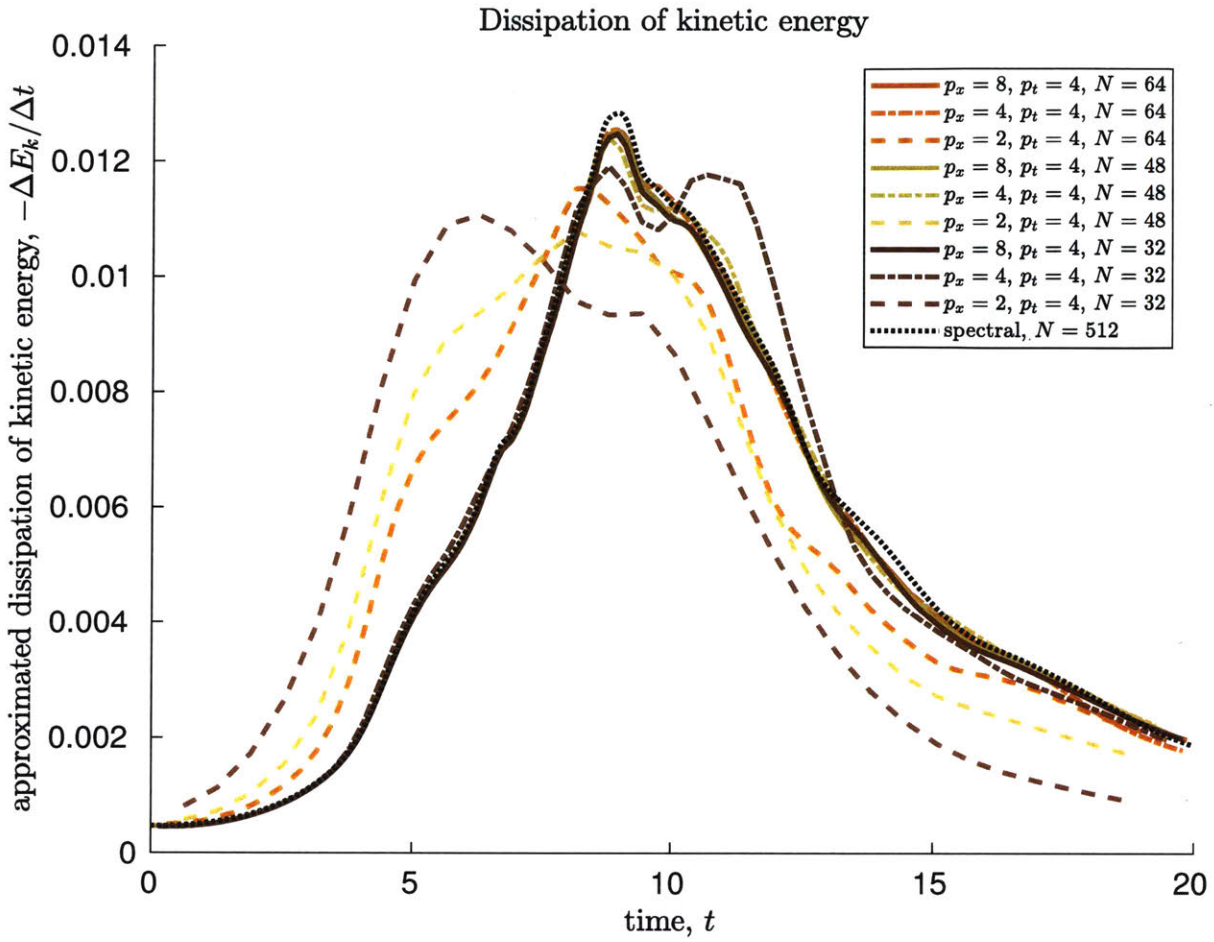

Figure 4-7: Evolution of kinetic energy dissipation for Taylor-Green vortex problem under varied discretizations with $p_t = 4$.

observations from the $p_t = 2$ case. We now seek some insight as to how the stabilization involved in our DG discretization relates to these effects.

4.2.4 Entropy evolution for the Taylor-Green vortex problem

We can see from the previous section that an underresolved DG scheme produces errors in the kinetic energy. In order to understand what causes this, we look into the entropy generation that underlies the spacetime DG simulation outlined here. To begin, consider the

entropy evolution outlined in (3.27). Rearranging slightly gives:

$$\left(\frac{\Delta S}{\Delta t}\right)^t_{\text{total}} = \left(\frac{\Delta S}{\Delta t}\right)^t_{\text{flux}} + \left(\frac{\Delta S}{\Delta t}\right)^t_{\text{disc}} = \left(\frac{\Delta S}{\Delta t}\right)^{\text{shear}}_{\text{prod}} + \left(\frac{\Delta S}{\Delta t}\right)^{\text{heat}}_{\text{prod}} - \left(\frac{\Delta S}{\Delta t}\right)^{I}_{\text{flux}} - \left(\frac{\Delta S}{\Delta t}\right)^{\text{heat}}_{\text{diff}} - \left(\frac{\Delta S}{\Delta t}\right)^{I}_{\text{disc}} - \left(\frac{\Delta S}{\Delta t}\right)^{V}_{\text{disc}} \tag{4.14}$$

Here, again, $(\Delta S)^t_{\text{total}}$ is the total variation of entropy from t^n to t^{n+1}. Figures 4-8 and 4-9

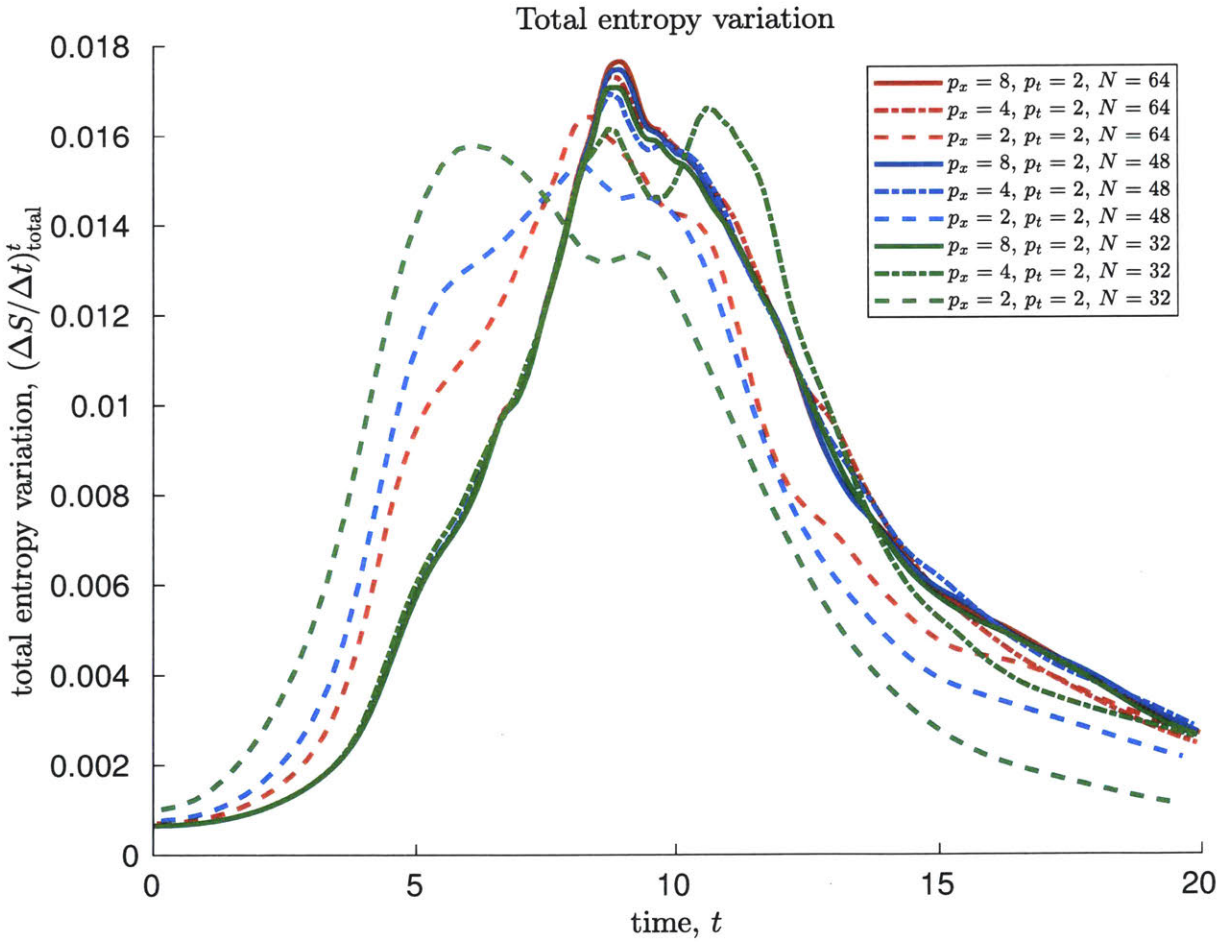

Figure 4-8: Evolution of total variation of entropy with $p_t = 2$.

show how $(\Delta S/\Delta t)^t_{\text{total}}$ evolves in time. We can see that the entropy generation on a given timeslab seems to correlate well with Figures 4-5 and 4-7. This indicates, as expected at this

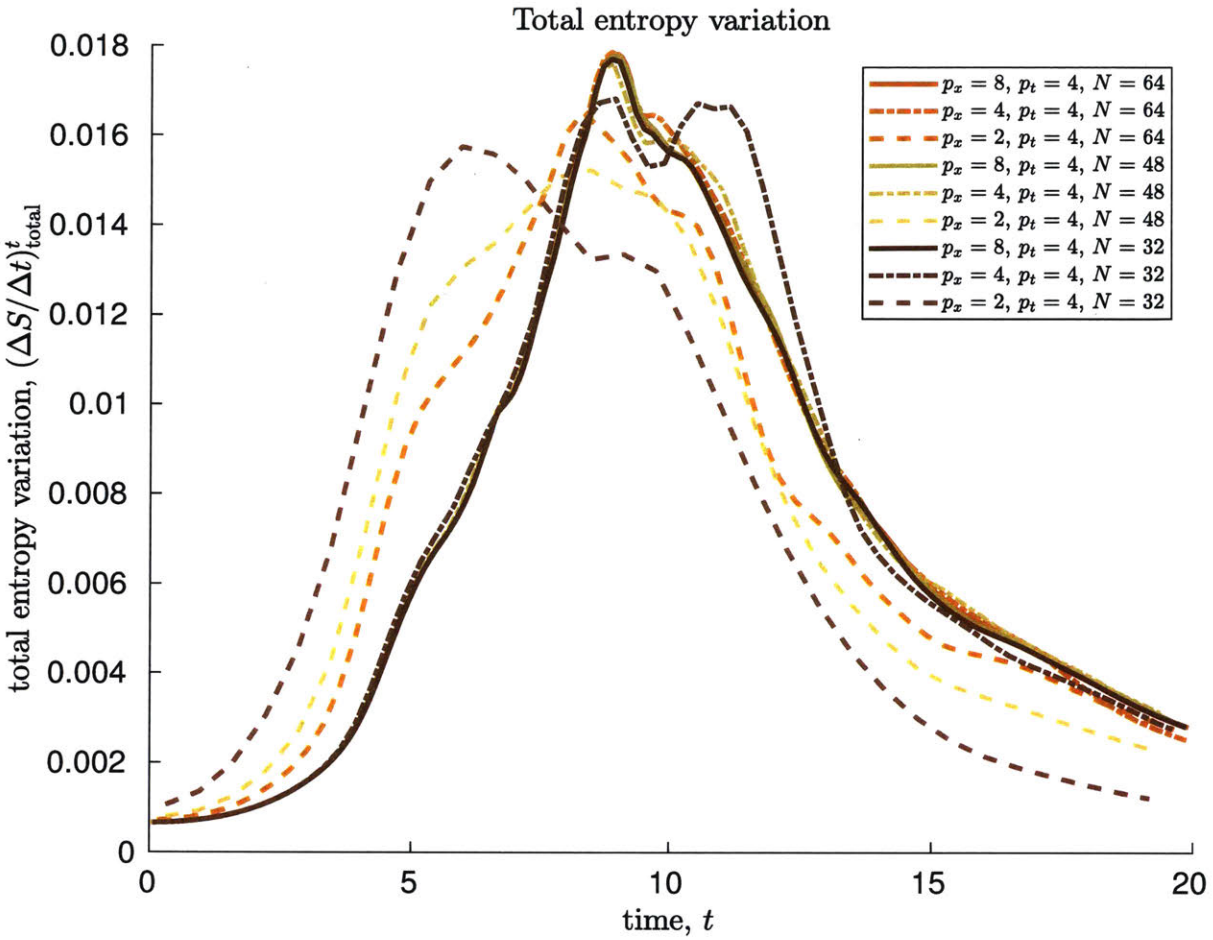

Figure 4-9: Evolution of total variation of entropy with $p_t = 4$.

low Mach number, that the processes that produce entropy and those that dissipate kinetic energy from the flow are the same. From (4.14), it can be seen that $(\Delta S/\Delta t)^t_{\text{total}}$ on a timeslab consists of contributions from both the resolved entropy flux in time, $(\Delta S/\Delta t)^t_{\text{flux}}$ and from the entropy generated by the jump due to the upwinding-in-time, $(\Delta S/\Delta t)^t_{\text{disc}}$. By studying Figures 4-10 and 4-11, we can see that, for $p_t = 2$, the effect of the discrete term $(\Delta S/\Delta t)^t_{\text{disc}}$ tends to destroy excess entropy from the resolved entropy variation and is beginning to converge as the flow is increasingly resolved. However, in spite of the fact that the discrete conribution to the temporal variation in entropy is large, these temporal jumps do not seem to induce large errors in the total variation of entropy, witnessed by the convergence seen in Figure 4-8.

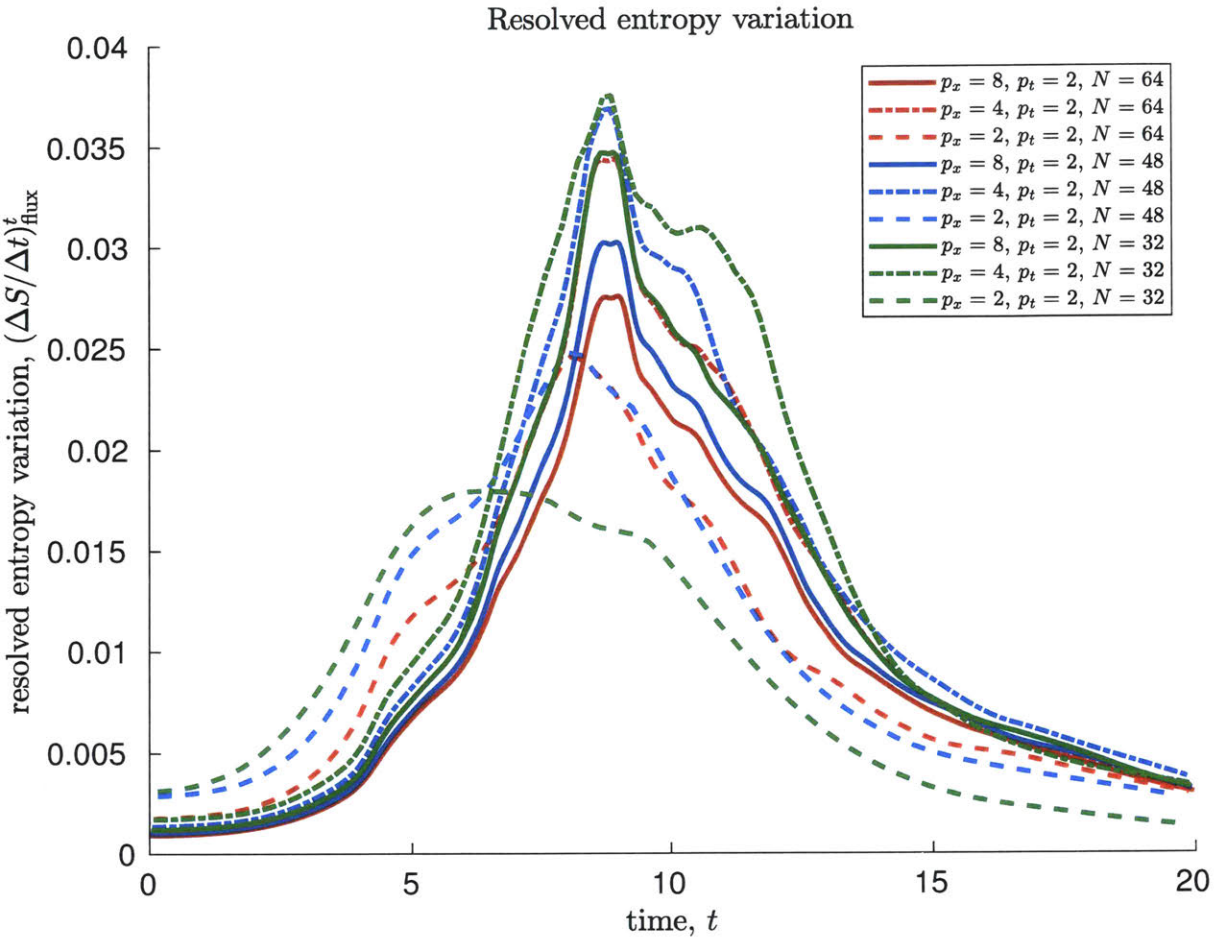

Figure 4-10: Evolution of resolved entropy variation with $p_t = 2$.

When the temporal order of approximation is increased to $p_t = 4$, almost all of $(\Delta S/\Delta t)^t_{\text{total}}$ is accounted for by the resolved terms. This effect can be clearly seen in Figure 4-13. Computation at high temporal order sharply reduces entropy contributions from the temporal upwinding scheme.

We can break down (4.14) again, into terms that are due to resolved production, inviscid

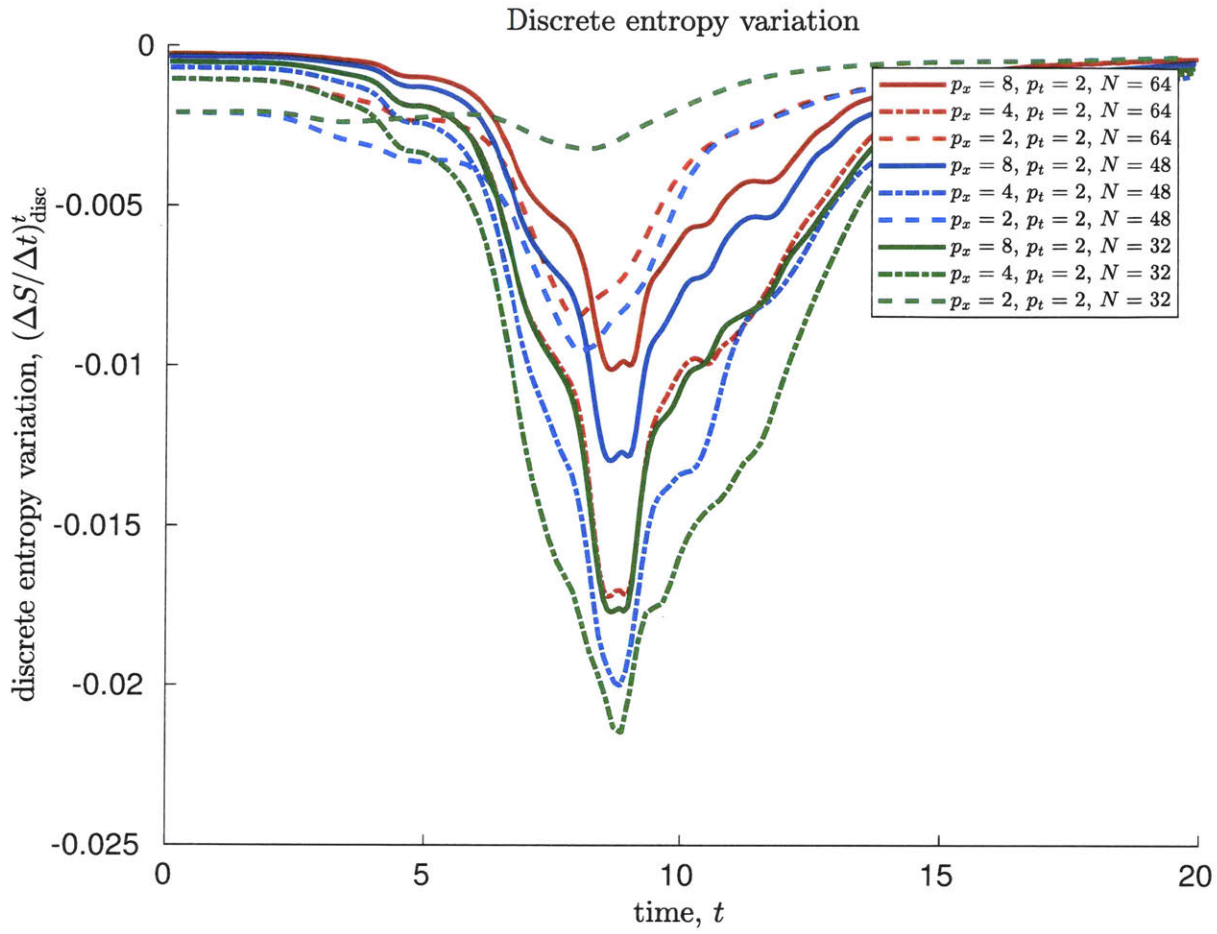

Figure 4-11: Evolution of discrete entropy variation with $p_t = 2$.

numerical flux, and viscous numerical flux contributions to the entropy variation.

$$\underbrace{\left(\frac{\Delta S}{\Delta t}\right)^t_{\text{flux}} + \left(\frac{\Delta S}{\Delta t}\right)^t_{\text{disc}}}_{\left(\frac{\Delta S}{\Delta t}\right)^t_{\text{total}}} = \underbrace{\left(\left(\frac{\Delta S}{\Delta t}\right)^{\text{shear}}_{\text{prod}} + \left(\frac{\Delta S}{\Delta t}\right)^{\text{heat}}_{\text{prod}}\right)}_{\left(\frac{\Delta S}{\Delta t}\right)_{\text{prod}}} - \underbrace{\left(\left(\frac{\Delta S}{\Delta t}\right)^I_{\text{flux}} + \left(\frac{\Delta S}{\Delta t}\right)^I_{\text{disc}}\right)}_{\left(\frac{\Delta S}{\Delta t}\right)^I} - \underbrace{\left(\left(\frac{\Delta S}{\Delta t}\right)^{\text{heat}}_{\text{diff}} + \left(\frac{\Delta S}{\Delta t}\right)^V_{\text{disc}}\right)}_{\left(\frac{\Delta S}{\Delta t}\right)^V} \tag{4.15}$$

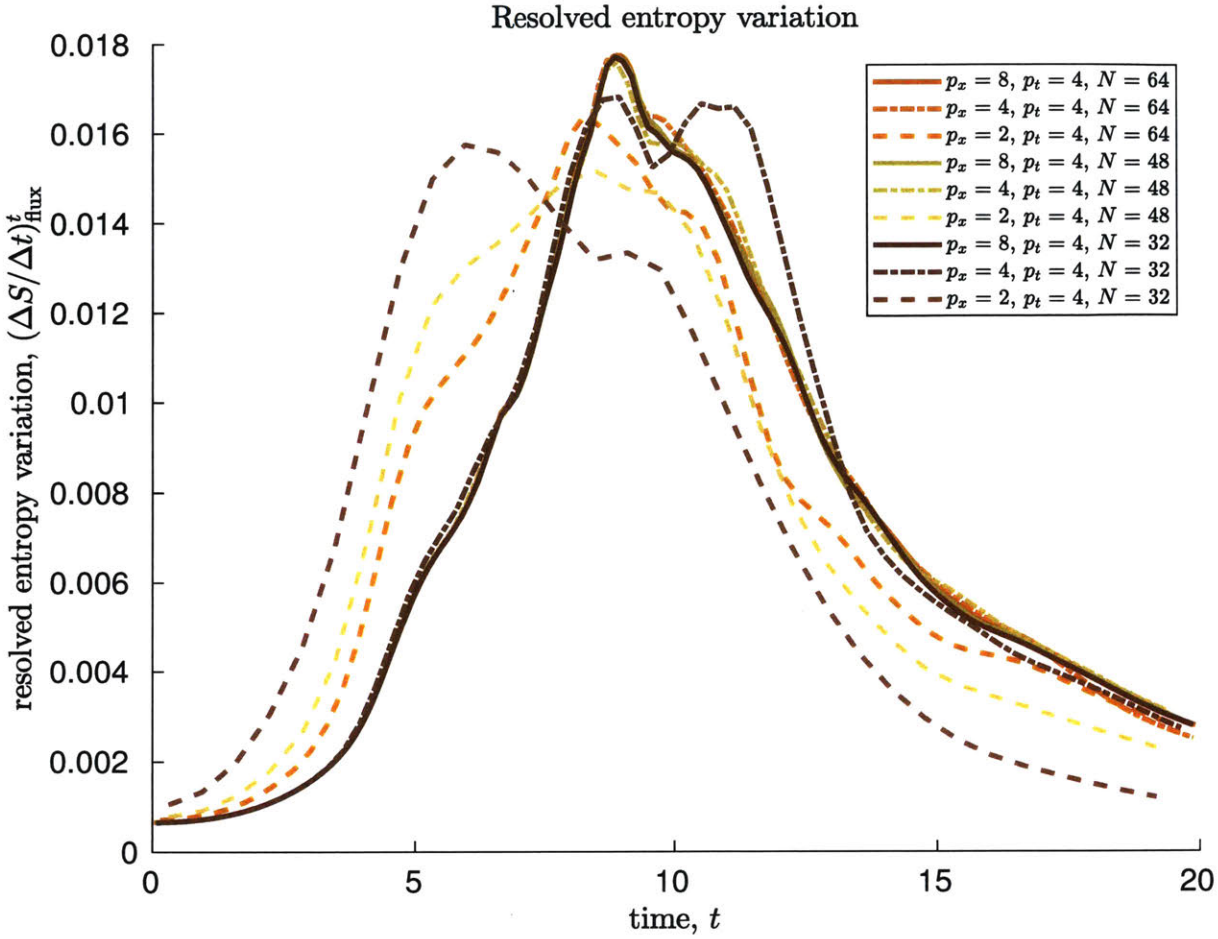

Figure 4-12: Evolution of resolved entropy variation with $p_t = 4$.

The results of this breakdown are seen in Figure 4-14, Figure 4-15, and Figure 4-16, for $N = 32$, $N = 48$, and $N = 64$, repectively. The results in these figures reinforce the observation that the difference between $p_t = 2$ and $p_t = 4$ is small, although some slight changes in the entropy evolution persist (see in particular the peak regions) due to this choice.

Particular observations can be made that, regardless of N, in the $p_x = 2$ cases the dominant cause of entropy generation is the inviscid terms. As p_x is decreased, this source of entropy generation decreases in all cases. For all of the cases shown here, regardless of N, p_x, and p_t, the entropy generated by the viscous terms is small but significant. It shows little sensitivity to the conditions of the discretization. The cases for which the viscous entropy

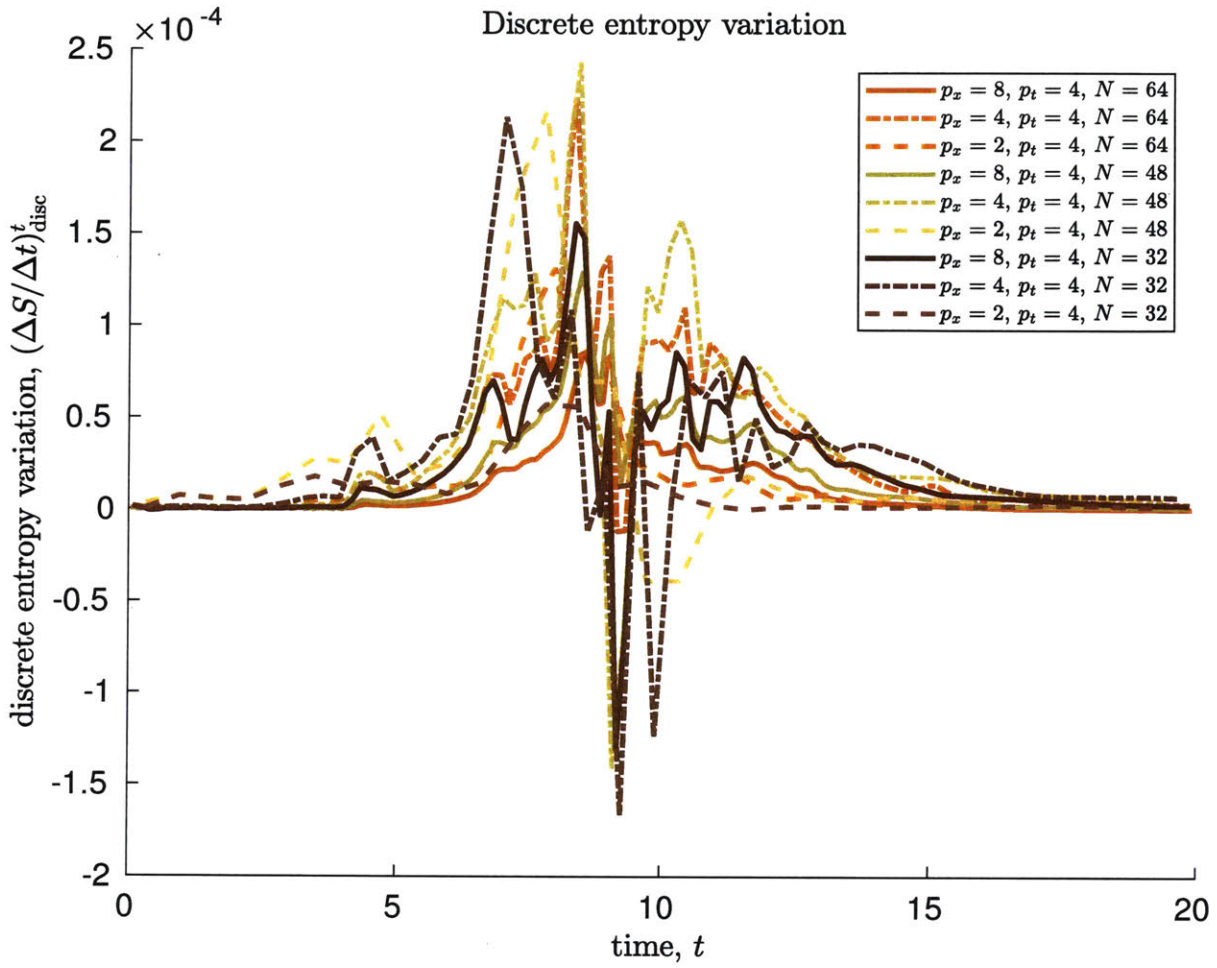

Figure 4-13: Evolution of discrete entropy variation with $p_t = 4$.

generation is changed seem to be largely the $p_x = 2$ cases, for which turbulent transition is triggered prematurely. In these cases, the viscous entropy generation also rises prematurely.

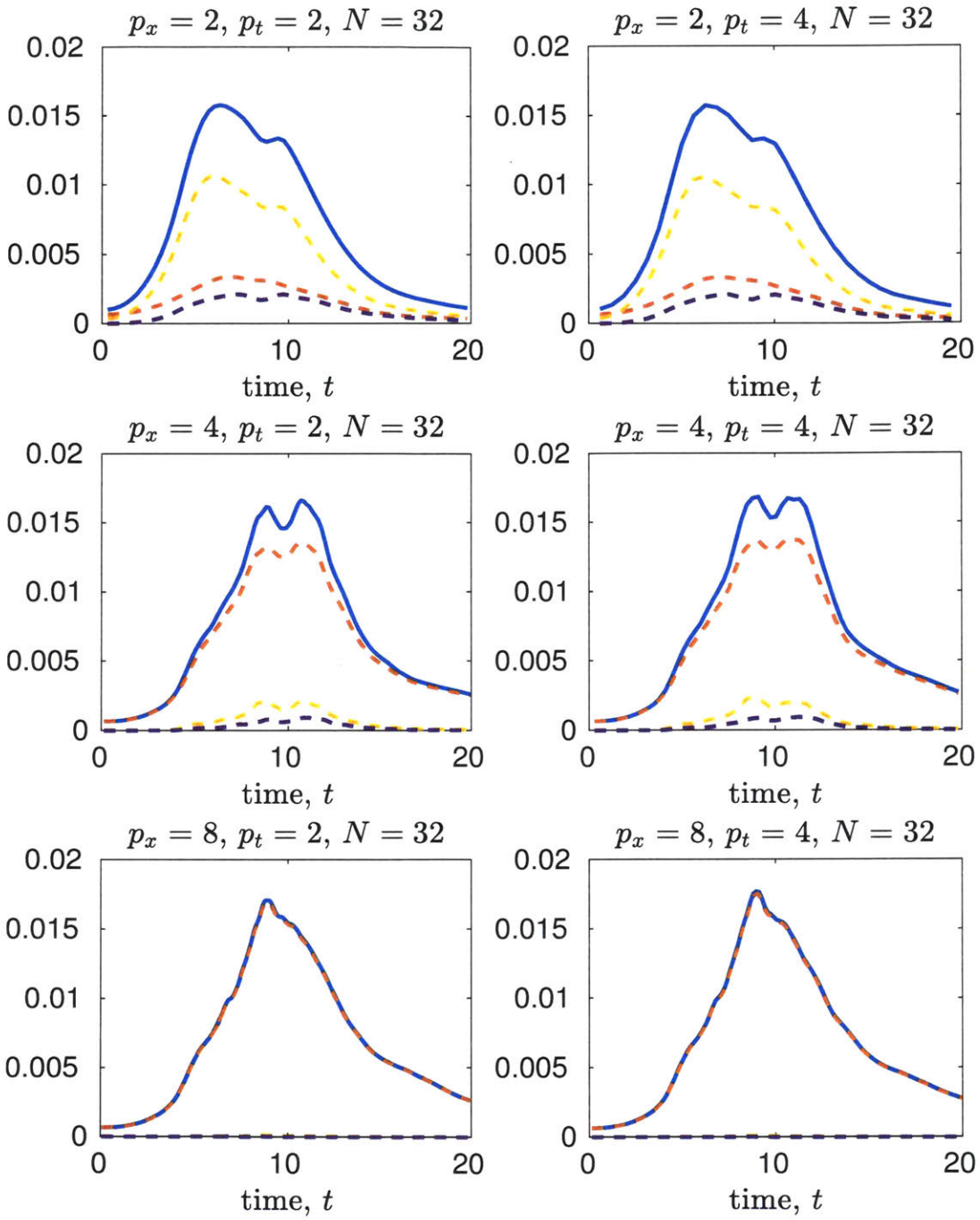

Figure 4-14: Breakdown of entropy generation for $N = 32$ cases. Solid blue line: $(\Delta S/\Delta t)^t_{\text{total}}$; red dashed line: $(\Delta S/\Delta t)_{\text{prod}}$; yellow dashed line:; $-(\Delta S/\Delta t)^I$; purple dashed line: $-(\Delta S/\Delta t)^V$.

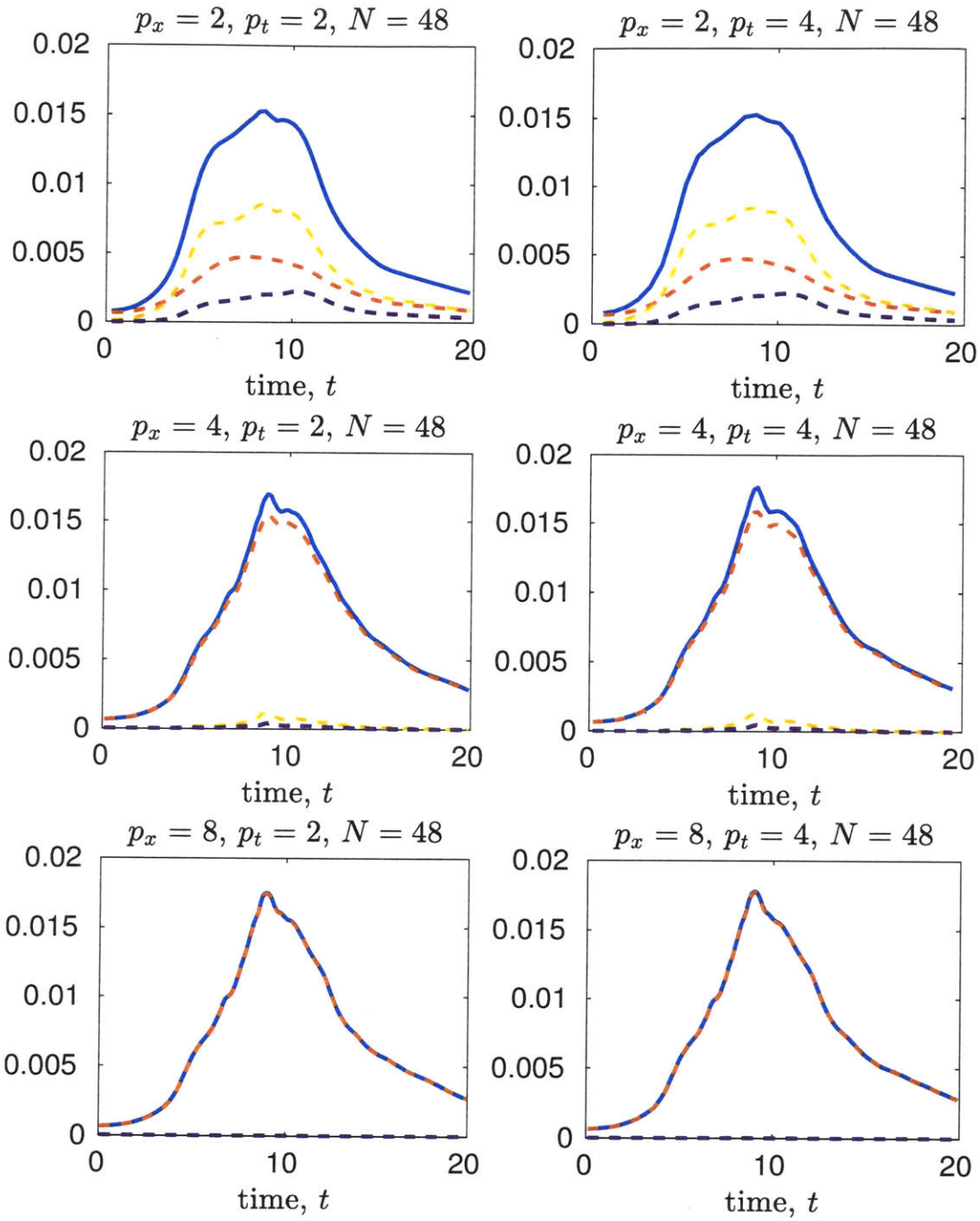

Figure 4-15: Breakdown of entropy generation for $N = 48$ cases. Solid blue line: $(\Delta S/\Delta t)^t_{\text{total}}$; red dashed line: $(\Delta S/\Delta t)_{\text{prod}}$; yellow dashed line:; $-(\Delta S/\Delta t)^I$; purple dashed line: $-(\Delta S/\Delta t)^V$.

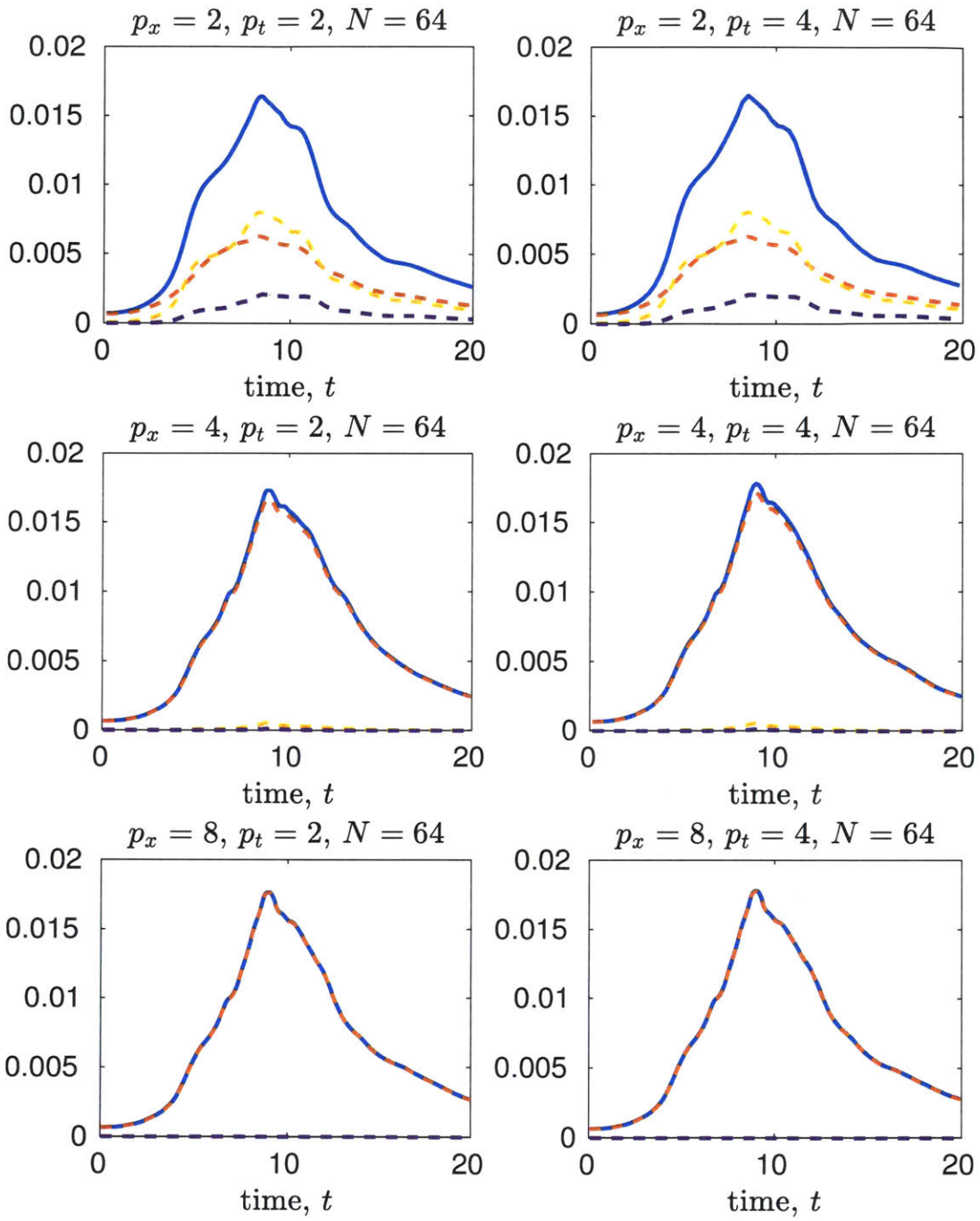

Figure 4-16: Breakdown of entropy generation for $N = 64$ cases. Solid blue line: $(\Delta S/\Delta t)^t_{\text{total}}$; red dashed line: $(\Delta S/\Delta t)_{\text{prod}}$; yellow dashed line:; $-(\Delta S/\Delta t)^I$; purple dashed line: $-(\Delta S/\Delta t)^V$.

4.2.5 Discrete contributions to the satisfaction of the second law of thermodynamics

We can now look at how the discrete terms in (3.27) work together to provide an entropy stable solution. The grouping of terms in (4.15) hides some details of what is happening in these solutions.

In Figures 4-17, 4-18, and 4-19, we can see that, as p_x decreases, paired contributions to the entropy transport from the convective flux of entropy on the domain and the inviscid numerical flux are present. We recall the definitions of the convective flux of entropy:

$$(\Delta S)^I_{\text{flux}} = \sum_\kappa \int_I \int_\kappa \nabla \cdot [\rho s \underline{V}] \ \mathrm{d}\mathbb{V} \ \mathrm{d}t \qquad \text{(3.20, reprise)}$$

and the entropy flux due to heat diffusion:

$$(\Delta S)^{\text{heat}}_{\text{diff}} = -\sum_\kappa \int_I \int_\kappa \frac{1}{R} \kappa_T \nabla \cdot \left(\frac{\nabla T}{T} \right) \ \mathrm{d}\mathbb{V} \ \mathrm{d}t \qquad \text{(3.21, reprise)}$$

Because of the periodicity of the domain, these terms should be zero by the divergence theorem. However, because of the use of the DG discretization, these divergences will not be satisfied exactly. The figures show that, when p_x is less resolved, these divergences are poorly behaved, and the numerical fluxes have to compensate for them.

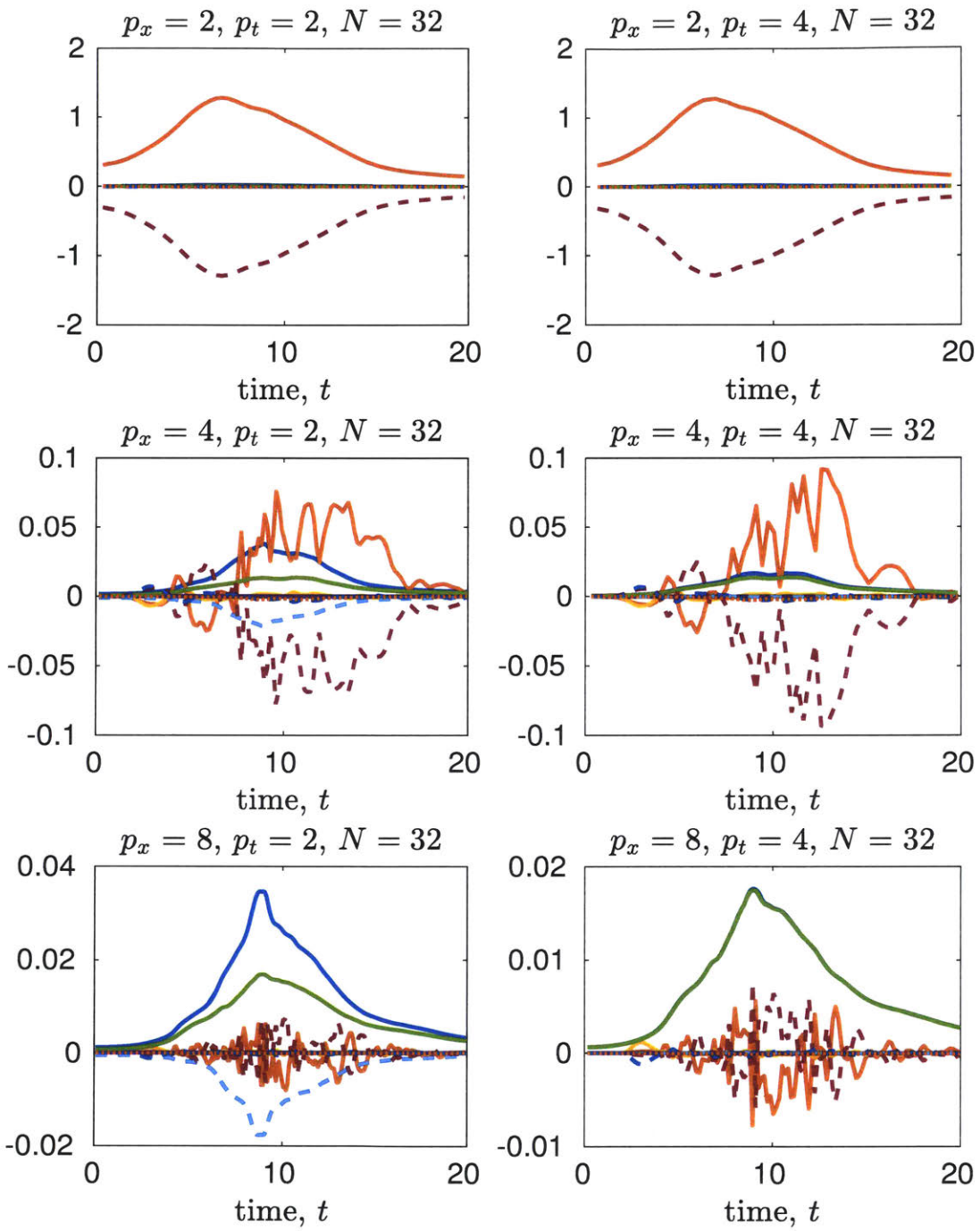

Figure 4-17: Entropy transport for $N = 32$ cases. Solid blue line: $(\Delta S/\Delta t)^{t}_{\text{flux}}$; solid orange line: $(\Delta S/\Delta t)^{I}_{\text{flux}}$; solid yellow line: $(\Delta S/\Delta t)^{\text{heat}}_{\text{diff}}$; solid purple line: $(\Delta S/\Delta t)^{\text{heat}}_{\text{prod}}$; solid green line: $(\Delta S/\Delta t)^{\text{shear}}_{\text{prod}}$; dashed cyan line: $(\Delta S/\Delta t)^{t}_{\text{disc}}$; dashed maroon line: $(\Delta S/\Delta t)^{I}_{\text{disc}}$; dashed navy line: $(\Delta S/\Delta t)^{V}_{\text{disc}}$; dotted yellow line: $(\Delta S/\Delta t)^{I}_{\text{flux}} + (\Delta S/\Delta t)^{I}_{\text{disc}}$.

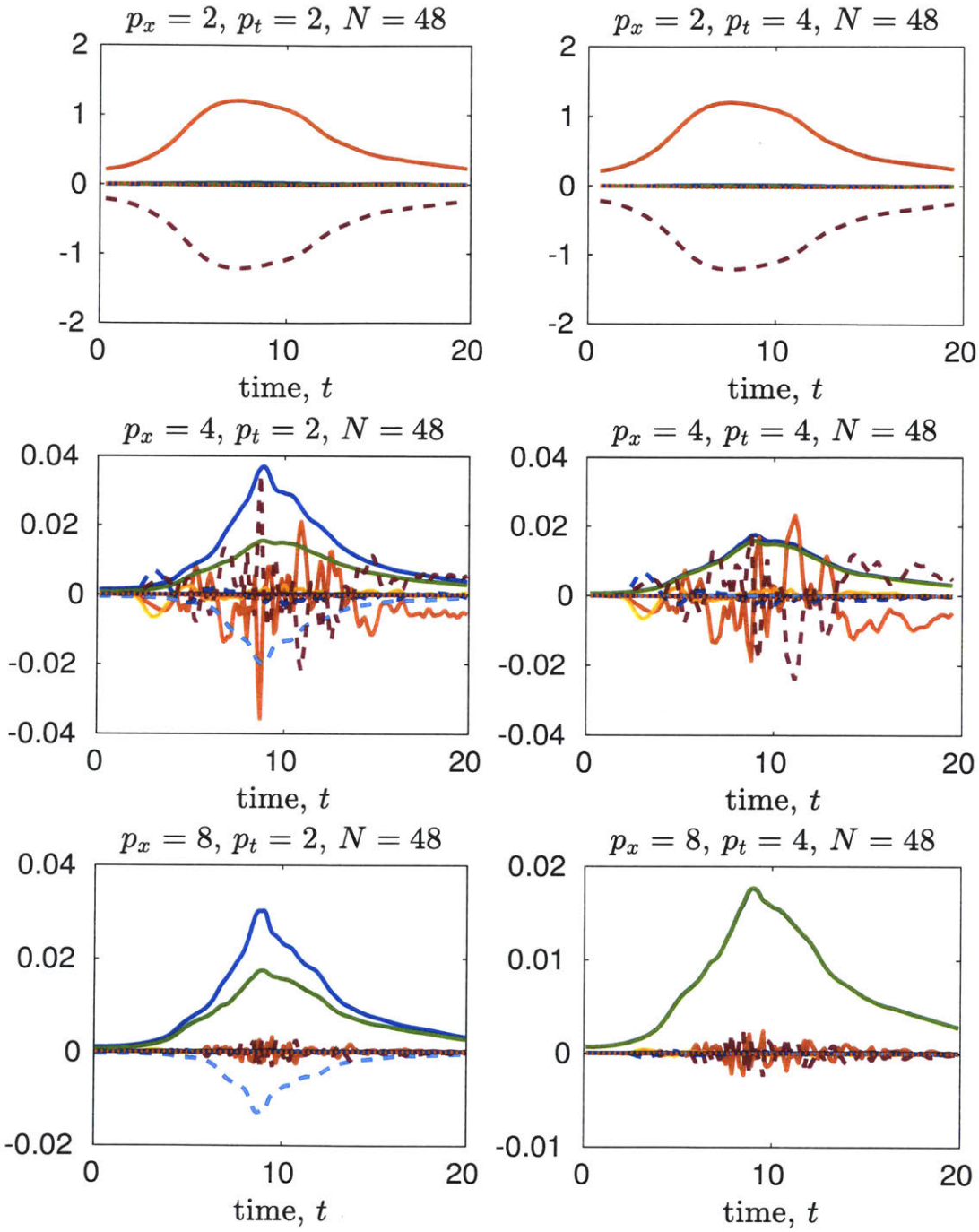

Figure 4-18: Entropy transport for $N = 48$ cases. Solid blue line: $(\Delta S/\Delta t)^{t}_{\text{flux}}$; solid orange line: $(\Delta S/\Delta t)^{I}_{\text{flux}}$; solid yellow line: $(\Delta S/\Delta t)^{\text{heat}}_{\text{diff}}$; solid purple line: $(\Delta S/\Delta t)^{\text{heat}}_{\text{prod}}$; solid green line: $(\Delta S/\Delta t)^{\text{shear}}_{\text{prod}}$; dashed cyan line: $(\Delta S/\Delta t)^{t}_{\text{disc}}$; dashed maroon line: $(\Delta S/\Delta t)^{I}_{\text{disc}}$; dashed navy line: $(\Delta S/\Delta t)^{V}_{\text{disc}}$; dotted yellow line: $(\Delta S/\Delta t)^{I}_{\text{flux}} + (\Delta S/\Delta t)^{I}_{\text{disc}}$.

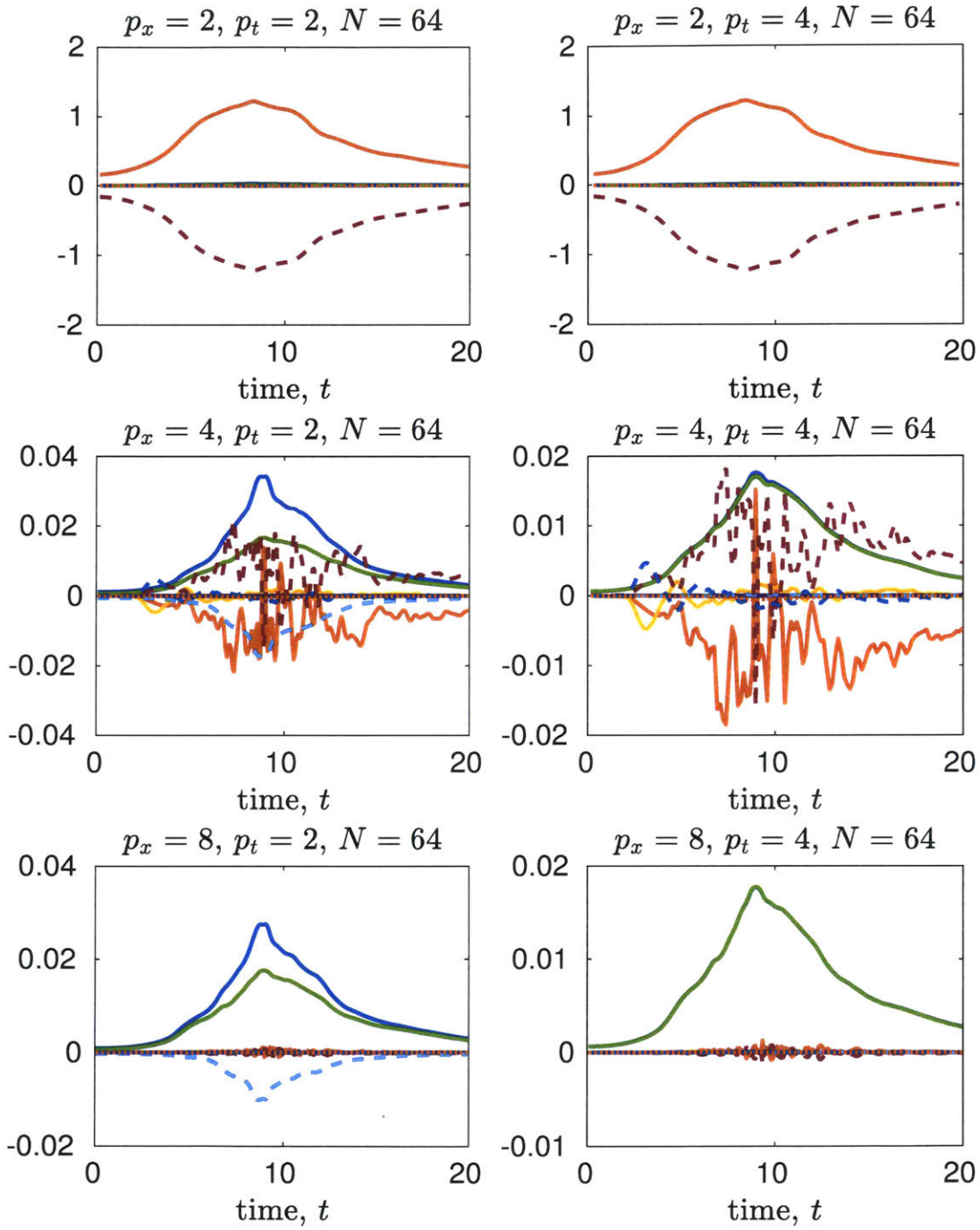

Figure 4-19: Entropy transport for $N = 64$ cases. Solid blue line: $(\Delta S/\Delta t)^{t}_{\text{flux}}$; solid orange line: $(\Delta S/\Delta t)^{I}_{\text{flux}}$; solid yellow line: $(\Delta S/\Delta t)^{\text{heat}}_{\text{diff}}$; solid purple line: $(\Delta S/\Delta t)^{\text{heat}}_{\text{prod}}$; solid green line: $(\Delta S/\Delta t)^{\text{shear}}_{\text{prod}}$; dashed cyan line: $(\Delta S/\Delta t)^{t}_{\text{disc}}$; dashed maroon line: $(\Delta S/\Delta t)^{I}_{\text{disc}}$; dashed navy line: $(\Delta S/\Delta t)^{V}_{\text{disc}}$; dotted yellow line: $(\Delta S/\Delta t)^{I}_{\text{flux}} + (\Delta S/\Delta t)^{I}_{\text{disc}}$.

4.2.6 Constant degree-of-freedom studies

In this section, we will consider variation of the results of cases with a similar number of spatial degrees of freedom. The number of degrees of freedom is just the number of unknowns per state variable in space:

$$N_{\mathrm{DOF},x} = Np_x \tag{4.16}$$

We first look at the case of $N_{\mathrm{DOF},x} = 128$, with $p_t = 4$. For these cases, we will have a resolution relative to DNS of $(\delta x/\eta) = 3.68$ and $(\delta t/\tau_\eta) = 1.73$. In Figures 4-20 and 4-21, we can see that the high-order solution has favorable results to the low order ones, in terms of converging to the spectral solution for the dissipation of kinetic energy. In Figure 4-22,

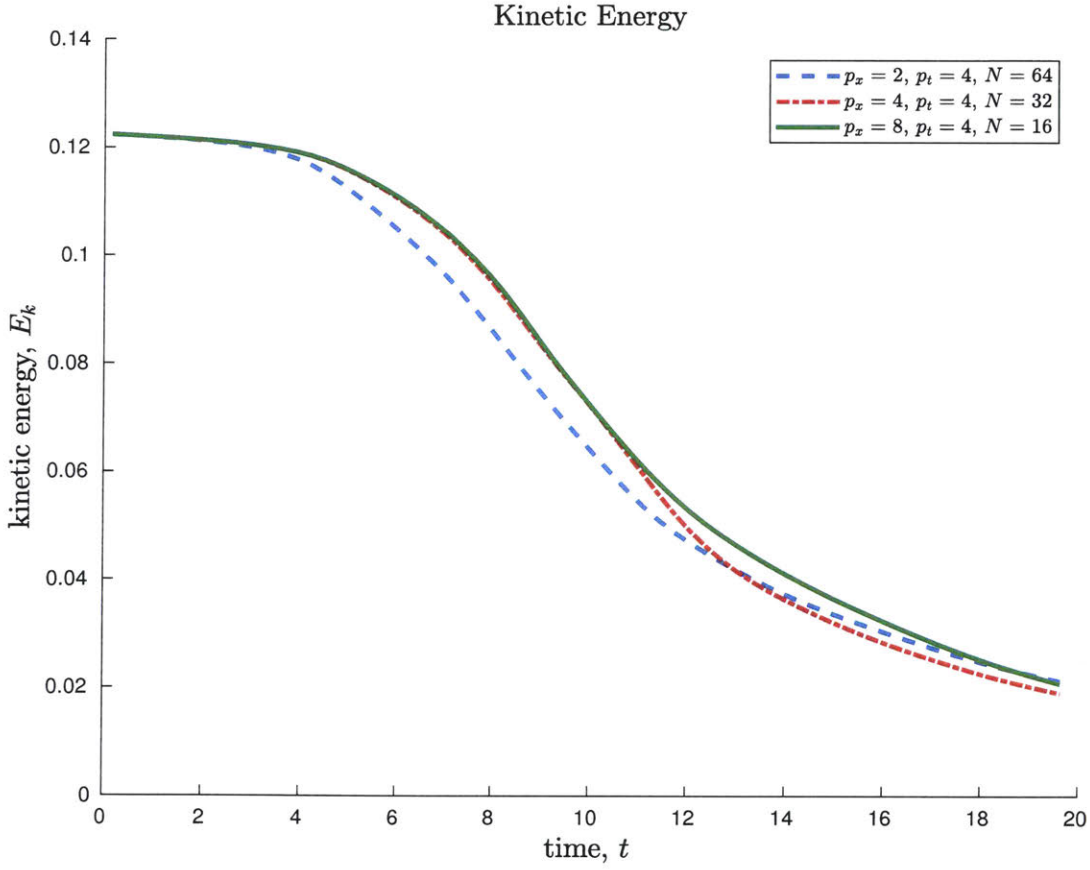

Figure 4-20: Kinetic energy evolution for Taylor-Green vortex problem with $N_{\mathrm{DOF},x} = 128$ and $p_t = 4$.

we can see that the inaccuracies are correlated to entropy production by the inviscid solver.

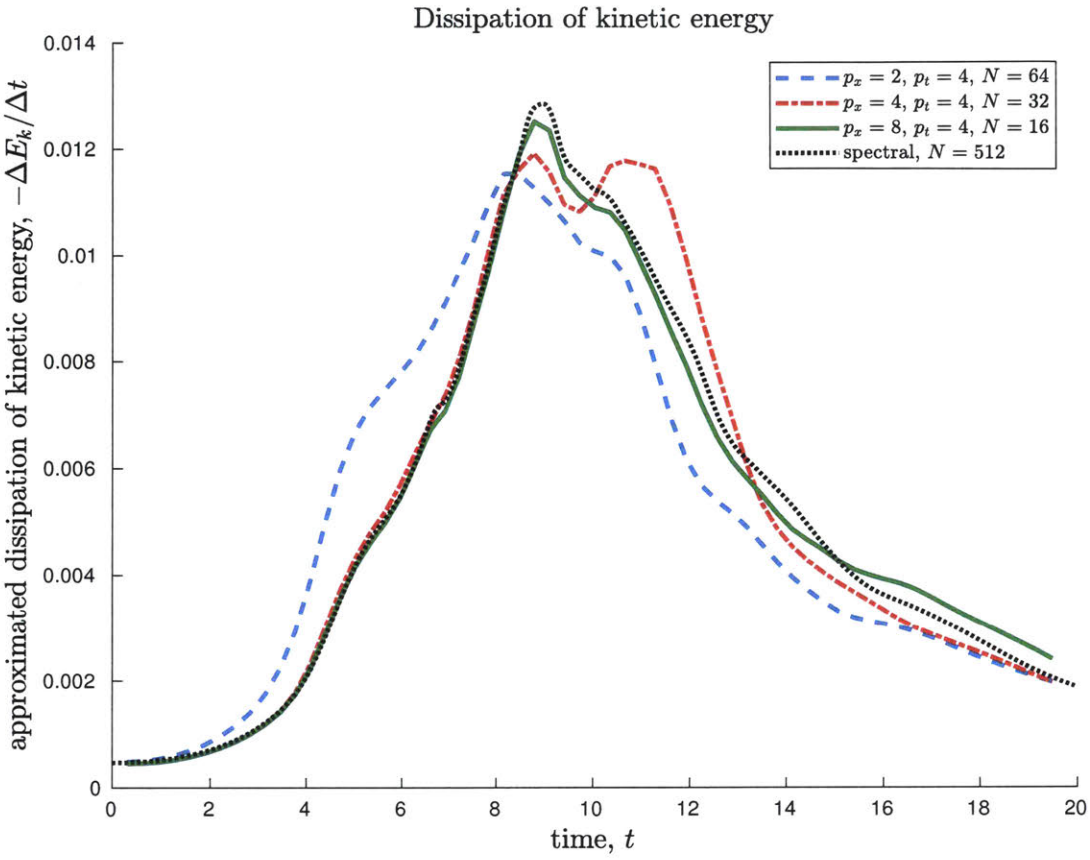

Figure 4-21: Dissipation of kinetic energy for Taylor-Green vortex problem with $N_{\mathrm{DOF},x} = 128$ and $p_t = 4$.

We repeat this analysis, this time using cases with $N_{\mathrm{DOF},x} = 64$ and $p_t = 4$, for which $(\delta x/\eta) = 7.36$ and $(\delta t/\tau_\eta) = 3.46$. The kinetic energy evolution is shown in Figure 4-23, and the dissipation is shown in Figure 4-24. At this level of underresolution, the high-order solution, for the first time, notably deviates from the spectral solution. However, even when it fails to capture the dissipative peak, it seems to capture the overall temporal evolution very well. Nonetheless, the high-order solution is the most accurate for a fixed $N_{\mathrm{DOF},x}$, and the lower-order solutions deteriorate in accuracy much more quickly than the high-order solutions.

Finally, we compare the results of all of the $p_x = 8$, $p_t = 4$ solutions that are used in this thesis. In Figures 4-25 and 4-26, we can see the kinetic energy evolution and dissipation

of kinetic energy for these cases. Overall, agreement looks good, with in particular the $N = 8$ solution showing some deviations from the other two cases. It seems, especially with the entropy peak being cutoff in the $N = 8$ solution, that the "modeling effect" of the DG discretization is doing a commendable job of generating entropy correctly. In Figure 4-27, we can see how each term contributes to the entropy variation in time. Based on these results, we can see that when high-order discretizations are used, the viscous and inviscid numerics both contribute to the so-called modeling effect and to the entropy variation of the system. In particular, at high-order, the presence of a significant inviscid flux does not necessarily correlate to a premature or excessive generation of entropy on the domain.

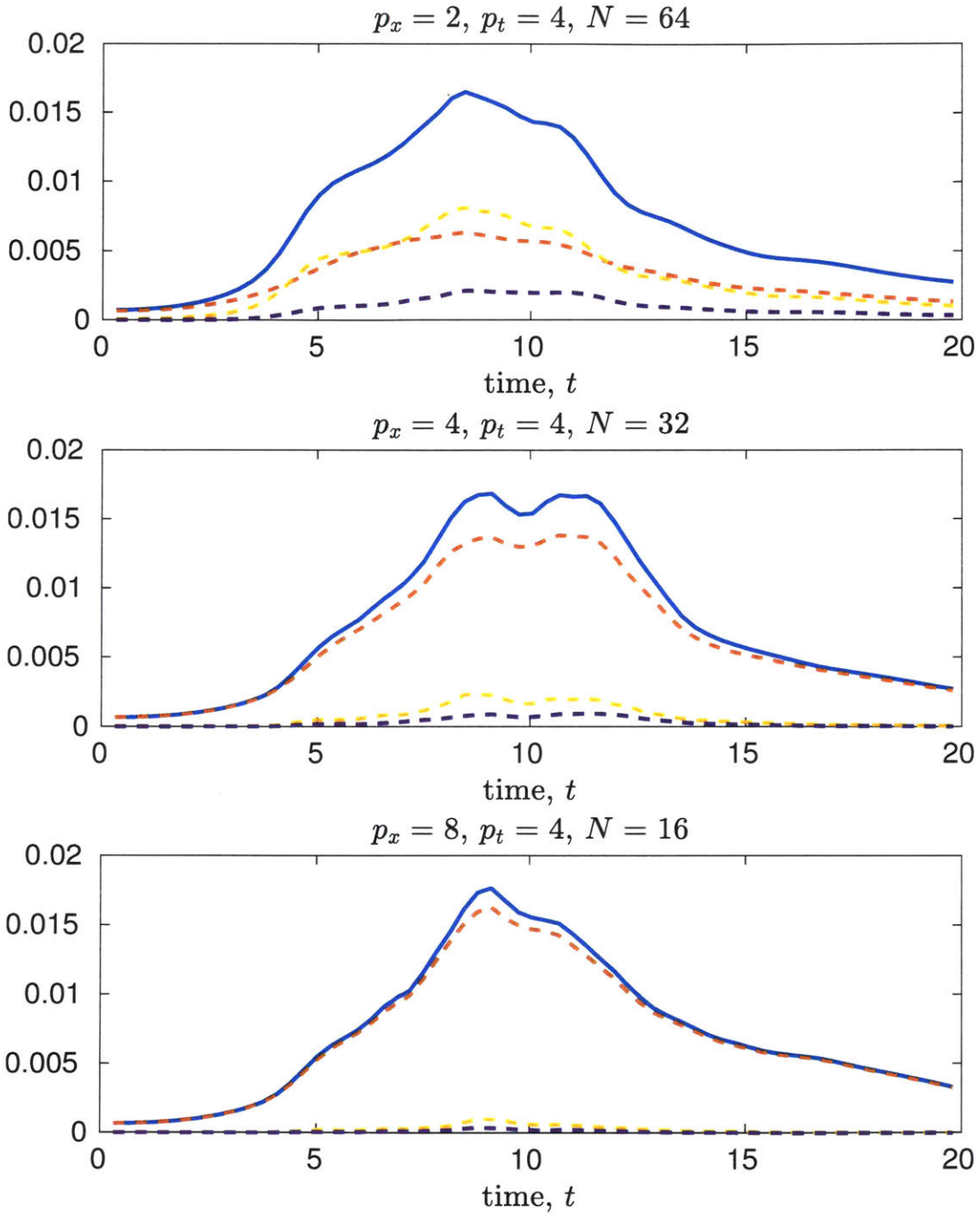

Figure 4-22: Breakdown of entropy generation for $N_{\mathrm{DOF},x} = 128$ cases. Solid blue line: $(\Delta S)^t_{\mathrm{total}}$, red dashed line: $(\Delta S)_{\mathrm{prod}}$, yellow dashed line: $-(\Delta S)^I$, purple dashed line: $-(\Delta S)^V$.

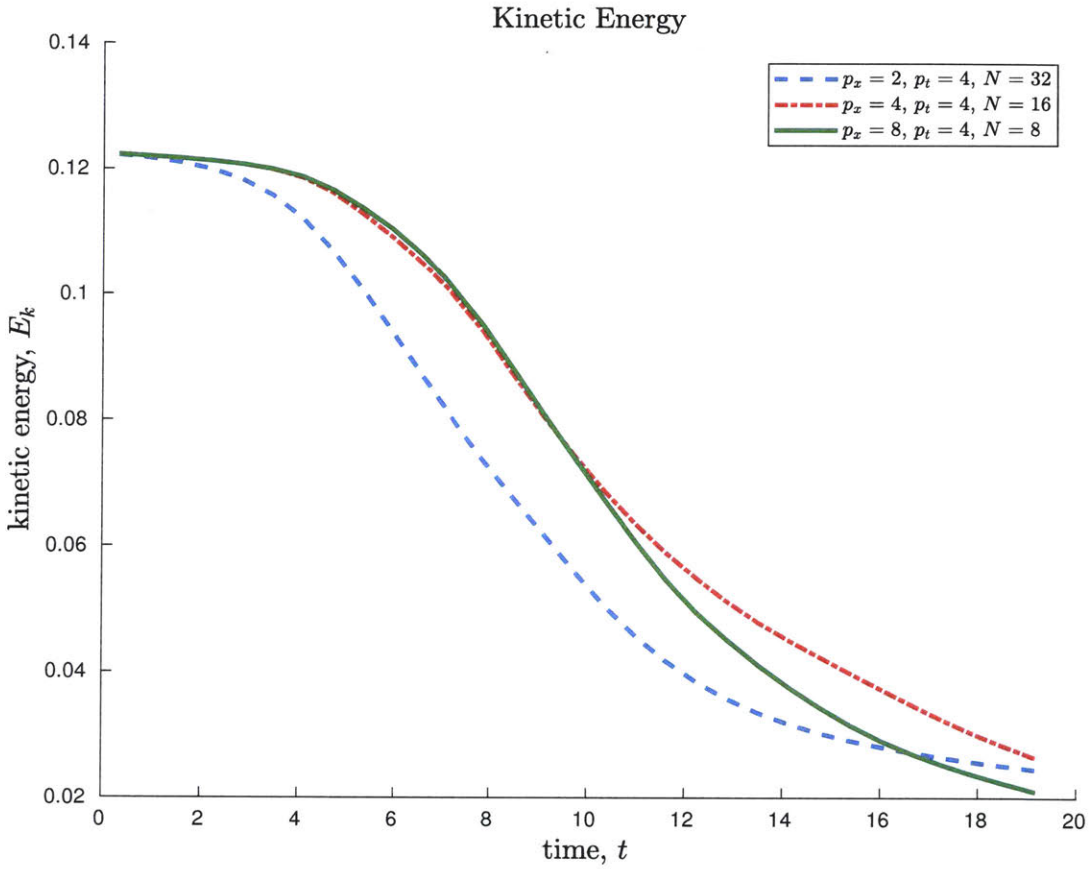

Figure 4-23: Kinetic energy evolution for Taylor-Green vortex problem with $N_{\mathrm{DOF},x} = 64$ and $p_t = 4$.

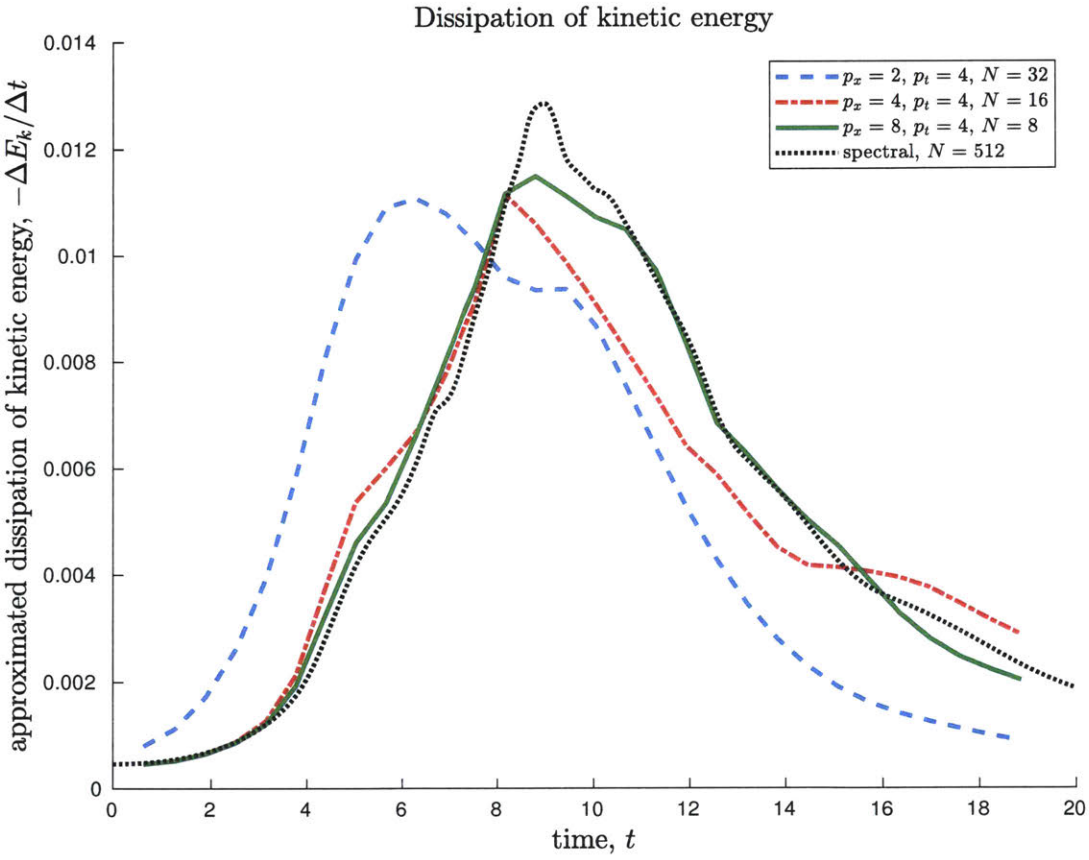

Figure 4-24: Dissipation of kinetic energy for Taylor-Green vortex problem with $N_{\mathrm{DOF},x} = 64$ and $p_t = 4$.

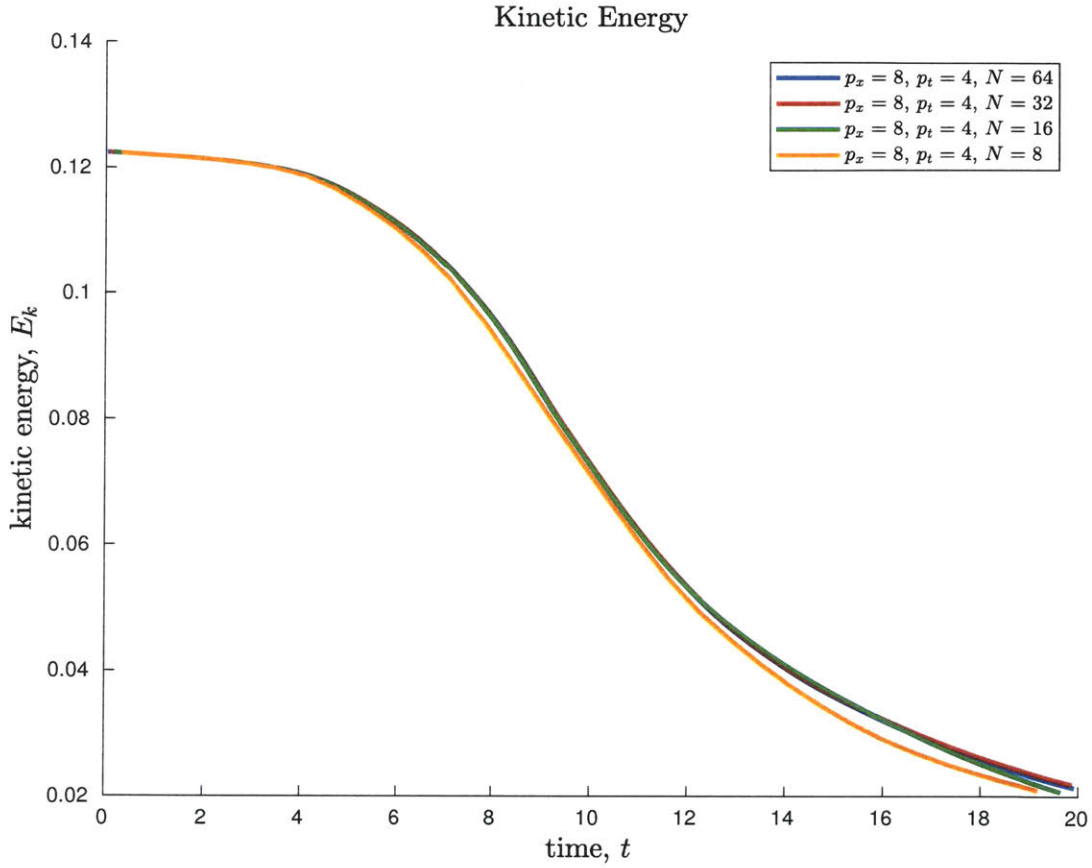

Figure 4-25: Kinetic energy evolution for Taylor-Green vortex problem with $p_x = 8$ and $p_t = 4$, with $N \in \{8, 16, 32\}$.

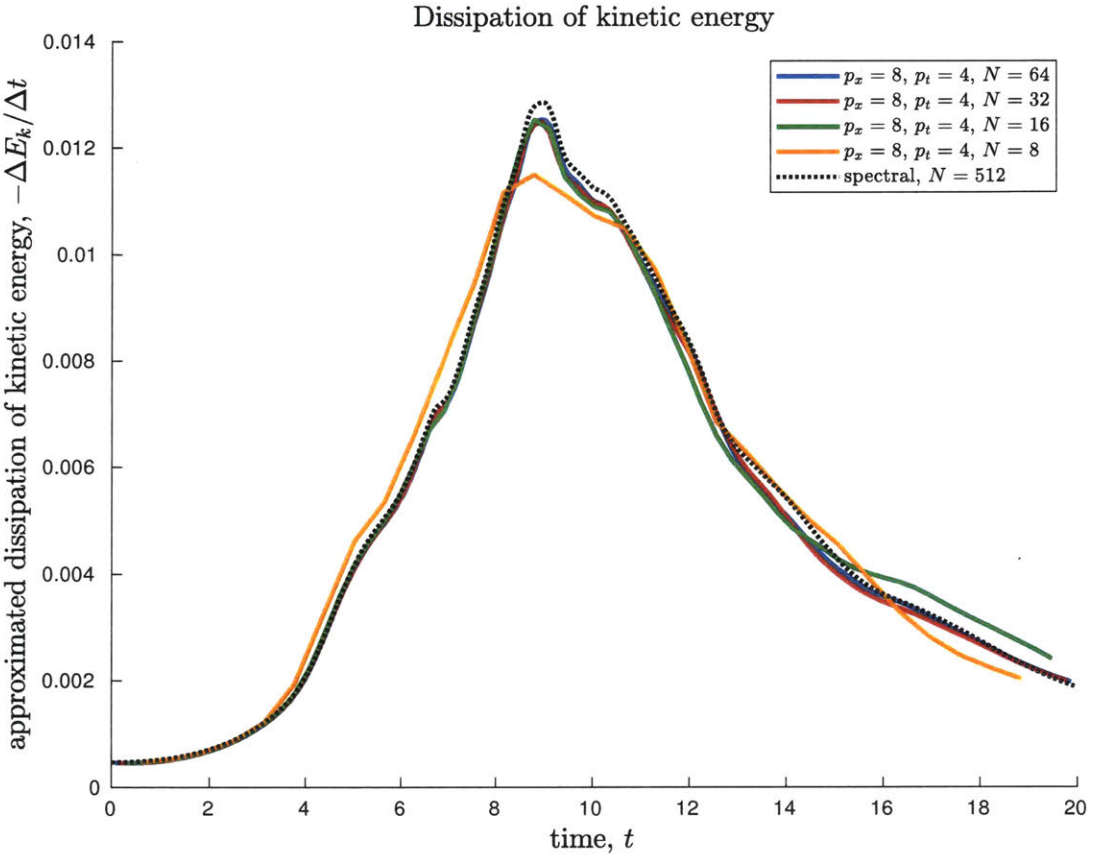

Figure 4-26: Dissipation of kinetic energy for Taylor-Green vortex problem with $p_x = 8$ and $p_t = 4$, with $N \in \{8, 16, 32\}$.

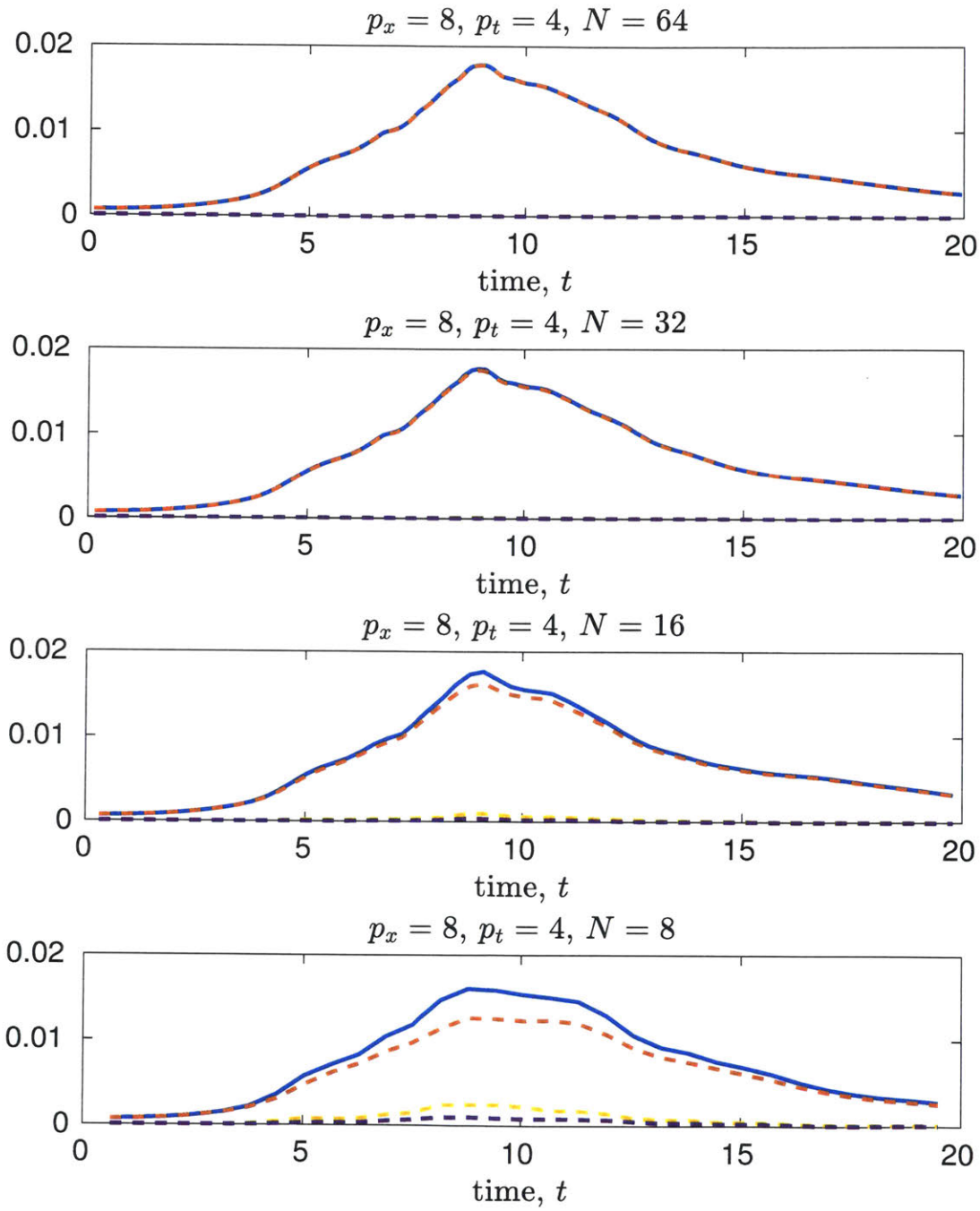

Figure 4-27: Breakdown of entropy generation for $p_x = 8$, $p_t = 4$ cases. Solid blue line: $(\Delta S)^t_{\text{total}}$, red dashed line: $(\Delta S)_{\text{prod}}$, yellow dashed line: $-(\Delta S)^I$, purple dashed line: $-(\Delta S)^V$.

Chapter 5

Conclusions and future work

5.1 Summary

We have developed a framework within the discontinuous Galerkin formulation for the Navier-Stokes equations to understand how the discretization produces or destroys entropy in order to satisfy a discrete version of the Clausius-Duhem statement. This framework was then used to look at how, in various underresolved simulations of the Taylor-Green vortex problem, entropy is generated by different stabilization terms introduced by the numerical flux functions.

We can see that when low spatial order (p_x) polynomials are used to represent the solution, excess entropy is generated by the inviscid numerical flux, which persists even into cases with large numbers of elements (N). This effect seems to penalize the use of low-order DG schemes for implicit LES of turbulent flows. At a fixed number of degrees of freedom, it seems that the simulation will be significantly inaccurate if p_x is chosen small and exhibit excess entropy generation from the inviscid solver.

The effect of the temporal discretization seems to be somewhat benign. When a low temporal order ($p_t = 2$) is chosen, the entropy generated by the temporal jump can be a large contributor to the total energy variation on a timeslab. However, when the contribution of the temporal jump is large, because it is not actively stabilized by the scheme, it does

not seem to contribute an aphysical entropy surplus. The effect of the temporal jump seems to be to prevent the inviscid and viscous solvers from contributing excess entropy to the system. With the higher temporal order ($p_t = 4$), entropy generated by the jump term is minimal, and the resolved entropy variaton on a timeslab accounts for almost all of the total entropy variation.

When a simulation uses a significantly high polynomial order, it seems that the entropy production converges quickly to that of the most resolved cases. The temporal evolution of kinetic energy is well captured for high p_x, even when relatively few elements are used in a given direction.

With this said, it seems that error is induced in the high-order simulations whenever the discretization terms are producing entropy. This tends to happen for high p_x cases on a fixed number of degrees of freedom. It seems that some care must be taken when evaluating LES discretizations at a fixed number of degrees of freedom. For a fixed number of degrees of freedom, the high p_x, low N results have apparently, more ability to resolve flow structures. The approximation for relating the resolved scales for polynomial respresentation in (4.6) and (4.7) may be too crude for this relationship, and a better rule-of-thumb may be appropriate for determining tradeoffs than the number of degrees of freedom.

5.2 Future directions

In light of these results, there is much to be further investigated. First of all, the limited Reynolds numbers used in this work are not enough to unequivocally state that the discretization adequately models the small scales. At $Re = 1600$, the flow is sufficiently turbulent, but it is quite possible that at higher Reynolds numbers, the accuracy when underresolved that we observe for high-order solutions may not be robust. Similarly, this effect may not be robust for flows that are not strictly in the low Mach number regime. Moreover, the choice of the Taylor-Green vortex problem means that the turbulence generated here is homogeneous and isotropic. This analysis can be extended to canonical problems of non-homogeneous turbulence, to evaluate how the stabilization accounts for unresolved entropy effects in these

more complex geometries.

Additionally, there may be potential for more local analysis of these terms. The analysis that leads to (3.16) and the analysis that follows is based on testing with $\mathbf{v}$. We can also test with a function $\mathbf{w}$ that only has support on a given element and takes the value of $\mathbf{v}$ on that element. This means we can effectively use (3.16) and the other analyses that are based on the weak form governing equations locally on the elements. Not only that, but by using the lifting operator (defined in Equation 3.5) on (3.16), we may be able to localize the entropy generation effects within elements. Using the data that would result from such an analysis, we could then consider how the entropy generation by the discretization localizes compared to known behaviors for the canonical flows of interest, via, for example, DNS studies.

Bibliography

[1] John D. Anderson. *Fundamentals of Aerodynamics.* McGraw-Hill, Boston, USA, 2001.

[2] Andrew Aspden, Nikos Nikiforakis, Stuart Dalziel, John Bell, et al. Analysis of implicit LES methods. *Communications in Applied Mathematics and Computational Science*, 3(1):103–126, 2008.

[3] Timothy J. Barth. Numerical methods for gasdynamic systems on unstructured meshes. In *An Introduction to Recent Developments in Theory and Numerics for Conservation Laws*, pages 195–285. Springer, 1999.

[4] F. Bassi and S. Rebay. GMRES discontinuous Galerkin solution of the compressible Navier-Stokes equations. In *Discontinuous Galerkin Methods*, pages 197–208. Springer, 2000.

[5] Laslo T. Diosady and Scott M. Murman. Design of a variational multiscale method for high reynolds number compressible flows. In *21st AIAA Computational Fluid Dynamics Conference*, 2013.

[6] Laslo T. Diosady and Scott M. Murman. Higher-order methods for compressible turbulent flows using entropy variables. In *53rd AIAA Aerospace Sciences Meeting*, 2015.

[7] Dimitris Drikakis, Marco Hahn, Fernando F Grinstein, Carl R. DeVore, Christer Fureby, Mattias Liefvendahl, and David L. Youngs. 4 Numerics for ILES 4a Limiting Algorithms. *Implicit Large Eddy Simulation: Computing Turbulent Fluid Dynamics*, page 94, 2007.

[8] A.J. Favre. Equations des gaz turbulents compressibles. 2. methode des vitesses moyennes methode des vitesses macroscopiques ponderees par la masse volumique. *Journal de Mecanique*, 4(4):391, 1965.

[9] Pablo Fernandez, N.C. Nguyen, and Jaime Peraire. Subgrid-scale modeling and implicit numerical dissipation in DG-based Large-Eddy Simulation. In *23rd AIAA Computational Fluid Dynamics Conference*, 2017.

[10] Eric Garnier, Nikolaus Adams, and Pierre Sagaut. *Large eddy simulation for compressible flows.* Springer Science & Business Media, 2009.

[11] Gregor J. Gassner and Andrea D. Beck. On the accuracy of high-order discretizations for underresolved turbulence simulations. *Theoretical and Computational Fluid Dynamics*, 27(3-4):221–237, 2013.

[12] A.E. Green and G.I. Taylor. Mechanism of the production of small eddies from larger ones. In *Proceedings of the Royal Society A*, volume 158, pages 499–521, 1937.

[13] Amiram Harten, James M. Hyman, Peter D. Lax, and Barbara Keyfitz. On finite-difference approximations and entropy conditions for shocks. *Communications on pure and applied mathematics*, 29(3):297–322, 1976.

[14] Thomas J.R. Hughes, L.P. Franca, and M. Mallet. A new finite element formulation for computational fluid dynamics: I. symmetric forms of the compressible Euler and Navier-Stokes equations and the second law of thermodynamics. *Computer Methods in Applied Mechanics and Engineering*, 54(2):223–234, 1986.

[15] Farzad Ismail and Philip L. Roe. Affordable, entropy-consistent euler flux functions ii: Entropy production at shocks. *Journal of Computational Physics*, 228(15):5410–5436, 2009.

[16] Brian Edward Launder and Dudley Brian Spalding. *Mathematical models of turbulence.* Academic Press, 1972.

[17] A. Leonard. Energy cascade in large-eddy simulations of turbulent fluid flows. In *Advances in Geophysics*, volume 18, pages 237–248. Elsevier, 1975.

[18] Marcel Lesieur and Olivier Metais. New trends in large-eddy simulations of turbulence. *Annual Review of Fluid Mechanics*, 28(1):45–82, 1996.

[19] M. Pino Martin, Ugo Piomelli, and Graham V. Candler. Subgrid-scale models for compressible large-eddy simulations. *Theoretical and Computational Fluid Dynamics*, 13(5):361–376, 2000.

[20] Ugo Piomelli. Large-eddy simulation: achievements and challenges. *Progress in Aerospace Sciences*, (35), 1999.

[21] Osbourne Reynolds. On the dynamical theory of incompressible viscous fluids and the determination of the criterion. *Philosophical Transactions of the Royal Society A*, 186, 1895.

[22] William Rider and Len Margolin. From numerical analysis to implicit subgrid turbulence modeling. In *16th AIAA Computational Fluid Dynamics Conference*, page 4101, 2003.

[23] Philip L. Roe. Approximate Riemann solvers, parameter vectors, and difference schemes. *Journal of Computational Physics*, 43(2):357–372, 1981.

[24] Robert S. Rogallo and Parviz Moin. Numerical simulation of turbulent flows. *Annual Review of Fluid Mechanics*, 16(1):99–137, 1984.

[25] Philipe R. Spalart and Steven Allmaras. A one-equation turbulence model for aerodynamic flows. In *30th AIAA Aerospace Sciences Meeting and Exhibition*, 1992.

[26] Philippe R. Spalart. Strategies for turbulence modelling and simulations. *International Journal of Heat and Fluid Flow*, 21(3):252–263, 2000.

[27] Eli Turkel. Improving the accuracy of central difference schemes. In *11th International Conference on Numerical Methods in Fluid Dynamics*, pages 586–591. Springer, 1989.

[28] Wim M. Van Rees, Anthony Leonard, D.I. Pullin, and Petros Koumoutsakos. A comparison of vortex and pseudo-spectral methods for the simulation of periodic vortical flows at high reynolds numbers. *Journal of Computational Physics*, 230(8):2794–2805, 2011.

[29] D.C. Wilcox. *Turbulence Modeling for CFD.* DCW Industries, California, USA, 2006.

Appendix A

Inviscid and viscous numerical fluxes

A simplified statement of the DG weak form for Navier-Stokes is given by:

$$\sum_{\kappa}\Big\{-\int_I\int_\kappa \frac{\partial \mathbf{w}}{\partial t}^T \mathbf{u}_h \;\mathrm{d}\mathbb{V}\,\mathrm{d}t + \int_\kappa \left(\mathbf{w}(t_-^{n+1})^T\mathbf{u}_h(t_-^{n+1}) - \mathbf{w}(t_+^{n})^T\mathbf{u}_h(t_-^{n})\right)\;\mathrm{d}\mathbb{V}$$
$$+\int_I\oint_{\partial\kappa}\left(\mathbf{w}^T\widehat{\underline{\mathbf{F}}^I\cdot\underline{n}} - \mathbf{w}^T\widehat{\underline{\mathbf{F}}^V\cdot\underline{n}}\right)\;\mathrm{d}\mathbb{S}\,\mathrm{d}t - \int_I\int_\kappa(\nabla\mathbf{w}^T)\cdot(\underline{\mathbf{F}}^I-\underline{\mathbf{F}}^V)\;\mathrm{d}\mathbb{V}\,\mathrm{d}t\Big\} = 0 \quad \text{(A.1)}$$

A.1 Inviscid fluxes

The inviscid numerical flux is basically given by the method of Roe [23]. The inviscid Roe flux computes:

$$\widehat{\mathbf{F}} = \frac{1}{2}\left(\mathbf{F}(\mathbf{u}^+) + \mathbf{F}(\mathbf{u}^-) + \left|\overline{\mathbf{A}}\right|\left(\mathbf{u}^+ - \mathbf{u}^-\right)\right) \quad \text{(A.2)}$$

where, $\overline{\mathbf{A}}$ is a flux Jacobian evaluated about the Roe-average state, which is to be defined. We will use a shorthand for the normal fluxes:

$$\mathbf{F}_n = \begin{bmatrix} \rho v_n \\ \rho v_n u + p n_x \\ \rho v_n v + p n_y \\ \rho v_n w + p n_z \\ \rho v_n H \end{bmatrix} \quad \text{(A.3)}$$

with the normal velocity given by $v_n = un_x + vn_y + wn_z$, and the enthalpy defined by $H = E + \frac{p}{\rho}$. The Roe-averaged state is given by:

$$\begin{aligned}
\rho^{\text{Roe}} &= \sqrt{\rho^+ \rho^-} \\
u^{\text{Roe}} &= \frac{\sqrt{\rho^+}u^+ + \sqrt{\rho^-}u^-}{\sqrt{\rho^+} + \sqrt{\rho^-}} \\
v^{\text{Roe}} &= \frac{\sqrt{\rho^+}v^+ + \sqrt{\rho^-}v^-}{\sqrt{\rho^+} + \sqrt{\rho^-}} \\
w^{\text{Roe}} &= \frac{\sqrt{\rho^+}w^+ + \sqrt{\rho^-}w^-}{\sqrt{\rho^+} + \sqrt{\rho^-}} \\
H^{\text{Roe}} &= \frac{\sqrt{\rho^+}H^+ + \sqrt{\rho^-}H^-}{\sqrt{\rho^+} + \sqrt{\rho^-}}
\end{aligned} \tag{A.4}$$

The eigenvalues of the flux Jacobian are given by:

$$\lambda_0 = v_n + a \quad \lambda_1 = v_n - a \quad \lambda_2 = v_n \tag{A.5}$$

where a is the speed of sound defined by:

$$a^2 = (\gamma - 1)\left(H - \frac{1}{2}(\underline{V} \cdot \underline{V})\right) \tag{A.6}$$

According to the appendix of [27], the flux Jacobian can be applied to a vector using the form:

$$\overline{\mathbf{A}}\mathbf{x} = \lambda_2 \mathbf{x} + \bar{\mathbf{z}}_1 \mathbf{R}_1 + \bar{\mathbf{z}}_2 \mathbf{R}_2 \tag{A.7}$$

with right vectors given by:

$$\mathbf{R}_1 = \begin{bmatrix} 1 \\ u \\ v \\ w \\ H \end{bmatrix} \quad \mathbf{R}_2 = \begin{bmatrix} 0 \\ n_x \\ n_y \\ n_z \\ v_n \end{bmatrix} \tag{A.8}$$

and $\overline{\mathbf{z}}_1$ and $\overline{\mathbf{z}}_2$ given by:

$$\begin{aligned} \overline{\mathbf{z}}_1 &= \frac{\sigma_1}{a^2}\mathbf{L}_1^T\mathbf{x} + \frac{\sigma_2}{a}\mathbf{L}_2^T\mathbf{x} \\ \overline{\mathbf{z}}_2 &= \frac{\sigma_2}{c}\mathbf{L}_1^T\mathbf{x} + \sigma_1\mathbf{L}_2^T\mathbf{x} \end{aligned} \tag{A.9}$$

where $\mathbf{L}_1$ and $\mathbf{L}_2$ are left vectors given by:

$$\mathbf{L}_1 = \begin{bmatrix} \frac{\gamma-1}{2}\left(u^2+v^2+w^2\right) \\ -(\gamma-1)u \\ -(\gamma-1)v \\ -(\gamma-1)w \\ (\gamma-1) \end{bmatrix} \quad \mathbf{L}_2 = \begin{bmatrix} -v_n \\ n_x \\ n_y \\ n_z \\ 0 \end{bmatrix} \tag{A.10}$$

with, finally, scaling parameters σ_1 and σ_2 given by:

$$\sigma_1 = \frac{1}{2}\left(\lambda_0 + \lambda_1\right) - \lambda_2 \quad \sigma_2 = \frac{1}{2}\left(\lambda_0 - \lambda_2\right) \tag{A.11}$$

It should be noted that the `eddy` implementation of Roe's inviscid solver uses a slightly different definition for σ_1. Finally, we can ensure that eigenvalues are bounded away from zero by applying an "entropy-fix" [13] where:

$$\widetilde{|\lambda|} = \begin{cases} \frac{1}{2}\left(\varepsilon + \frac{\lambda^2}{\varepsilon}\right) & |\lambda| < \varepsilon \\ |\lambda| & \text{otherwise} \end{cases} \tag{A.12}$$

This method is used to compute $\widehat{\underline{\mathbf{F}}^I \cdot \underline{n}}$.

A.2 Viscous fluxes

For the viscous numerical flux term, $\mathbf{w}^T\widehat{\underline{\mathbf{F}}^V \cdot \underline{n}}$, we first note that this term uses a simplified form. In reality, this term incorporates all of the effects of the implementation of the second method of Bassi and Rebay, even though these effects are not captured in that particular

form. We can elaborate them completely by starting with the form of the viscous flux. The viscous flux can be restated as:

$$\underline{\mathbf{F}}^V = \underline{\underline{\overline{\mathbf{K}}}}(\mathbf{u}_h)\,\nabla\mathbf{u}_h \tag{A.13}$$

The second method of Bassi and Rebay replaces the residual terms due to the viscosity:

$$R^{\text{diff}}(\mathbf{u}_h,\mathbf{w}) = \sum_{\kappa}\left\{-\int_I\oint_{\partial\kappa}\widehat{\mathbf{w}^T\underline{\mathbf{F}}^V}\cdot\underline{n}\ \mathrm{dS}\ \mathrm{d}t + \int_I\int_\kappa\left(\nabla\mathbf{w}^T\right)\cdot\underline{\mathbf{F}}^V\ \mathrm{d}\mathbb{V}\ \mathrm{d}t\right\} \tag{A.14}$$

with:

$$\begin{aligned}
R^{\text{diff}}(\mathbf{u}_h,\mathbf{w}) = &\sum_{\kappa}\int_I\int_\kappa\left(\nabla\mathbf{w}^T\right)\cdot\underline{\underline{\overline{\mathbf{K}}}}(\mathbf{u}_h)\,\nabla\mathbf{u}_h\ \mathrm{d}\mathbb{V}\ \mathrm{d}t\\
&-\sum_{f\in\Gamma_i}\int_I\int_f\Big[\left\{\underline{\underline{\overline{\mathbf{K}}}}^T(\mathbf{u}_h)\left(\nabla\mathbf{w}\right)\right\}^T\cdot[[\mathbf{u}_h]]\\
&\qquad+[[\mathbf{w}]]\cdot\left\{\underline{\underline{\overline{\mathbf{K}}}}(\mathbf{u}_h)\left(\nabla\mathbf{u}_h+\eta_f\underline{r}_f\left([[\mathbf{u}_h]]\right)\right)\right\}\Big]\ \mathrm{dS}\ \mathrm{d}t\\
&-\sum_{f\in\Gamma_b}\int_I\int_f\Big[\left(\underline{n}^+\cdot\underline{\underline{\overline{\mathbf{K}}}}(\mathbf{u}_b)\left(\nabla\mathbf{w}\right)^+\right)^T\left(\mathbf{u}_h^+-\mathbf{u}_b\right)\\
&+\left(\mathbf{w}^+\right)^T\mathcal{F}^b\left(\underline{n}^+\cdot\underline{\underline{\overline{\mathbf{K}}}}(\mathbf{u}_b)\left(\left(\nabla\mathbf{u}_h\right)^+ +\eta_f\underline{r}_f^b\left(\mathbf{u}_h^+-\mathbf{u}_b\right)\underline{n}^+\right);\ \text{B.C.}\right)\Big]\ \mathrm{dS}\ \mathrm{d}t
\end{aligned} \tag{A.15}$$

We introduced a few things here. The lifting operator $\underline{r}_f : [\mathcal{V}_h(f)]^d \mapsto [\mathcal{V}_h]^d$ associated with a face f is given by:

$$\sum_{\kappa\in\kappa_f}\int_\kappa\nabla\boldsymbol{\phi}\cdot^T\underline{r}_f(\boldsymbol{\psi})\ \ \mathrm{d}\mathbb{V} = -\int_f\{\boldsymbol{\phi}\cdot\underline{n}\}^T\boldsymbol{\psi}\ \ \mathrm{dS}\ \ \forall\,\boldsymbol{\phi}\in[\mathcal{V}_h]^d \tag{3.5}$$

and κ_f is defined as the set of all elements sharing a face f. The averaging operator of an arbitrary quantity X on a face f is given by:

$$\{X\} = \frac{1}{2}\left((X)^+ + (X)^-\right) \tag{A.16}$$

Meanwhile, the jump operator on a face f applied to an arbitrary quantity X is given by:

$$[[X]] = (X)^+ \underline{n}^+ + (X)^- \underline{n}^- \tag{A.17}$$

This can be rewritten as:

$$\begin{aligned}
R^{\text{diff}}(\mathbf{u}_h, \mathbf{w}) = &\sum_{\kappa} \int_I \int_{\kappa} (\nabla \mathbf{w}^T) \cdot \underline{\underline{\overline{\mathbf{K}}}} \cdot (\nabla \mathbf{u}_h) \quad \mathrm{d}\mathbb{V}\, \mathrm{d}t \\
&- \sum_{f \in \Gamma_i} \int_I \int_f \Big[\frac{1}{2} \left(\left(\underline{\underline{\overline{\mathbf{K}}}}(\mathbf{u}_h^+) \right)^T (\nabla \mathbf{w})^+ + \left(\underline{\underline{\overline{\mathbf{K}}}}(\mathbf{u}_h^-) \right)^T (\nabla \mathbf{w})^- \right) \cdot \left(\mathbf{u}_h^+ \underline{n}^+ + \mathbf{u}_h^- \underline{n}^- \right) \\
&\qquad + \left(\mathbf{w}^+ \underline{n}^+ + \mathbf{w}^- \underline{n}^- \right) \cdot \frac{1}{2} \left(\underline{\underline{\overline{\mathbf{K}}}}(\mathbf{u}_h^+) \left(\nabla \mathbf{u}_h^+ + \eta_f \underline{r}_f \left([[\mathbf{u}_h]] \right) \right) \right. \\
&\qquad\qquad \left. + \underline{\underline{\overline{\mathbf{K}}}}(\mathbf{u}_h^-) \left(\nabla \mathbf{u}_h^- + \eta_f \underline{r}_f \left([[\mathbf{u}_h]] \right) \right) \right) \Big] \quad \mathrm{dS}\, \mathrm{d}t \\
&- \sum_{f \in \Gamma_b} \int_I \int_f \Big[\left(\underline{n}^+ \cdot \underline{\underline{\overline{\mathbf{K}}}}(\mathbf{u}_b) (\nabla \mathbf{w})^+ \right)^T \left(\mathbf{u}_h^+ - \mathbf{u}_b \right) \\
&\qquad + \left(\mathbf{w}^+ \right)^T \mathcal{F}^b \left(\underline{n}^+ \cdot \underline{\underline{\overline{\mathbf{K}}}}(\mathbf{u}_b) \left((\nabla \mathbf{u}_h)^+ + \eta_f \underline{r}_f^b \left(\mathbf{u}_h^+ - \mathbf{u}_b \right) \underline{n}^+ \right) ;\ \text{B.C.} \right) \Big] \quad \mathrm{dS}\, \mathrm{d}t
\end{aligned} \tag{A.18}$$

For the cases of periodic boundaries, $\Gamma_b = \emptyset$ and Γ_i is the set of all spatial faces. Thus we can ignore the contributions from the boundary faces, $f \in \Gamma_b$ and we can say:

$$\begin{aligned}
R^{\text{diff}}(\mathbf{u}_h, \mathbf{w}) = &\sum_{\kappa} \int_I \int_{\kappa} (\nabla \mathbf{w}^T) \cdot \underline{\underline{\overline{\mathbf{K}}}} (\nabla \mathbf{u}_h) \quad \mathrm{d}\mathbb{V}\, \mathrm{d}t \\
&- \sum_{f \in \Gamma_i} \int_I \int_f \Big[\frac{1}{2} \left(\left(\underline{\underline{\overline{\mathbf{K}}}}(\mathbf{u}_h^+) \right)^T (\nabla \mathbf{w})^+ + \left(\underline{\underline{\overline{\mathbf{K}}}}(\mathbf{u}_h^-) \right)^T (\nabla \mathbf{w})^- \right) \cdot \left(\mathbf{u}_h^+ \underline{n}^+ + \mathbf{u}_h^- \underline{n}^- \right) \\
&\qquad + \left(\mathbf{w}^+ \underline{n}^+ + \mathbf{w}^- \underline{n}^- \right) \cdot \frac{1}{2} \left(\underline{\underline{\overline{\mathbf{K}}}}(\mathbf{u}_h^+) \left(\nabla \mathbf{u}_h^+ + \eta_f \underline{r}_f \left([[\mathbf{u}_h]] \right) \right) \right. \\
&\qquad\qquad \left. + \underline{\underline{\overline{\mathbf{K}}}}(\mathbf{u}_h^-) \left(\nabla \mathbf{u}_h^- + \eta_f \underline{r}_f \left([[\mathbf{u}_h]] \right) \right) \right) \Big] \quad \mathrm{dS}\, \mathrm{d}t
\end{aligned} \tag{A.19}$$

and for an equivalent statement, we can move these contributions to the element:

$$R^{\text{diff}}(\mathbf{u}_h, \mathbf{w}) = \sum_{\kappa} \Bigg\{ \int_I \int_\kappa \left(\nabla \mathbf{w}^T\right) \cdot \overline{\underline{\underline{\mathbf{K}}}} \left(\nabla \mathbf{u}_h\right) \ \mathrm{d}\mathbb{V} \ \mathrm{d}t$$
$$- \int_I \oint_{\partial\kappa} \Bigg[\frac{1}{2} \overline{\underline{\underline{\mathbf{K}}}}^T \left(\mathbf{u}_h\right) \left(\nabla \mathbf{w}\right) \cdot [[\mathbf{u}_h]]$$
$$+ \mathbf{w}^T \left\{ \overline{\underline{\underline{\mathbf{K}}}} \left(\mathbf{u}_h\right) \left(\nabla \mathbf{u}_h\right) \right\} \cdot \underline{n}$$
$$+ \mathbf{w}^T \left\{ \overline{\underline{\underline{\mathbf{K}}}} \left(\mathbf{u}_h\right) \right\} \eta_f \underline{r}_f \left([[\mathbf{u}_h]]\right) \cdot \underline{n} \Bigg] \ \mathrm{d}S \ \mathrm{d}t \Bigg\} \quad \text{(A.20)}$$

For hexahedra, it can be shown that the lifting operator on a face can be rewritten:

$$\underline{r}_f \left([[\mathbf{u}]]\right) = \underline{L} \, [[\mathbf{u}]] \quad \text{(A.21)}$$

where L is some parameter that is constant with respect to the solution but dependent on the geometry of the mesh, the discretization choice, etc. We will roll this dependent parameter into the definition $\underline{\eta}_f$ in the remainder of this appendix and in the main body of the text.

Now, we can write the total residual equation explicitly as it's calculated in the code:

$$-\sum_{\kappa} \int_I \int_\kappa \frac{\partial \mathbf{w}^T}{\partial t} \mathbf{u}_h \ \mathrm{d}\mathbb{V} \ \mathrm{d}t + \sum_{\kappa} \int_\kappa \left(\mathbf{w}(t_-^{n+1})^T \mathbf{u}_h(t_-^{n+1}) - \mathbf{w}(t_+^n)^T \mathbf{u}_h(t_-^n) \right) \ \mathrm{d}\mathbb{V}$$
$$- \sum_{\kappa} \int_I \int_\kappa \nabla \mathbf{w}^T \cdot \underline{\mathbf{F}}^I \ \mathrm{d}\mathbb{V} \ \mathrm{d}t + \sum_{\kappa} \int_I \int_\kappa \nabla \mathbf{w}^T \cdot \underline{\mathbf{F}}^V \ \mathrm{d}\mathbb{V} \ \mathrm{d}t$$
$$+ \sum_{f \in \Gamma_i} \int_I \int_f \left(\left(\mathbf{w}^T \widehat{\underline{\mathbf{F}}^I \cdot \underline{n}} \right)^+ + \left(\mathbf{w}^T \widehat{\underline{\mathbf{F}}^I \cdot \underline{n}} \right)^- \right) \ \mathrm{d}S \ \mathrm{d}t$$
$$- \sum_{f \in \Gamma_i} \int_I \int_f \frac{1}{2} \left(\left(\overline{\underline{\underline{\mathbf{K}}}}(\mathbf{u}_h^+) \right)^T \left(\nabla \mathbf{w}\right)^+ + \left(\overline{\underline{\underline{\mathbf{K}}}}(\mathbf{u}_h^-) \right)^T \left(\nabla \mathbf{w}\right)^- \right) \cdot \left(\mathbf{u}_h^+ \underline{n}^+ + \mathbf{u}_h^- \underline{n}^- \right) \ \mathrm{d}S \ \mathrm{d}t$$
$$- \sum_{f \in \Gamma_i} \int_I \int_f \left(\mathbf{w}^+ \underline{n}^+ + \mathbf{w}^- \underline{n}^- \right) \cdot \frac{1}{2} \left(\overline{\underline{\underline{\mathbf{K}}}}(\mathbf{u}_h^+) \left(\nabla \mathbf{u}_h^+ + \underline{\eta}_f [[\mathbf{u}_h]] \right) \right.$$
$$\left. + \overline{\underline{\underline{\mathbf{K}}}}(\mathbf{u}_h^-) \left(\nabla \mathbf{u}_h^- + \underline{\eta}_f [[\mathbf{u}_h]] \right) \right) \ \mathrm{d}S \ \mathrm{d}t = 0 \quad \text{(3.4)}$$

Appendix B

Entropy variable formulation

B.1 Transformations between conservative variable and entropy variable formulations

In this section, we formulate an entropy variable form that follows closely the methodology enumerated by [14], but disposes some less optimal choices, to ultimately get results similar to [3].

We have a new statement of the strong form:

$$\frac{\partial \mathbf{u}}{\partial t} + \nabla \cdot \left(\underline{\mathbf{F}}^{I} - \underline{\mathbf{F}}^{V^*} - \underline{\mathbf{F}}^{H^*} \right) = 0 \tag{B.1}$$

where, here the heat contribution is separated from the viscous contribution proper, with, as above:

$$\mathbf{u} = \begin{pmatrix} \rho \\ \rho u \\ \rho v \\ \rho w \\ \rho E \end{pmatrix} \quad \underline{V} = \begin{pmatrix} u \\ v \\ w \end{pmatrix} \tag{2.16, reprise}$$

$$\underline{\mathbf{F}}^I = \begin{bmatrix} \rho\underline{V}^T \\ \rho\underline{V}\underline{V}^T + p\underline{\underline{I}} \\ \rho\underline{V}^T(E + \frac{p}{\rho}) \end{bmatrix} = \begin{bmatrix} \rho u & \rho v & \rho w \\ \rho uu + p & \rho uv & \rho uw \\ \rho uv & \rho vv + p & \rho vw \\ \rho uw & \rho vw & \rho ww + p \\ \rho u\left(E + \frac{p}{\rho}\right) & \rho v\left(E + \frac{p}{\rho}\right) & \rho w\left(E + \frac{p}{\rho}\right) \end{bmatrix} \qquad \text{(2.18, reprise)}$$

and, slightly modified from above:

$$\underline{\mathbf{F}}^{V^*} = \begin{bmatrix} \underline{0}^T \\ \underline{\underline{\tau}} \\ \underline{V}^T\underline{\underline{\tau}} \end{bmatrix} = \begin{bmatrix} 0 & 0 & 0 \\ \tau_{11} & \tau_{12} & \tau_{13} \\ \tau_{21} & \tau_{22} & \tau_{23} \\ \tau_{31} & \tau_{32} & \tau_{33} \\ \underline{V}\cdot\underline{\tau}_1 & \underline{V}\cdot\underline{\tau}_2 & \underline{V}\cdot\underline{\tau}_3 \end{bmatrix} \qquad \text{(B.2)}$$

$$\underline{\mathbf{F}}^{H^*} = \begin{bmatrix} \underline{0}^T \\ \underline{\underline{0}} \\ -\kappa_T\nabla T \end{bmatrix} = \begin{bmatrix} 0 & 0 & 0 \\ 0 & 0 & 0 \\ 0 & 0 & 0 \\ 0 & 0 & 0 \\ -\kappa_T\frac{\partial T}{\partial x} & -\kappa_T\frac{\partial T}{\partial y} & -\kappa_T\frac{\partial T}{\partial z} \end{bmatrix} \qquad \text{(B.3)}$$

with our familiar definitions:

$$p = (\gamma - 1)\left(\rho E - \frac{1}{2}\rho\underline{V}\cdot\underline{V}\right) \qquad \text{(1.6, reprise)}$$

and

$$\tau_{ij} = \mu\left(\frac{\partial u_i}{\partial x_j} + \frac{\partial u_j}{\partial x_i}\right) - \frac{2}{3}\mu\frac{\partial u_k}{\partial x_k}\delta_{ij} \qquad \text{(1.3, reprise)}$$

We note that $\underline{\mathbf{F}}^V = \underline{\mathbf{F}}^{V^*} + \underline{\mathbf{F}}^{H^*}$.

We can show that non-dimensional entropy can be viewed as an increasing function of

time that falls out of the state for an ideal gas:

$$s = \ln\left(p\rho^{-\gamma}\right) + C \tag{2.5}$$

with some constant C. We take $C = 0$ for simplicity. One thing leads to another and we get to the set of symmetrizing entropy variables:

$$\mathbf{v} = \begin{bmatrix} -\frac{s}{\gamma-1} + \frac{\gamma+1}{\gamma-1} - \frac{\rho E}{p} \\ \frac{\rho u}{p} \\ \frac{\rho v}{p} \\ \frac{\rho w}{p} \\ -\frac{\rho}{p} \end{bmatrix} \tag{2.22}$$

which corresponds to a general entropy function $H = -\frac{\rho s}{\gamma-1}$

Using $u_i = [\mathbf{u}]_i$, we can write the pressure in terms of the state function:

$$p = (\gamma - 1)\left(u_5 - \frac{1}{2}\frac{(u_2^2 + u_3^2 + u_4^2)}{u_1}\right) \tag{B.4}$$

and, leveraging that definition, the nondimensional state entropy:

$$s = \ln\left(pu_1^{-\gamma}\right) = \ln\left((\gamma - 1)\left(u_5 - \frac{1}{2}\frac{(u_2^2 + u_3^2 + u_4^2)}{u_1}\right)u_1^{-\gamma}\right) \tag{B.5}$$

And, with these, we can write the nonlinear transformation between $\mathbf{u}$ and $\mathbf{v}$:

$$\begin{aligned}
v_1 = & -\frac{s}{\gamma-1}+\frac{\gamma+1}{\gamma-1}-\frac{\rho E}{p} \\
= & -\frac{1}{\gamma-1}\ln\left((\gamma-1)\left(u_5-\frac{1}{2}\frac{(u_2^2+u_3^2+u_4^2)}{u_1}\right)u_1^{-\gamma}\right) \\
& +\frac{\gamma+1}{\gamma-1}-\frac{1}{(\gamma-1)}\frac{u_1u_5}{\left(u_1u_5-\frac{1}{2}(u_2^2+u_3^2+u_4^2)\right)} \\
v_2 = & \frac{\rho u}{p}=\frac{1}{\gamma-1}\frac{u_1u_2}{u_1u_5-\frac{1}{2}(u_2^2+u_4^2+u_4^2)} \\
v_3 = & \frac{\rho v}{p}=\frac{1}{\gamma-1}\frac{u_1u_3}{u_1u_5-\frac{1}{2}(u_2^2+u_4^2+u_4^2)} \\
v_4 = & \frac{\rho w}{p}=\frac{1}{\gamma-1}\frac{u_1u_4}{u_1u_5-\frac{1}{2}(u_2^2+u_4^2+u_4^2)} \\
v_5 = & -\frac{\rho}{p}=-\frac{1}{\gamma-1}\frac{u_1^2}{u_1u_5-\frac{1}{2}(u_2^2+u_4^2+u_4^2)}
\end{aligned}$$

In order to reverse this transformation, we examine the definition of v_1:

$$v_1=-\frac{s}{\gamma-1}+\frac{\gamma+1}{\gamma-1}-\frac{\rho E}{p} \tag{B.6}$$

We reorder and substitute using the definition of pressure in (1.6):

$$\begin{aligned}
s &= -(\gamma-1)v_1+(\gamma+1)-\frac{(\gamma-1)}{p}\left(\frac{p}{(\gamma-1)}+\frac{1}{2}\rho\left(u^2+v^2+w^2\right)\right) \\
&= -(\gamma-1)v_1+(\gamma+1)-\left(1+\frac{1}{2}(\gamma-1)\left(\left(\frac{\rho u}{p}\right)^2+\left(\frac{\rho v}{p}\right)^2+\left(\frac{\rho w}{p}\right)^2\right)\frac{p}{\rho}\right) \\
s &= \gamma-(\gamma-1)v_1+\frac{1}{2}(\gamma-1)\frac{v_2^2+v_3^2+v_4^2}{v_5}
\end{aligned}$$

Now, with $s=s(\mathbf{v})$, we just need the pressure to fully define $\mathbf{u}$ with respect to $\mathbf{v}$. We

consider the definition of s and use logarithm tricks to start.

$$\begin{aligned} s &= \ln\left(p\rho^{-\gamma}\right) = \ln p - \gamma \ln \rho \\ -\frac{s}{\gamma-1} &= -\frac{1}{\gamma-1}\ln p + \frac{\gamma}{\gamma-1}\ln\rho \\ \exp\left(-\frac{s}{\gamma-1}\right) &= p^{-\frac{1}{\gamma-1}}\rho^{\frac{\gamma}{\gamma-1}} = (\gamma-1)^{-\frac{1}{\gamma-1}}\left(\frac{p}{\gamma-1}\right)^{-\frac{1}{\gamma-1}}\rho^{\frac{\gamma}{\gamma-1}} \\ (\gamma-1)^{\frac{1}{\gamma-1}}\exp\left(-\frac{s}{\gamma-1}\right)\left(\frac{\rho}{p}\right)^{\frac{-\gamma}{\gamma-1}} &= p^{\frac{\gamma}{\gamma-1}}\left(\frac{p}{\gamma-1}\right)^{-\frac{1}{\gamma-1}} = (\gamma-1)^{\frac{1}{\gamma-1}}p \end{aligned} \tag{B.7}$$

And we can write:

$$p = \exp\left[-\frac{s}{\gamma-1}\right]\left(-\frac{1}{v_5}\right)^{\frac{\gamma}{\gamma-1}} \tag{B.8}$$

Now, we consider the last four terms of $\mathbf{v}$:

$$\begin{aligned} v_2 &= \frac{\rho u}{p} &&= \frac{u_2}{p} \\ v_3 &= \frac{\rho v}{p} &&= \frac{u_3}{p} \\ v_4 &= \frac{\rho w}{p} &&= \frac{u_4}{p} \\ v_5 &= -\frac{\rho}{p} &&= -\frac{u_1}{p} \end{aligned} \tag{B.9}$$

Hey-o! We can work with that. Now we note that $\frac{\rho E}{p} = \frac{u_5}{p}$ in the definition of v_1, which

allows us to write a nonlinear transformation from $\mathbf{v}$ to $\mathbf{u}$:

$$\begin{aligned}
u_1 &= -v_5 p &&= -v_5 \exp\left[-\frac{s}{\gamma-1}\right]\left(-\frac{1}{v_5}\right)^{\frac{\gamma}{\gamma-1}} \\
u_2 &= v_2 p &&= v_2 \exp\left[-\frac{s}{\gamma-1}\right]\left(-\frac{1}{v_5}\right)^{\frac{\gamma}{\gamma-1}} \\
u_3 &= v_3 p &&= v_3 \exp\left[-\frac{s}{\gamma-1}\right]\left(-\frac{1}{v_5}\right)^{\frac{\gamma}{\gamma-1}} \\
u_4 &= v_4 p &&= v_4 \exp\left[-\frac{s}{\gamma-1}\right]\left(-\frac{1}{v_5}\right)^{\frac{\gamma}{\gamma-1}} \\
u_5 &= \left[-\frac{1}{\gamma-1}s + \frac{\gamma+1}{\gamma-1} - v_1\right] p &&= \left[-\frac{1}{\gamma-1}s + \frac{\gamma+1}{\gamma-1} - v_1\right] \exp\left[-\frac{s}{\gamma-1}\right]\left(-\frac{1}{v_5}\right)^{\frac{\gamma}{\gamma-1}}
\end{aligned} \tag{B.10}$$

B.2 Deriving second law of thermodynamics properties

As stated in the literature [3, 14], testing using the entropy variables, such that $w = v$, should result in a statement that states the Clausius-Duhem inequality or the second law of theromodynamics. We can use our expanded form in (3.14) to investigate the artificial generation of entropy due to the underresolution of the scheme:

$$\begin{aligned}
\sum_{\kappa} \Bigg\{ \int_I \int_\kappa \mathbf{v}^T \frac{\partial \mathbf{u}_h}{\partial t} \, \mathrm{d}\mathbb{V} \, \mathrm{d}t + \int_\kappa \left(\mathbf{v}^T \left(\hat{\mathbf{u}}_h - \mathbf{u}_h\right)\right)\Big|_{t_+^n}^{t_-^{n+1}} \, \mathrm{d}\mathbb{V} \\
+ \int_I \oint_{\partial\kappa} \mathbf{v}^T \left(\left(\widehat{\underline{\mathbf{F}}^I \cdot \underline{n}} - \underline{\mathbf{F}}^I \cdot \underline{n}\right) - \left(\widehat{\underline{\mathbf{F}}^V \cdot \underline{n}} - \underline{\mathbf{F}}^V \cdot \underline{n}\right)\right) \, \mathrm{dS} \, \mathrm{d}t \\
+ \int_I \int_\kappa \mathbf{v}^T \left(\nabla \cdot \left(\underline{\mathbf{F}}^I - \underline{\mathbf{F}}^V\right)\right) \, \mathrm{d}\mathbb{V} \, \mathrm{d}t + R^{\text{quad}}_{\mathrm{s},\kappa,0} + R^{\text{quad}}_{\mathrm{t},\kappa,0} \Bigg\} = 0
\end{aligned} \tag{B.11}$$

We start with the first term and the last integral term, which constitute the infinite-resolution case terms. These, simplified, should simplify to a simple statement of the Clausius-Duhem

statement. We start with the temporal term:

$$
\begin{aligned}
\mathbf{v}^T \frac{\partial \mathbf{u}_h}{\partial t} &= -\frac{1}{\gamma-1} s \frac{\partial \rho}{\partial t} + \frac{\gamma+1}{\gamma-1}\frac{\partial \rho}{\partial t} - \frac{\rho E}{p}\frac{\partial \rho}{\partial t} + \frac{\rho u}{p}\frac{\partial(\rho u)}{\partial t} + \frac{\rho v}{p}\frac{\partial(\rho v)}{\partial t} + \frac{\rho w}{p}\frac{\partial(\rho w)}{\partial t} - \frac{\rho}{p}\frac{\partial(\rho E)}{\partial t} \\
&= -\frac{1}{\gamma-1} s \frac{\partial \rho}{\partial t} + \frac{\gamma+1}{\gamma-1}\frac{\partial \rho}{\partial t} - \frac{\partial}{\partial t}\left[\frac{\rho^2 E}{p}\right] + \rho\frac{\partial}{\partial t}\left[\frac{\rho E}{p}\right] + \frac{\partial}{\partial t}\left[\frac{\rho^2}{p}\left(\underline{V}\cdot\underline{V}\right)\right] \\
&\quad - \rho\underline{V}\cdot\frac{\partial}{\partial t}\left[\frac{\rho\underline{V}}{p}\right] - \frac{\partial}{\partial t}\left[\frac{\rho^2 E}{p}\right] + \frac{\rho E}{p}\frac{\partial \rho}{\partial t} - \frac{\rho^2 E}{p}\frac{\partial \rho}{\partial t} \\
&= -\frac{1}{\gamma-1} s \frac{\partial \rho}{\partial t} + \frac{\gamma+1}{\gamma-1}\frac{\partial \rho}{\partial t} - 2\frac{\partial}{\partial t}\left[\frac{\rho}{p}\left(\rho E - \frac{1}{2}\rho\left(\underline{V}\cdot\underline{V}\right)\right)\right] + \rho\frac{\partial}{\partial t}\left[\frac{\rho E}{p}\right] \\
&\quad - \rho\underline{V}\cdot\frac{\partial}{\partial t}\left[\frac{\rho\underline{V}}{p}\right] + \frac{\rho E}{p}\frac{\partial \rho}{\partial t} - \frac{\rho^2 E}{p^2}\frac{\partial \rho}{\partial t} \\
&= -\frac{1}{\gamma-1} s \frac{\partial \rho}{\partial t} + \frac{\gamma+1}{\gamma-1}\frac{\partial \rho}{\partial t} - \frac{2}{\gamma-1}\frac{\partial \rho}{\partial t} + \rho\frac{\partial}{\partial t}\left[\frac{\rho E}{p}\right] \\
&\quad - \rho\frac{\partial}{\partial t}\left[\frac{\rho\left(\underline{V}\cdot\underline{V}\right)}{p}\right] + \frac{\rho^2\underline{V}}{p}\cdot\frac{\partial \underline{V}}{\partial t} + \frac{\rho E}{p}\frac{\partial \rho}{\partial t} - \frac{\rho^2 E}{p^2}\frac{\partial \rho}{\partial t} \\
&= -\frac{1}{\gamma-1} s \frac{\partial \rho}{\partial t} + \frac{\partial \rho}{\partial t} + \rho\frac{\partial}{\partial t}\left[\frac{\rho E}{p}\right] - \rho\frac{\partial}{\partial t}\left[\frac{\rho\left(\underline{V}\cdot\underline{V}\right)}{p}\right] \\
&\quad + \frac{\rho^2}{p}\frac{\partial}{\partial t}\left[\frac{1}{2}\left(\underline{V}\cdot\underline{V}\right)\right] + \rho\frac{\partial}{\partial t}\left[\frac{\rho E}{p}\right] - \rho^2\frac{\partial}{\partial t}\left[\frac{E}{p}\right] - \frac{\rho^2 E}{p}\frac{\dot{p}}{p} \\
&= -\frac{1}{\gamma-1} s \frac{\partial \rho}{\partial t} + \frac{\partial \rho}{\partial t} + 2\rho\frac{\partial}{\partial t}\left[\frac{1}{p}\left(\rho E - \frac{1}{2}\rho\left(\underline{V}\cdot\underline{V}\right)\right)\right] + \frac{\rho^2}{p}\frac{\partial}{\partial t}\left(\frac{1}{2}\left(\underline{V}\cdot\underline{V}\right)\right) - \frac{\rho^2}{p}\frac{\partial E}{\partial t} \\
&= -\frac{1}{\gamma-1} s \frac{\partial \rho}{\partial t} + \frac{\partial \rho}{\partial t} - \frac{\rho^2}{p}\frac{\partial}{\partial t}\left[E - \frac{1}{2}\left(\underline{V}\cdot\underline{V}\right)\right]
\end{aligned}
\tag{B.12}
$$

Here, we have used the definition of p from (1.6). We can continue to use this definition by taking the derivative of (1.6)!

$$
\begin{aligned}
\frac{\partial p}{\partial t} &= (\gamma-1)\left[\frac{\partial \rho}{\partial t}E + \rho\frac{\partial E}{\partial t} - \frac{1}{2}\frac{\partial \rho}{\partial t}\left(\underline{V}\cdot\underline{V}\right) - \frac{1}{2}\rho\frac{\partial}{\partial t}\left(\frac{1}{2}\left(\underline{V}\cdot\underline{V}\right)\right)\right] \\
\frac{\partial p}{\partial t} &= (\gamma-1)\left[\frac{\partial \rho}{\partial t}\left(E - \frac{1}{2}\left(\underline{V}\cdot\underline{V}\right)\right) + \rho\frac{\partial}{\partial t}\left(E - \frac{1}{2}\left(\underline{V}\cdot\underline{V}\right)\right)\right] \qquad \text{(B.13)} \\
\rho\frac{\partial}{\partial t}\left[E - \frac{1}{2}\left(\underline{V}\cdot\underline{V}\right)\right] &= \frac{1}{\gamma-1}\frac{\partial p}{\partial t} - \frac{\partial \rho}{\partial t}\left[E - \frac{1}{2}\left(\underline{V}\cdot\underline{V}\right)\right]
\end{aligned}
$$

Back into the temporal term:

$$\mathbf{v}^T \frac{\partial \mathbf{u}_h}{\partial t} = -\frac{1}{\gamma - 1} s \frac{\partial \rho}{\partial t} + \frac{\partial \rho}{\partial t} - \frac{1}{\gamma - 1} \frac{\rho}{p} \frac{\partial p}{\partial t} + \frac{\rho}{p} \frac{\partial \rho}{\partial t} \left[E - \frac{1}{2} (\underline{V} \cdot \underline{V}) \right] \tag{B.14}$$

We can use the definition of s from (2.5) and expand using logarithm rules.

$$\begin{aligned}
\mathbf{v}^T \frac{\partial \mathbf{u}_h}{\partial t} =& -\frac{1}{\gamma - 1} \frac{\partial \rho}{\partial t} \log p + \frac{\gamma}{\gamma - 1} \frac{\partial \rho}{\partial t} \log \rho + \frac{\partial \rho}{\partial t} \\
& - \frac{1}{\gamma - 1} \rho \frac{\dot{p}}{p} + \frac{\rho}{p} \frac{\partial \rho}{\partial t} \left[E - \frac{1}{2} (\underline{V} \cdot \underline{V}) \right] \\
=& -\frac{1}{\gamma - 1} \frac{\partial \rho}{\partial t} \log p + \frac{\gamma}{\gamma - 1} \frac{\partial \rho}{\partial t} \log \rho + \frac{\partial \rho}{\partial t} - \frac{1}{\gamma - 1} \rho \frac{\partial}{\partial t} (\log p) \\
& + \frac{\rho}{p} \frac{\partial}{\partial t} \left[\rho E - \frac{1}{2} \rho (\underline{V} \cdot \underline{V}) \right] - \frac{\rho^2}{p} \frac{\partial}{\partial t} \left[E - \frac{1}{2} (\underline{V} \cdot \underline{V}) \right] \\
=& -\frac{1}{\gamma - 1} \frac{\partial}{\partial t} [\rho \log p] + \frac{\gamma}{\gamma - 1} \frac{\partial}{\partial t} [\rho \log \rho] \\
& - \frac{1}{\gamma - 1} \frac{\partial \rho}{\partial t} + \frac{\rho}{p} \frac{\partial \rho}{\partial t} \left[E - \frac{1}{2} (\underline{V} \cdot \underline{V}) \right] \\
=& -\frac{1}{\gamma - 1} \frac{\partial}{\partial t} \left[\rho \log \left(p \rho^{-\gamma} \right) \right] - \frac{1}{\gamma - 1} \frac{\partial \rho}{\partial t} + \frac{\partial \rho}{\partial t} \frac{1}{p} \left[\frac{p}{\gamma - 1} \right]
\end{aligned} \tag{B.15}$$

Thus, we have:

$$\mathbf{v}^T \frac{\partial \mathbf{u}_h}{\partial t} = -\frac{1}{\gamma - 1} \frac{\partial}{\partial t} [\rho s] \tag{2.27}$$

We can approach the inviscid divergence term, $\mathbf{v}^T (\nabla \cdot \underline{\mathbf{F}}^I)$, similarly. We start with the divergence of the fluxes:

$$\nabla \cdot \underline{\mathbf{F}}^I = \begin{pmatrix} \nabla \rho \cdot \underline{V} + \rho \nabla \cdot \underline{V} \\ u(\nabla \rho \cdot \underline{V}) + \rho u (\nabla \cdot \underline{V}) + \rho \nabla u \cdot \underline{V} + \frac{\partial p}{\partial x} \\ v(\nabla \rho \cdot \underline{V}) + \rho v (\nabla \cdot \underline{V}) + \rho \nabla v \cdot \underline{V} + \frac{\partial p}{\partial y} \\ w(\nabla \rho \cdot \underline{V}) + \rho w (\nabla \cdot \underline{V}) + \rho \nabla w \cdot \underline{V} + \frac{\partial p}{\partial z} \\ H(\nabla \rho \cdot \underline{V}) + \rho H (\nabla \cdot \underline{V}) + \rho \underline{V} \cdot \nabla H \end{pmatrix} \tag{B.16}$$

$$\nabla \cdot \underline{\underline{\mathbf{F}}}^{V^*} = \begin{pmatrix} 0 \\ \nabla \cdot \underline{\underline{\tau}} \\ \nabla \cdot (\underline{V} \cdot \underline{\underline{\tau}}) \end{pmatrix} \quad \nabla \cdot \underline{\underline{\mathbf{F}}}^{H^*} = \begin{pmatrix} 0 \\ 0 \\ -\kappa_T \nabla^2 T \end{pmatrix} \tag{B.17}$$

So we can write:

$$\begin{aligned}
\mathbf{v}^T(\nabla \cdot \underline{\underline{\mathbf{F}}}^I) = & \left(-\frac{s}{\gamma-1} + \frac{\gamma+1}{\gamma-1} - \frac{\rho E}{p}\right)(\nabla\rho \cdot \underline{V}) + \left(-\frac{s}{\gamma-1} + \frac{\gamma+1}{\gamma-1} - \frac{\rho E}{p}\right)\rho\,(\nabla \cdot \underline{V}) \\
& + \frac{\rho u^2}{p}(\nabla\rho \cdot \underline{V}) + \frac{\rho v^2}{p}(\nabla\rho \cdot \underline{V}) + \frac{\rho w^2}{p}(\nabla\rho \cdot \underline{V}) + \frac{\rho^2 u^2}{p}(\nabla \cdot \underline{V}) \\
& + \frac{\rho^2 v^2}{p}(\nabla \cdot \underline{V}) + \frac{\rho^2 w^2}{p}(\nabla \cdot \underline{V}) + \frac{\rho^2 u}{p}\nabla u \cdot \underline{V} + \frac{\rho^2 v}{p}\nabla v \cdot \underline{V} + \frac{\rho^2 w}{p}\nabla w \cdot \underline{V} \\
& + \frac{\rho u}{p}\frac{\partial p}{\partial x} + \frac{\rho v}{p}\frac{\partial p}{\partial y} + \frac{\rho w}{p}\frac{\partial p}{\partial z} - \frac{\rho}{p}\left(E + \frac{p}{\rho}\right)(\nabla\rho \cdot \underline{V}) \\
& - \frac{\rho^2}{p}\left(E + \frac{p}{\rho}\right)(\nabla \cdot \underline{V}) - \frac{\rho^2}{p}\nabla\left(E + \frac{p}{\rho}\right) \cdot \underline{V} \\
= & \left[-\frac{1}{\gamma-1}s + \frac{\gamma+1}{\gamma-1} - 2\frac{\rho E}{p} + \frac{\rho}{p}(\underline{V} \cdot \underline{V})\right](\nabla\rho \cdot \underline{V}) \\
& + \left[-\frac{1}{\gamma-1}\rho s + \frac{\gamma+1}{\gamma-1}\rho - 2\frac{\rho^2 E}{p} + \frac{\rho^2}{p}(\underline{V} \cdot \underline{V}) - \rho\right](\nabla \cdot \underline{V}) \\
& + \frac{\rho^2}{p}\underline{V} \cdot (\nabla \underline{V}) \cdot \underline{V} - \frac{\rho^2}{p}(\nabla E \cdot \underline{V}) \\
= & \left[-\frac{1}{\gamma-1}s + \frac{\gamma+1}{\gamma-1} - \frac{2}{p}\left(\rho E - \frac{1}{2}\rho(\underline{V} \cdot \underline{V})\right)\right](\nabla\rho \cdot \underline{V}) \\
& + \left[-\frac{1}{\gamma-1}\rho s + \frac{\gamma+1}{\gamma-1}\rho - \frac{2\rho}{p}\left(\rho E - \frac{1}{2}\rho(\underline{V} \cdot \underline{V})\right) - \rho\right](\nabla \cdot \underline{V}) \\
& + \frac{\rho^2}{p}\underline{V} \cdot (\nabla \underline{V}) \cdot \underline{V} - \frac{\rho^2}{p}(\nabla E \cdot \underline{V}) \\
= & \left[-\frac{1}{\gamma-1}s + \frac{\gamma}{\gamma-1} - \frac{1}{\gamma-1}\right](\nabla\rho \cdot \underline{V}) + \left[-\frac{1}{\gamma-1}s + \frac{\gamma}{\gamma-1} - \frac{1}{\gamma-1} - 1\right]\rho\,(\nabla \cdot \underline{V}) \\
& + \frac{\rho^2}{p}\left(\nabla\left(\frac{1}{2}(\underline{V} \cdot \underline{V})\right) \cdot \underline{V}\right) - \frac{\rho^2}{p}(\nabla E \cdot \underline{V})
\end{aligned} \tag{B.18}$$

Now, we note that the gradient of (1.6) is given by:

$$\nabla p = (\gamma - 1)\left[(\nabla\rho)\,E + \rho\,(\nabla E) - \frac{1}{2}(\nabla\rho)\,(\underline{V} \cdot \underline{V}) - \rho\nabla\left(\frac{1}{2}(\underline{V} \cdot \underline{V})\right)\right] \tag{B.19}$$

Substituting and returning to the inviscid spatial flux:

$$\begin{aligned}
\mathbf{v}^T(\nabla\cdot\underline{\mathbf{F}}^I) &= \left[-\frac{1}{\gamma-1}s+\frac{\gamma}{\gamma-1}-\frac{1}{\gamma-1}\right](\nabla\rho\cdot\underline{V})+\left[-\frac{1}{\gamma-1}s+\frac{\gamma}{\gamma-1}-\frac{1}{\gamma-1}-1\right]\rho(\nabla\cdot\underline{V})\\
&\quad+\frac{\rho}{p}\left[-\frac{1}{\gamma-1}\nabla p\cdot\underline{V}+\left(E-\frac{1}{2}(\underline{V}\cdot\underline{V})\right)(\nabla\rho\cdot\underline{V})\right]\\
&=\left[-\frac{1}{\gamma-1}s+\frac{\gamma}{\gamma-1}-\frac{1}{\gamma-1}\right](\nabla\rho\cdot\underline{V})+\left[-\frac{1}{\gamma-1}s+\frac{\gamma}{\gamma-1}-\frac{1}{\gamma-1}-1\right]\rho(\nabla\cdot\underline{V})\\
&\quad-\frac{1}{\gamma-1}\rho\frac{\nabla p}{p}\cdot\underline{V}+\frac{1}{\gamma-1}(\nabla\rho\cdot\underline{V})\\
&=\left[-\frac{1}{\gamma-1}s+\frac{\gamma}{\gamma-1}\right](\nabla\rho\cdot\underline{V})+\left[-\frac{1}{\gamma-1}s\right](\nabla\cdot\underline{V})-\frac{1}{\gamma-1}\rho\frac{\nabla p}{p}\cdot\underline{V}\\
&=-\frac{1}{\gamma-1}s\left[\nabla\rho\cdot\underline{V}+\rho(\nabla\underline{V})\right]+\frac{\gamma}{\gamma-1}(\nabla\rho\cdot\underline{V})-\frac{1}{\gamma-1}\rho\frac{\nabla p}{p}\cdot\underline{V}\\
&=-\frac{1}{\gamma-1}s(\nabla\cdot(\rho\underline{V}))+\frac{\gamma}{\gamma-1}(\nabla\rho\cdot\underline{V})-\frac{1}{\gamma-1}\rho\frac{\nabla p}{p}\cdot\underline{V}\\
&=-\frac{1}{\gamma-1}(\nabla\cdot(\rho s\underline{V}))+\frac{1}{\gamma-1}\nabla s\cdot(\rho\underline{V})+\frac{\gamma}{\gamma-1}\nabla\cdot(\rho\underline{V})\\
&\quad-\frac{\gamma}{\gamma-1}\rho(\nabla\cdot\underline{V})-\frac{1}{\gamma-1}\rho\underline{V}\cdot\nabla(\log p)\\
&=-\frac{1}{\gamma-1}(\nabla\cdot(\rho s\underline{V}))-\frac{\gamma}{\gamma-1}\rho\underline{V}\cdot\nabla(\log\rho)+\frac{\gamma}{\gamma-1}\nabla\rho\cdot\underline{V}\\
&=-\frac{1}{\gamma-1}(\nabla\cdot(\rho s\underline{V}))-\frac{\gamma}{\gamma-1}\rho\underline{V}\cdot\frac{\nabla\rho}{\rho}+\frac{\gamma}{\gamma-1}\nabla\rho\cdot\underline{V}\\
\mathbf{v}^T(\nabla\cdot\underline{\mathbf{F}}^I) &= -\frac{1}{\gamma-1}(\nabla\cdot(\rho s\underline{V}))
\end{aligned}\tag{B.20}$$

For the divergence of the heat flux term, $\mathbf{v}^T(\nabla\cdot\underline{\mathbf{F}}^{H^*})$, we have:

$$\begin{aligned}
\mathbf{v}^T(\nabla\cdot\underline{\mathbf{F}}^{H^*}) &= -\frac{\rho}{p}\left[-\kappa_T\nabla^2T\right]=\frac{1}{RT}\kappa_T\nabla\cdot\nabla T\\
&=\frac{1}{R}\kappa_T\nabla\cdot\left(\frac{\nabla T}{T}\right)-\frac{1}{R}\kappa_T(\nabla T)\cdot\nabla\left(\frac{1}{T}\right)\\
\mathbf{v}^T(\nabla\cdot\underline{\mathbf{F}}^{H^*}) &= \frac{1}{R}\kappa_T\nabla\cdot\left(\frac{\nabla T}{T}\right)+\frac{1}{R}\kappa_T\left(\frac{\nabla T\cdot\nabla T}{T^2}\right)
\end{aligned}\tag{B.21}$$

Here, we pause and note that the rightmost term is always negative! Now, we look at the

divergence of the viscous flux term, $\mathbf{v}^T(\nabla \cdot \underline{\underline{\mathbf{F}}}^{V^*})$. We have:

$$\begin{aligned}
\mathbf{v}^T(\nabla \cdot \underline{\underline{\mathbf{F}}}^{V^*}) &= \frac{\rho \underline{V}}{p} \cdot (\nabla \cdot \underline{\underline{\tau}}) - \frac{\rho}{p} \nabla \cdot (\underline{V} \cdot \underline{\underline{\tau}}) \\
&= \frac{\rho}{p} \left[\underline{V} \cdot \nabla \cdot \underline{\underline{\tau}} - \nabla \cdot (\underline{V} \cdot \underline{\underline{\tau}}) \right] \\
&= -\frac{\rho}{p} \left\langle \nabla \underline{V}, \underline{\underline{\tau}} \right\rangle_F = -\frac{\rho}{p} \left\langle \nabla \underline{V}, \mu \left(\nabla \underline{V} + (\nabla \underline{V})^T \right) - \frac{2}{3} \mu \operatorname{tr} \left((\nabla \underline{V})^T \nabla \underline{V} \right) \right\rangle_F \\
&= -\frac{\rho}{p} \left[\mu \langle \nabla \underline{V}, \nabla \underline{V} \rangle_F + \mu \langle \nabla \underline{V}, (\nabla \underline{V})^T \rangle_F - \frac{2}{3} \mu \operatorname{tr} \left((\nabla \underline{V})^T \nabla \underline{V} \right) \right] \\
&= -\frac{\rho}{p} \left[2\mu \left(\left(\frac{\partial u}{\partial x} \right)^2 + \left(\frac{\partial v}{\partial w} \right)^2 + \left(\frac{\partial w}{\partial z} \right)^2 \right) \right. \\
&\qquad + \left(\frac{\partial u}{\partial y} + \frac{\partial v}{\partial x} \right)^2 + \left(\frac{\partial u}{\partial z} + \frac{\partial w}{\partial x} \right)^2 + \left(\frac{\partial u}{\partial z} + \frac{\partial w}{\partial x} \right)^2 \\
&\qquad \left. - \frac{2}{3} \mu \left(\left(\frac{\partial u}{\partial x} \right)^2 + \left(\frac{\partial v}{\partial w} \right)^2 + \left(\frac{\partial w}{\partial z} \right)^2 \right) \right] \\
\mathbf{v}^T(\nabla \cdot \underline{\underline{\mathbf{F}}}^{V^*}) &= -\frac{\rho}{p} \left[\frac{4}{3} \mu \left(\left(\frac{\partial u}{\partial x} \right)^2 + \left(\frac{\partial v}{\partial w} \right)^2 + \left(\frac{\partial w}{\partial z} \right)^2 \right) \right. \\
&\qquad \left. + \left(\frac{\partial u}{\partial y} + \frac{\partial v}{\partial x} \right)^2 + \left(\frac{\partial u}{\partial z} + \frac{\partial w}{\partial x} \right)^2 + \left(\frac{\partial u}{\partial z} + \frac{\partial w}{\partial x} \right)^2 \right]
\end{aligned} \tag{B.22}$$

We note again that this term is always negative. We can now take the discovered terms and substitute them into (B.11), assuming for the moment that the solution is continuous. This gives:

$$\begin{aligned}
\sum_\kappa \left\{ \int_I \int_\kappa \frac{\partial}{\partial t} \left(-\frac{1}{\gamma - 1} \rho s \right) \, \mathrm{d}\mathbb{V} \, \mathrm{d}t + \int_I \int_\kappa \left(-\frac{1}{\gamma - 1} \nabla \cdot [\rho s \underline{V}] \right) \, \mathrm{d}\mathbb{V} \, \mathrm{d}t \right. \\
+ \int_I \int_\kappa \frac{\kappa_T}{R} \nabla \cdot \frac{\nabla T}{T} \, \mathrm{d}\mathbb{V} \, \mathrm{d}t + \int_I \int_\kappa \frac{\kappa_T}{R} \left(\frac{\nabla T \cdot \nabla T}{T^2} \right) \, \mathrm{d}\mathbb{V} \, \mathrm{d}t \\
\left. - \int_I \int_\kappa \mathbf{v}^T (\nabla \cdot \underline{\underline{\mathbf{F}}}^{V^*}) \, \mathrm{d}\mathbb{V} \, \mathrm{d}t \right\} = 0
\end{aligned} \tag{B.23}$$

We can jimmy this to show:

$$\sum_{\kappa}\left\{\int_I\int_\kappa \frac{\partial}{\partial t}(\rho s)\ \ \mathrm{d}\mathbb{V}\ \mathrm{d}t + \int_I\int_\kappa \nabla\cdot\left[\rho s\underline{V}\right]\ \ \mathrm{d}\mathbb{V}\ \mathrm{d}t - \int_I\int_\kappa \kappa_T\frac{\gamma-1}{R}\nabla\cdot\left(\frac{\nabla T}{T}\right)\ \ \mathrm{d}\mathbb{V}\ \mathrm{d}t\right\} =$$
$$\sum_{\kappa}\left\{\int_I\int_\kappa \kappa_T\frac{\gamma-1}{R}\left(\frac{\nabla T\cdot\nabla T}{T^2}\right)\ \ \mathrm{d}\mathbb{V}\ \mathrm{d}t - (\gamma-1)\mathbf{v}^T(\nabla\cdot\underline{\mathbf{F}}^{V^*})\right\} \geq 0 \quad \text{(B.24)}$$

This shows that the DG discretization in the infinite limit of resolution satisfies the Clausius-Duhem inequality [14].